arXiv:astro-ph/9904411v1 29 Apr 1999

University of Naples "Federico II"

Faculty of Mathematical, Physical and Natural Sciences

Ph.D. Thesis in Physics

Primordial Nucleosynthesis: accurate predictions for light element abundances

Salvatore Esposito

Advisors:

Dr. G. Mangano
Dr. G. Miele
Prof. F. Buccella

The heavens declare the glory of God;
and the firmament sheweth his handywork.

Day unto day uttereth speech,
and night unto night sheweth knowledge.

No speech nor language,
their voice is not heard.

Their line is gone out through all the earth,
and their words to the end of the world.

(Psalms 19)

Contents

Introduction **iv**

1 The standard cosmology: an overview **1**

1.1 Homogeneity and Isotropy 2
1.2 Cosmological equations 4
    1.2.1 Evolution of the Universe 6
    1.2.2 Driving the expansion 8
1.3 Thermodynamics of the Universe 9
    1.3.1 Equilibrium thermodynamics 9
    1.3.2 Energy density and pressure in the Universe 13
    1.3.3 Total entropy density in the comoving volume 13
    1.3.4 Decoupling 14
    1.3.5 Time - temperature relationship 16
1.4 Thermal evolution of the Universe 16
    1.4.1 Neutrino decoupling 18

2 Primordial Nucleosynthesis **22**

2.1 Preliminaries 22
2.2 Observed primordial abundances 24
    2.2.1 D 24
    2.2.2 ^3He 25
    2.2.3 ^4He 26
    2.2.4 ^7Li 28
2.3 Production of the light elements 29

2.3.1 $T \gtrsim 1\,MeV$ ($t \lesssim 1\,s$) 29

2.3.2 $T \simeq 0.3 \div 0.1\,MeV$ ($t \simeq 1 \div 3\,min$) 31

2.4 Calculation of the primordial abundances 34

2.4.1 Equation for R 35

2.4.2 Equation for n_B 36

2.4.3 Equation for ϕ_e 36

2.4.4 Equation for T 36

2.4.5 Equations for Y_i 38

2.5 Theory versus observations. Constraints from BBN 39

3 The Born rates for $n \leftrightarrow p$ reactions 42

3.1 The reaction $\nu_e + n \to e^- + p$ and the other processes 44

3.2 Radiative electromagnetic corrections: the neutron lifetime 46

3.3 Results for the reaction rates 53

4 Finite nucleon mass corrections 56

4.1 Corrections to the transition amplitude 57

4.2 Kinematical corrections 59

5 QED thermal radiative corrections 64

5.1 Mass shift correction 67

5.2 Wavefunction renormalization correction 69

5.3 Vertex correction 70

5.4 Photon emission and absorption 72

5.5 Corrections to the equation of state 75

6 Calculations of Big Bang Nucleosynthesis. Results 77

6.1 Primordial nucleosynthesis: cosmology and particle physics inputs 77

6.2 Prediction on the ^4He abundance 86

6.3 Building the BBN code 88

6.3.1 Numerical tricks 89

Acknowledgments 94

Bibliography **95**

A Non equilibrium distribution of species **102**

B Neutrino-photon temperature relation **106**

C Nuclear reaction network **108**

D Nuclide mass excess **113**

E Finite nucleon mass corrected matrix element **115**

F Finite temperature and density QED **117**

F.1 The Real Time Formalism . . . 117
F.2 Electron self-energy . . . 118
F.3 Wavefunction renormalization . . . 122
F.4 Photon self-energy . . . 125

Introduction

Primordial Big Bang Nucleosynthesis (BBN) [1]-[7] represents one of the greatest successes of the hot Big Bang model, along with the Hubble expansion and the Cosmic Microwave Background Radiation. Of the three, BBN probes the Universe to the earliest times, from a fraction of a second to thousands of seconds from its born, and its formulation predicted the existence of cosmic microwave background radiation [8]. Its emergence as a cosmological cornerstone relies on the basic consistency of the predictions for the abundances of the light elements, such as D, ^3He, ^4He, ^7Li, with their measured abundances, which span over more than nine orders of magnitude.

BBN took place in the early Universe when the temperature scale was less than $1\,MeV$. The key events leading to the synthesis of the light nuclides followed from the period when the weak interaction rates were in equilibrium, thus fixing the ratio of number densities of neutrons to protons; at temperatures $T \gg 1\,MeV$ this ratio was $n/p \simeq 1$. As the temperature fell and approached the point where the weak interaction rates were no longer fast enough to maintain equilibrium, the neutron to proton ratio was given approximately by the Boltzmann factor, $(n/p) \simeq \exp\{-\Delta m/T\}$, where Δm is the neutron-proton mass difference.

The nucleosynthesis chain begins with the formation of deuterium through the process $p + n \to D + \gamma$. However, because of the large number of photons relative to nucleons (of the order of 10^{10}), deuterium production is delayed past until the temperature falls well below the deuterium binding energy of $2.2\,MeV$ (the average photon energy in a blackbody is $< E_\gamma > \simeq 2.7\,T$).

The dominant product of BBN is ^4He, resulting in a mass abundance close to 25 %. Smaller amounts of other light elements are produced: D and ^3He at the level of about 10^{-5}, and ^7Li at the level of 10^{-10} per hydrogen nucleus. In the standard model (see below) the abundances depend only on one free parameter, the baryon to photon ratio η, and remarkablya single value for $\eta \sim 10^{-10}$ may accommodate all observed orders of magnitude for ^4He, D, ^3He and ^7Li data. Furthermore, the primeval yield of ^4He is also relatively insensitive to this quantity (pinning down η to 20 % pegs its value to 1 % precision).

The resulting abundances of the light elements are shown in Figure 1, where we report the predictions for the ^4He mass fraction Y, and D, ^3He, ^7Li abundances relative to H as function of η. We also report the present observational situation (a complete discussion is presented in chapter 2). The general agreement between experimental data and expectations emerging from this figure, ranging over many orders of magnitude, is the great success of the Big Bang model which we referred to above. The essential problem in attempting to compare [7, 10] the theoretical predictions with the observational data is that the primordial abundances have been significantly altered during the lifetime of the Universe through nuclear processing in stars and other galactic chemical evolution effects (we will discuss this subject in chapter 2). The most stable nucleus, ^4He, grows in abundance with time since it is always created in stars, while D, the most weakly bound, is always destroyed. The history of ^3He and ^7Li is more complicated since these elements may be both destroyed and created during stellar evolutiom. To avoid corrections which are difficult to treat quantitatively, it is necessary to measure abundances in the most primordial available material. Observations of light element abundances have dramatically improved over the past few years [10]. Although D and ^3He abundances have about a 10 % uncertainty and ^7Li data are even more uncertain, as an example we mention the fact that ^4He data are now reaching a precision [11] of one per mille.

This perspective, however, the fact that BBN is now entering in his maturity and precision era, demands similar improvements in the precision of the theoretical analysis, in order to reduce as much as possible all uncertainties in the predictions. An increasing precision in the measurements of ^4He mass fraction at the level of 10^{-4} requires, for example, a reliability of neutron-proton conversion rates at the same level of precision of all other effects which are relevant for the neutron to proton ratio at the onset of nucleosynthesis [12, 13].

This is the main goal of this thesis.

The physics of BBN is well understood [14, 15]: basically, it can be seen as a nuclear reactor in an expanding box. Therefore nuclear and particle physics and cosmology are the two basic inputs for studying primordial nucleosynthesis. Since BBN involves events

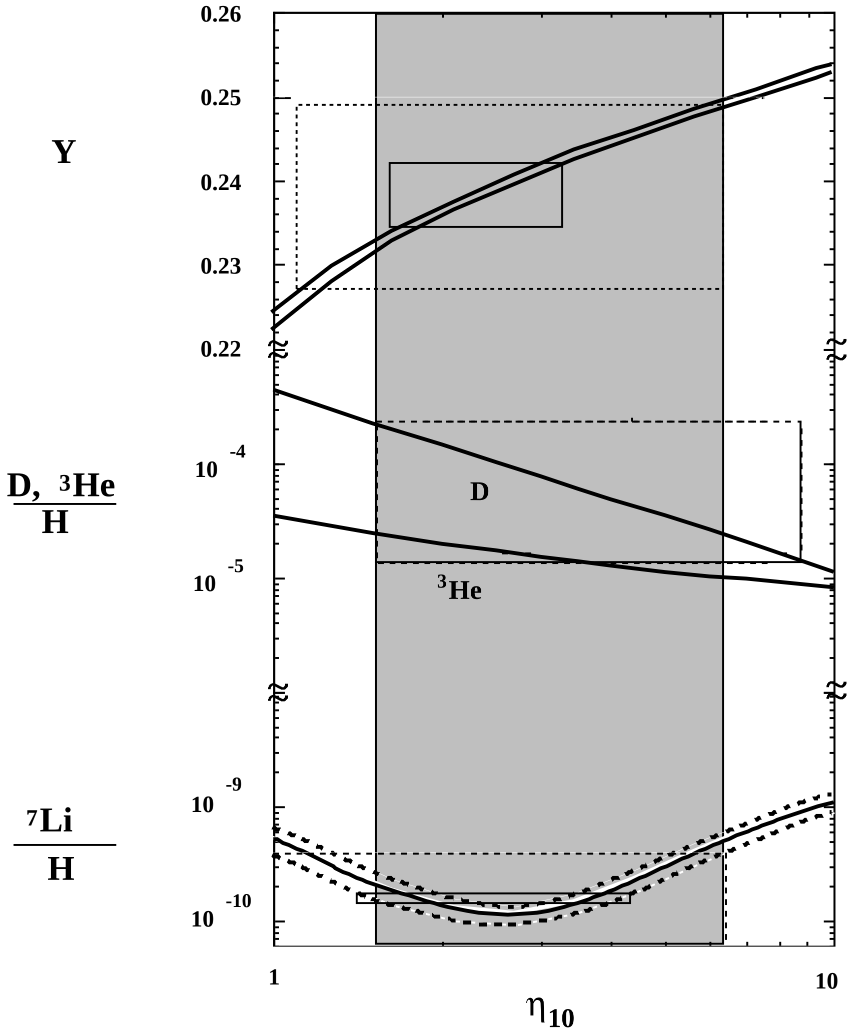

Figure 1: Predicted abundances (solid curves) of primordial ^4He, D, ^3He and ^7Li along with their experimental determination (rectangles) as a function of $\eta_{10} = 10^{10}\eta$. The two curves for ^4He correspond to the 1σ experimental values for the neutron lifetime, while the theoretical uncertainties on ^7Li are as discussed in Ref. [9]. Uncertainties on D and ^3He curves cannot be appreciated on the scale of this figure. The filled zone is the range of η representing the agreement between BBN theory and measurements (taken from [10]).

that occurred at temperatures of order $1\,MeV$, it naturally plays a key role in forging the connection between cosmology and nuclear and particle physics. It is interesting to note how the increasing interaction between particle physics and cosmology has largely resulted from the establishments of "standard models" in both fields which satisfactorily describe all known phenomena. Regarding cosmology, there are of course many possibilities for departures from its standard model [7], e.g. an inhomogeneous nucleon distribution or non zero neutrino chemical potentials. However, recent developments do not motivate such non standard scenarios and moreover they are highly constrained by the observational data. It is therefore reasonable, and we hereafter shall do so, to adopt the standard picture. In our calculations we will also use the standard model of strong and electroweak interactions [16], but it is very intriguing to observe how BBN can constrain new physics beyond the standard $SU(3)\times SU(2)\times U(1)$ model [7]. This is well illustrated by the BBN limit to the number of light neutrino species [17]. The amount of synthesized ^4He strongly depends upon the expansion rate: a faster expansion rate leads to the production of a larger amount of ^4He since nuclear reactions begin earlier when the neutron fraction is higher. The expansion rate itself is determined by the energy density of relativistic particles and the larger the latter, the larger the former. Now, since the energy density increases by adding new neutrino species, this can overproduce ^4He, thus violating the observational evidences. The BBN limit on the number N_ν of light neutrino flavours is close to three, although more work, both observational and theoretical, is still needed. It is impressive and interesting to compare this result with the LEP limit based upon the shape of the Z^0 resonance: $N_\nu = 2.994\pm0.012$ [18]. While it is unlike that the BBN limit will ever achieve such precision, the cosmological and laboratory limits are complementary. The neutrino limit based upon the shape of the Z^0 counts the number of "active" particle species that have a mass smaller than half the Z^0 mass, weighted by their coupling to the Z^0. Differently, BBN constrains the energy density due to any relativistic particle specie around the time of primordial nucleosynthesis and thus is sensitive to any particle species lighter than about $1\,MeV$.

Other several interesting constraints on physics beyond the standard model of elementary particles, coming from BBN considerations, can be obtained [7], but this is not our subject. We only stress the fact that accurate BBN predictions, along with precise experimental observations, greatly helps also our understanding of fundamental physics.

Summarizing, this thesis is devoted to the study of precision effects intervening during primordial nucleosynthesis. Our present goal is to give an estimate of the primeval ^4He mass fraction confident, at least, at the third significant digit (the actual experimental accuracy). The following step is to write down a new numerical BBN code [19] employing our results to further improve light element abundance predictions.

The thesis is organized as follows. Chapters 1 and 2 review standard cosmology and, in particular, primordial nucleosynthesis. The subsequent three chapters are devoted to the calculations of the mentioned precision effects. In particular we discuss the calculation of QED radiative corrected Born rates for the weak reactions fixing the neutron to proton ratio at freeze out, along with the calculation of corrections to this quantities arising from finite nucleon mass and QED thermal plasma effects. Finally, in chapter 6 we summarize our results and give our prediction for the ^4He mass fraction.

Throughout this thesis, unless otherwise specificated, we use natural units in which $\hbar = c = k = 1$.

Chapter 1

The standard cosmology: an overview

The standard cosmological model is based on three observational pillars:

i) the uniform distribution of matter in the Universe on large scales and the isotropic expansion of it that maintains the uniformity;

ii) the existence of a nearly uniform and accurately thermal cosmic background radiation (CBR);

iii) the abundances (relative to hydrogen) of the light elements D, ^{3}He, ^{4}He, ^{7}Li.

As we will see, the validity of the Hubble's expansion law, namely the proportionality between the observed red-shift z (see below) and the distance d from the Earth of a given source [1]

$$H_0\, d \;\simeq\; z \quad . \tag{1.1}$$

through the Hubble constant H_0, out to red-shifts $z \sim 0.2$, supports the general notion of an expanding Universe [20]. The Hubble constant H_0, defining the present expansion rate, is usually parametrized as

$$H_0 \;=\; 100\, h_0 \; Km\, s^{-1}\, Mpc^{-1} \quad , \tag{1.2}$$

where, observationally [21], [22]

$$0.6 \;\leq\; h_0 \;\leq\; 0.8 \quad . \tag{1.3}$$

---

[1] In astronomy, this distance is defined as $d^2 \;=\; \mathcal{L}/(4\pi\mathcal{F})$, with $\mathcal{L}$ the absolute luminosity (energy per unit time produced by the source in its rest frame) and $\mathcal{F}$ the measured energy flux (energy per unit time and surface measured by a detector in the expanding Universe).

The distribution of matter and radiation in such a Universe is observed to be homogeneous and isotropic when averaged on scales exceeding a few hundred Mpc [23]. Instead, the CBR provides a firm evidence of a hot, dense beginning of the Universe itself ("Big Bang"); the spectrum of the CBR is a perfect blackbody, at temperature [24]

$$T_0 \;=\; 2.728 \pm 0.002\,K \quad , \tag{1.4}$$

with deviations that are less than 0.03 %.

Observations of the primordial light element abundances finally provide the complete success of the hot Big Bang model, and they will be discussed in the next chapter.

1.1 Homogeneity and Isotropy

Space-time events in a homogeneous and isotropic Universe are described by the maximally symmetric Robertson-Walker metric which, in the comoving reference frame (defined by the property that an observer at rest in this frame has constant spatial coordinates in time), takes the form [25]

$$ds^2 \;=\; dt^2 \;-\; R^2(t)\left(\frac{dr^2}{1\;-\;kr^2} \;+\; r^2\,d\theta^2 \;+\; r^2\,\sin^2\theta\,d\phi^2\right) \quad , \tag{1.5}$$

where $t \in [0,+\infty)$ is the proper time measured by an observer at rest in the comoving frame, and with $r \in [0,1]$, $\theta \in [0,\pi]$, $\phi \in [0,2\pi]$ the (dimensionless) spherical coordinates in this frame. The parameter k =+1,0,-1 gives the spatial curvature of the Universe. The homogeneity and isotropy of space allows us to describe the dynamics in the space-time in terms of only a quantity (with dimension of a length), the cosmic scale factor $R(t)$, depending on the time t only.

Since, in the Robertson-Walker metric, $R(t)$ is a function of time, the distance between two space points depends on time; if the space described by this metric is expanding or contracting, the motion of a particle is influenced by this expansion/contraction. In fact, let us consider, for example, a particle in free motion with momentum $\mathbf{p_1}$ at time t_1; since the momentum has dimension of an inverse of length, at a later time t_2 the particle momentum will be rescaled by a factor proportional to R^{-1}, that is

$$p_2 \;=\; p_1\,\frac{R(t_1)}{R(t_2)} \quad . \tag{1.6}$$

Furthermore, due to the finite propagation velocity of light signals, in an expanding/contracting Universe it is meaningful to introduce the concept of a "distance to the horizon" $d_H(t)$: for a comoving observer, this is the distance at which a light signal emitted at $t = 0$ reaches him at (or before) time t. If $d_H(t)$ is finite, then there are sources from which light has not yet reached us [26]: a boundary exists (termed "horizon") between the visible Universe and the part of Universe from which light signals have not reached us. The distance $d_H(t)$ can be calculated in the following way: from the isotropy of space, we can consider an observer at $r = 0$ for which $d\theta = d\phi = 0$; hence

$$d_H(t) \;=\; \int_0^{r_H} \sqrt{g_{rr}}\, dr \;=\; R(t) \int_0^{r_H} \frac{dr}{\sqrt{1 - kr^2}} \quad . \tag{1.7}$$

For a light signal $ds^2 = 0$, thus

$$dt' \;=\; R(t') \frac{dr}{\sqrt{1 - kr^2}} \quad , \tag{1.8}$$

and correspondingly

$$d_H(t) \;=\; R(t) \int_0^t \frac{dt'}{R(t')} \quad . \tag{1.9}$$

The explicit form of $d_H(t)$ depends on the expression for $R(t)$ which is determined by the cosmological equations (see next section); however, we note that the behaviour of $R(t)$ near the initial singularity determines the finiteness of $d_H(t)$. In the standard cosmology this is indeed finite and $d_H(t) \sim t$.

Another interesting property of an expanding/contracting Universe is that if at a given point P_1 a photon is emitted with a wavelength λ_1, at a distant point P_0 it will be detected with a different wavelength λ_0. In a space described by the Robertson-Walker metric, on dimensional grounds we have in fact that

$$\frac{\lambda_1}{\lambda_0} \;=\; \frac{R(t_1)}{R(t_0)} \quad . \tag{1.10}$$

The red-shift (or blue-shift) z of a given object is defined as the ratio between the variation in the detected wavelength and the emitted wavelength:

$$z \;=\; \frac{\lambda_0 - \lambda_1}{\lambda_1} \quad . \tag{1.11}$$

From (1.10) we then have

$$1 + z \;=\; \frac{R(t_0)}{R(t_1)} \quad . \tag{1.12}$$

An increase (or decrease) in the cosmic scale factor then leads to a red-shift (or blue-shift) of the light from distant sources. The Hubble law (1.1), relating the distance to a galaxy with the observed red-shift through the Hubble parameter at the present epoch

$$H_0 \; = \; \frac{\dot{R}(t_0)}{R(t_0)} \quad , \tag{1.13}$$

t_0 being the present time, is a direct consequence of the Robertson-Walker metric (its derivation is reported in [4], for example); it is only an approximate relation [27], and corrections are necessary for cosmological large distances. The present age is set by the Hubble time

$$H_0^{-1} \; \simeq \; 9.778 \times 10^9 \, h_0^{-1} \, yr \quad , \tag{1.14}$$

corresponding to a local spatial scale for the Universe

$$H_0^{-1} \; \simeq \; 3000 \, h_0^{-1} \, Mpc \tag{1.15}$$

(Hubble radius).

1.2 Cosmological equations

As anticipated in the previous section, the cosmic scale factor governing the dynamics of the processes in the Universe is determined by the Einstein field equations relating the energy-momentum tensor $T_{\mu\nu}$ to the space-time curvature:

$$R_{\mu\nu} \; - \; \frac{1}{2} R_c \, g_{\mu\nu} \; = \; 8\pi \, G \, T_{\mu\nu} \quad . \tag{1.16}$$

Here $G \; = \; M_P^{-2}$ is the Newton gravitational constant, while $R_{\mu\nu}$ is the Ricci tensor and R_c its trace (the scalar curvature). For a perfect fluid, as the Universe is assumed to be (see the next section), the energy-momentum tensor takes the form

$$T_{\mu\nu} \; = \; - \mathrm{p} \, g_{\mu\nu} \; + \; (\mathrm{p} \, + \, \rho) \; u_\mu \, u_\nu \quad , \tag{1.17}$$

p and ρ being the pressure and energy density respectively, while $u_\mu \; = \; dx_\mu / ds$ is the fluid 4-velocity. In a comoving frame ($u_\mu = (1, \mathbf{0})$), Eq. (1.17) simplifies to

$$T_{\mu\nu} \; = \; \begin{pmatrix} \rho & & & \\ & \mathrm{p} & & \\ & & \mathrm{p} & \\ & & & \mathrm{p} \end{pmatrix} \quad . \tag{1.18}$$

Note that from homogeneity and isotropy of space it follows that ρ and p, as well as R, only depend on the time t. The Ricci tensor for the Robertson-Walker metric is instead given by

$$R_{00} = -3\frac{\ddot{R}}{R} \quad , \qquad R_{0i} = 0 \quad , \tag{1.19}$$

$$R_{ij} = -\left\{ \frac{\ddot{R}}{R} + 2\,\frac{\dot{R}^2}{R^2} + 3\,\frac{k}{R^2} \right\} g_{ij} \quad , \tag{1.20}$$

and

$$R_c = -6\left\{ \frac{\ddot{R}}{R} + \frac{\dot{R}^2}{R^2} + \frac{k}{R^2} \right\} \quad . \tag{1.21}$$

Substituting these expressions in the Einstein equations (1.16), we then obtain the following two independent equations [2]:

$$\left(\frac{\dot{R}}{R}\right)^2 + \frac{k}{R^2} = \frac{8\pi\, G}{3}\,\rho \quad , \tag{1.23}$$

$$\frac{\ddot{R}}{R} = -\frac{4\pi\, G}{3}\,(\rho + 3\mathrm{p}) \quad . \tag{1.24}$$

For both matter and radiation $\rho +$ 3p is positive, thus $\ddot{R}$ is always negative. Since we know that now $\dot{R} > 0$ (the Universe is now expanding), at a given remote (but finite) time t_{BB} in the past we have had that $R(t_{BB}) = 0$; this event is called the "Big Bang", and it is usually chosen as the starting reference time ($t_{BB} = 0$).

In the Eqs. (1.23),(1.24) the energy-momentum conservation equation $D_\nu T^{\mu\nu} = 0$ (D_ν being the covariant derivative in the Robertson-Walker metric) is also contained; in fact, deriving (1.23) with respect to time and substituting (1.24), we get

$$\dot{\rho} = -3\,H\,(\rho + \mathrm{p}) \quad , \tag{1.25}$$

where we have introduced the Hubble parameter (depending on time)

$$H = \frac{\dot{R}}{R} \quad . \tag{1.26}$$

An alternative form of (1.25) is as follows:

$$d\left(\rho R^3\right) = -\,\mathrm{p}\,d\left(R^3\right) \quad , \tag{1.27}$$

---

[2] The equation (1.23) can also be cast in the intriguing form

$$\frac{1}{2}\,v^2 - \frac{G\,M}{R} = -\,\frac{k}{2} \quad , \tag{1.22}$$

with $v = \dot{R}$ and $M = \frac{4}{3}\pi R^3\rho$, showing that the sign of k is deciding about the final destiny of our Universe.

Radiation	p $= \frac{1}{3}\rho$	$\rho \sim R^{-4}$
Matter	p $= 0$	$\rho \sim R^{-3}$
Vacuum	p $= -\rho$	$\rho \sim$ constant

Table 1.1: Equations of state for radiation, matter and vacuum.

expressing just the first law of thermodynamics for the expanding Universe.

Equations (1.23) and (1.25)

$$H^2 = \frac{8\pi G}{3}\rho - \frac{k}{R^2} \quad , \tag{1.28}$$

$$\dot{\rho} = -3H(\rho + \mathrm{p}) \quad , \tag{1.29}$$

are usually considered as the two basic independent equations governing the dynamics of the Universe. They are known as the cosmological Friedmann-Lemaitre equations. Obviously, only two equations are not sufficient to determine the three unknowns $R(t)$, $\rho(t)$, and p(t). The third relation to add to the Friedmann-Lemaitre equations is the equation of state relating pressure and energy density, that can be written as

$$\mathrm{p}(t) = w\,\rho(t) \quad , \tag{1.30}$$

where, for simplicity, we will assume the coefficient w to be time independent. From (1.25) we then have

$$\rho \sim R^{-3(1+w)} \quad . \tag{1.31}$$

The interesting case of radiation (relativistic particles), matter (non relativistic particles) and vacuum are summarized in Table 1.1.

1.2.1 Evolution of the Universe

The evolution of the Universe is determined by the curvature term k/R^2 in (1.28) which is positive, zero or negative if the energy density is greater than, equal to or less than the critical density

$$\rho_c = \frac{3H^2}{8\pi G} \quad , \tag{1.32}$$

respectively, since Eq. (1.28) can equivalently be written as

$$\frac{k}{H^2R^2} = \Omega - 1 \quad , \tag{1.33}$$

with

$$\Omega = \frac{\rho}{\rho_c} \quad . \tag{1.34}$$

For $k = -1$, $\dot{R}^2$ is always strictly positive and $R \to t$ as $t \to \infty$. Instead, for $k = 0$, $\dot{R}^2$ goes to zero as $R \to \infty$ while, for $k = -1$, $\dot{R}^2$ drops to zero at $R_{max} = \sqrt{3/(8\pi G\rho)}$ after which R begins decreasing. Thus $\Omega < 1$ corresponds to an open Universe which will expand forever, $\Omega = 1$ is a flat Universe which will asymptotically expand to infinity while $\Omega > 1$ corresponds to a closed Universe which will eventually recollapse.

The critical density today is (from (1.32))

$$\rho_{c0} = \left(2.999\times10^{-12}\sqrt{h_0}\,GeV\right)^4 = 1.054\times10^{-5}\,h_0^2\,GeV\,cm^{-3} \quad . \tag{1.35}$$

From dynamical measurements of the present energy density in all gravitating matter (and excluding the nowadays negligible contribution of relativistic particles) we deduce [23, 28]

$$\Omega_0 \approx 0.1 \div 1 \quad . \tag{1.36}$$

The present energy of photon background alone is known with a very good accuracy from measurements of the temperature of the cosmic microwave background radiation (1.4), which gives (see sect. 1.3.1)

$$\rho_{\gamma 0} = \frac{\pi^2 T_0^4}{15} \simeq 2.02\times10^{-21}\left(\frac{T_0}{2.73\,K}\right)^4 GeV^4 \quad , \tag{1.37}$$

and then

$$\Omega_{\gamma 0} = \frac{\rho_{\gamma 0}}{\rho_{c0}} \simeq 2.49\times10^{-5}\left(\frac{T_0}{2.73\,K}\right)^4 h_0^{-2} \quad . \tag{1.38}$$

Including the contribution of a primordial background of three massless neutrinos (see sect. 1.4.1) we have

$$\Omega_{R0} = \Omega_{\gamma 0} + \Omega_{\nu 0} \simeq 1.68\,\Omega_{\gamma 0} \simeq 4.18\times10^{-5}\left(\frac{T_0}{2.73\,K}\right)^4 h_0^{-2} \quad . \tag{1.39}$$

Comparing (1.36) with (1.39) we then see that the present Universe is dominated by non relativistic particles; however, as we will see in the next subsection, the evolution to this situation has been highly not trivial.

1.2.2 Driving the expansion

The equation (1.28) for the expansion rate of the Universe can be conveniently normalized to present values of the quantities involved ($R_0 = R(t_0)$, $H_0 = H(t_0)$ and $\Omega_0 = \rho/\rho_{c0}$, t_0 being the present time), obtaining

$$\left(\frac{H}{H_0}\right)^2 = \Omega_0(t) - \frac{k}{H_0^2 R_0^2}\left(\frac{R_0}{R}\right)^2 \quad . \tag{1.40}$$

From Table 1.1 we then see that

$$\Omega_0(t) = \Omega_{R0}(t)\left(\frac{R_0}{R}\right)^4 + \Omega_{M0}(t)\left(\frac{R_0}{R}\right)^3 \tag{1.41}$$

(the pedices $i = R, M$ indicating radiation and matter respectively), where Ω_{i0} themselves are in general functions of time which can be assumed, for simplicity, to be step function -like:

$$\Omega_{i0}(t) = \begin{cases} \Omega_{i0} & t \in [t_i^{in}, t_i^{fin}] \\ \\ 0 & t \notin [t_i^{in}, t_i^{fin}] \end{cases} \quad . \tag{1.42}$$

Thus we get

$$\left(\frac{H}{H_0}\right)^2 = \Omega_{R0}\left(\frac{R_0}{R}\right)^4 + \Omega_{M0}\left(\frac{R_0}{R}\right)^3 - \frac{k}{H_0^2 R_0^2}\left(\frac{R_0}{R}\right)^2 \quad . \tag{1.43}$$

Given the different powers of R for the terms in (1.43) determining the expansion rate, we see that the early Universe ($R << R_0$) was dominated by radiation (RD era), afterwards matter becomes dominating (MD era). The transition between the RD and MD era can be approximately dated back at $R_{EQ} \sim 10^{-4} R_0$. Since in the first stages of evolution of the Universe the curvature term can be neglected, we find that

$$\text{RD era} \qquad \mathrm{H}^2 \sim R^{-4} \tag{1.44}$$

$$\text{MD era} \qquad \mathrm{H}^2 \sim R^{-3} \tag{1.45}$$

and thus, from (1.33),

$$|\Omega - 1| \sim \begin{cases} \frac{R}{R_0} = (1+z)^{-1} & \text{MD era} \\ \\ \frac{R_{EQ}}{R_0}\left(\frac{R}{R_{EQ}}\right)^2 = 10^4\,(1+z)^{-2} & \text{RD era} \end{cases} \quad . \tag{1.46}$$

Note that, apparently, at very earlier epochs the Universe was very nearly critical (of the order of one part over 10^4). However, at these times a period of "inflation" (exponential growth of the expansion) is believed to have occurred [29], but a thorough analysis of this issue is beyond the scope of this thesis.

1.3 Thermodynamics of the Universe

In this section we will study the properties of the Universe considered as a thermodynamic system composed by different species (electrons, photons, neutrinos, nucleons, etc.) which, in the early phases, were to a good approximation in thermodynamic equilibrium, established through rapid interactions. Obviously, coming back to the past, decreasing the cosmic scale factor we have an increase of the temperature. In this thesis we will mainly concern ourselves with cosmological processes occurred during the RD era, thus the discussion is greatly simplified by assuming the Universe as an ideal gas. This assumption is justified by the fact that, as we will see in the next chapter, the particle densities do not usually become high enough for many-body interactions to be important.

1.3.1 Equilibrium thermodynamics

In a gas of a given specie with g_i internal (spin) degrees of freedom and energy $E_i = \sqrt{p^2 + m_i^2}$, *kinetic equilibrium* is established by sufficiently rapid elastic scattering processes; in this case, for an ideal gas, the equilibrium phase-space density is

$$f_i(p) = \left(\exp\left\{\frac{E_i - \mu_i}{T_i}\right\} \pm 1\right)^{-1} \quad , \tag{1.47}$$

where +/- refers to Fermi-Dirac/Bose-Einstein statistics and μ_i is the chemical potential. In general each specie has its own equilibrium temperature T_i, and the entire Universe can be represented as a plasma with different temperatures. However, if several species strongly interact among them, they will reach a mutual chemical equilibrium and a common temperature; this is indeed the situation at early times. As the Universe expands and cools down, some species may start interacting more and more weakly and eventually decouple. As we will see in sect. 1.4, we can consider the photon temperature T_γ as the plasma reference temperature T of the Universe.

In *chemical equilibrium*, established by processes which can create and destroy particles (differently from kinetic equilibrium), the chemical potential is additively conserved. So it is zero for particles such as photons and Z^0 which can be emitted and absorbed in any number and consequently opposite for a particle and its antiparticle which can annihilate into such bosons.

The quantities of interest are the number density, energy density and pressure of a given specie, defined in general as:

$$\begin{aligned} n_i &= g_i \int \frac{d^3\mathbf{p}}{(2\pi)^3}\, f_i(p) \quad , & (1.48)\\ \rho_i &= g_i \int \frac{d^3\mathbf{p}}{(2\pi)^3}\, E_i\, f_i(p) \quad , & (1.49)\\ \mathrm{p}_i &= g_i \int \frac{d^3\mathbf{p}}{(2\pi)^3}\, \frac{|\mathbf{p}|^{\mathbf{2}}}{3E_i}\, f_i(p) \quad . & (1.50) \end{aligned}$$

In kinetic equilibrium the phase-space density $f_i(p)$ is given in (1.47), and these quantities evolve according to temperature.

For non relativistic species ($T_i \ll m_i$) we have (for both Fermi-Dirac and Bose-Einstein statistics)

$$\begin{aligned} n_i &\simeq g_i \left(\frac{m_i T_i}{2\pi}\right)^{\frac{3}{2}} e^{-\frac{m_i-\mu_i}{T}} \quad , & (1.51)\\ \rho_i &\simeq n_i \left(m_i + \frac{3}{2}T_i\right) \quad , & (1.52)\\ \mathrm{p}_i &\simeq n_i\, T_i \ll \rho_i & (1.53) \end{aligned}$$

(and so we recover Boltzmann statistics). The average energy per particle $< E_i >\equiv \rho_i/n_i$ and net number density are instead given by

$$\begin{aligned} < E_i > &\simeq m_i + \frac{3}{2}T_i \quad , & (1.54)\\ n_{i+} - n_{i-} &\simeq 2g_i \left(\frac{m_i T_i}{2\pi}\right)^{\frac{3}{2}} \sinh\frac{\mu_i}{T}\, e^{-\frac{m_i}{T}} & (1.55) \end{aligned}$$

(assuming $\mu_{i+} = -\mu_{i-} \equiv \mu_i$) .

For relativistic species ($T_i \gg m_i$) we obtain:

- non degenerate case ($T_i \gg \mu_i$)

$$\begin{aligned} n_i &\simeq \begin{cases} \frac{3}{4}\;\; \frac{1}{\pi^2}\,\zeta(3)\, g_i\, T_i^3 & FD \\ \\ \frac{1}{\pi^2}\,\zeta(3)\, g_i\, T_i^3 & BE \end{cases} & (1.56)\\ \rho_i &\simeq \begin{cases} \frac{7}{8}\;\; \frac{\pi^2}{30}\, g_i\, T_i^4 & FD \\ \\ \frac{\pi^2}{30}\, g_i\, T_i^4 & BE \end{cases} & (1.57)\\ \mathrm{p}_i &\simeq \frac{1}{3}\,\rho_i & (1.58)\\ < E_i > &\simeq \begin{cases} \frac{7}{6}\;\; \frac{\pi^4}{30}\,\zeta(3)\, T_i \simeq 3.15\, T_i & FD \\ \\ \frac{\pi^4}{30}\,\zeta(3)\, T_i \simeq 2.70\, T_i & BE \end{cases} & (1.59)\\ n_{i+} - n_{i-} &\simeq 0 & (1.60) \end{aligned}$$

- weak degeneracy ($\mu_i < 0$ [3], $|\mu_i| < T_i$) [4]

$$\begin{aligned} n_i &\simeq \frac{1}{\pi^2}\, g_i\, T_i^3\, e^{\frac{\mu_i}{T_i}} && (1.61)\\ \rho_i &\simeq 3\,\frac{1}{\pi^2}\, g_i\, T_i^4\, e^{\frac{\mu_i}{T_i}} && (1.62)\\ \mathrm{p}_i &\simeq \frac{1}{3}\,\rho_i && (1.63)\\ < E_i > &\simeq 3\, T_i && (1.64)\\ n_{i+} - n_{i-} &\simeq 2\,\frac{1}{\pi^2}\, g_i\, T_i^3\, \sinh\frac{\mu_i}{T_i} && (1.65) \end{aligned}$$

- degenerate case ($T_i \ll \mu_i$)

$$\begin{aligned} n_i &\simeq \frac{1}{6\pi^2}\, g_i\, \mu_i^3 && (1.66)\\ \rho_i &\simeq \frac{1}{8\pi^2}\, g_i\, \mu_i^4 && (1.67)\\ \mathrm{p}_i &\simeq \frac{1}{3}\,\rho_i && (1.68)\\ < E_i > &\simeq \frac{3}{4}\,\mu_i && (1.69)\\ n_{i+} - n_{i-} &\simeq \frac{1}{6\pi^2}\, g_i\, T_i^3 \left(\left(\frac{\mu_i}{T_i}\right)^3 + \pi^2\left(\frac{\mu_i}{T_i}\right)\right) \quad . && (1.70) \end{aligned}$$

In the relations above $\zeta(x)$ is the Riemann zeta-function, and $\zeta(3) \simeq 1.2021....$

Another important quantity for the evolution of a thermodynamic system is its entropy S which, for thermal equilibrium, is defined by the second law of thermodynamics:

$$T\, dS = \delta Q \quad . \tag{1.71}$$

Assuming zero chemical potentials, for a given comoving volume element ($V = R^3$) we have

$$T_i\, dS_i = d(\rho_i V) + \mathrm{p}_i dV = d((\rho_i + \mathrm{p}_i)\, V) - V\, d\mathrm{p}_i \tag{1.72}$$

(note that ρ_i and p_i are the energy density and pressure of species at equilibrium). The entropy function is subject to the integrability condition

$$\frac{\partial^2 S_i}{\partial T_i\, \partial V} = \frac{\partial^2 S_i}{\partial V\, \partial T_i} \quad , \tag{1.73}$$

---

[3] For bosons with $\mu_i > 0$ Bose condensation may take place

[4] The following results hold for both FD and BE

which explicitly implies that

$$-\frac{\mathrm{p}_i + \rho_i}{T_i^2} + \frac{1}{T_i}\frac{d\mathrm{p}_i}{dT_i} + \frac{1}{T_i}\frac{d\rho_i}{dT_i} = \frac{1}{T_i}\frac{d\rho_i}{dT_i} \quad , \tag{1.74}$$

or

$$d\mathrm{p}_i = \frac{\mathrm{p}_i + \rho_i}{T_i}\, dT_i \quad . \tag{1.75}$$

This relation is in fact verified by (1.49), (1.50) with the equilibrium distribution (1.47). Substituting in (1.72) we then have

$$dS_i = d\left(V\,\frac{\mathrm{p}_i + \rho_i}{T_i}\right) \quad , \tag{1.76}$$

from which we found that the entropy per comoving volume ($V \propto R^3$) is defined, up to an additive constant, by

$$S_i = V\,\frac{\mathrm{p}_i + \rho_i}{T_i} = R^3\,\frac{\mathrm{p}_i + \rho_i}{T_i} \quad . \tag{1.77}$$

Note that from the first law of thermodynamics (1.27) and (1.72)

$$dS_i = 0 \quad , \tag{1.78}$$

i.e. in thermal equilibrium [5] the entropy in the comoving volume is conserved.

It is also useful to define the entropy density in the comoving volume,

$$s_i \equiv \frac{S_i}{V} = \frac{\mathrm{p}_i + \rho_i}{T_i} \quad , \tag{1.79}$$

which, from (1.78), varies as

$$s_i \propto R^{-3} \quad . \tag{1.80}$$

The total number of particles of a given specie in the comoving volume $N_i = V n_i = R^3 n_i$ is thus proportional to n_i/s_i,

$$N_i \propto \frac{n_i}{s_i} \quad . \tag{1.81}$$

Finally, if chemical potentials are not zero, Eq. (1.71) specializes into

$$T_i\, dS_i = d(\rho_i V) + \mathrm{p}_i dV - \mu_i\, d(n_i V) \quad , \tag{1.82}$$

and then the entropy is now given by

$$S_i = R^3\,\frac{\mathrm{p}_i + \rho_i - \mu_i n_i}{T_i} \quad , \tag{1.83}$$

which replaces Eq. (1.77).

---

[5] During phase transitions entropy is not conserved, in general.

1.3.2 Energy density and pressure in the Universe

In the Friedmann-Lemaitre equations (1.28), (1.29), assuming a perfect fluid, the total energy density ρ and pressure p of the cosmological fluid are involved; let us evaluate these quantities considering all the particles in thermal equilibrium in the Universe and express them in terms of photon temperature $T_\gamma \equiv T$:

$$\rho = T^4 \sum_i \left(\frac{T_i}{T}\right)^4 \frac{g_i}{2\pi^2} \int_{x_i}^{\infty} \frac{(u_i^2 - x_i^2)^{1/2}\, u_i^2\, du_i}{\exp\{u_i - y_i\} \pm 1} \quad , \tag{1.84}$$

$$\mathrm{p} = T^4 \sum_i \left(\frac{T_i}{T}\right)^4 \frac{g_i}{6\pi^2} \int_{x_i}^{\infty} \frac{(u_i^2 - x_i^2)^{3/2}\, du_i}{\exp\{u_i - y_i\} \pm 1} \quad , \tag{1.85}$$

where the sums run over all species and $u_i = E_i/T_i$, $x_i = m_i/T_i$, $y_i = \mu_i/T_i$. Note that from (1.51), (1.52), non relativistic particles contribute negligibly to the energy density in the radiation dominated era, since their energy density is exponentially suppressed with respect to the case of relativistic particles; thus we can neglect the contribution of non relativistic species in the sums above. Assuming all species non degenerate, we then get

$$\rho \simeq \frac{\pi^2}{30} g_* T^4 \quad , \tag{1.86}$$

$$\mathrm{p} \simeq \frac{1}{3}\rho = \frac{\pi^2}{90} g_* T^4 \quad , \tag{1.87}$$

where in g_* contribute only the relativistic degrees of freedom

$$g_* \simeq \sum_B g_i \left(\frac{T_i}{T}\right)^4 + \frac{7}{8} \sum_F g_i \left(\frac{T_i}{T}\right)^4 \tag{1.88}$$

($B =$ bosons, $F =$ fermions). Note that g_* is in general a function of T, since the number of degrees of freedom becoming relativistic at a given temperature depends on T itself. Moreover, at a given time, not all (relativistic) particles in the bath are in equilibrium at a common temperature T. A particle will be in kinetic equilibrium with the background plasma (that is $T_i = T$) only as long as its interaction with the plasma is fast enough; although the conditions for this to occur will be discussed in sect. 1.4, it is obvious that these involve a comparison between the particle interaction and the expansion rate H.

1.3.3 Total entropy density in the comoving volume

From (1.79) and (1.86), (1.87) we can evaluate the total entropy density in the comoving volume, obtaining

$$s = \frac{2\pi^2}{45} g_{*s} T^3 \quad , \tag{1.89}$$

with

$$g_{*s} \simeq \sum_B g_i \left(\frac{T_i}{T}\right)^3 + \frac{7}{8} \sum_F g_i \left(\frac{T_i}{T}\right)^3 \quad , \tag{1.90}$$

and the sums again run only over the relativistic degrees of freedom in equilibrium (in the considered approximation). Note that s in (1.89) can be parametrized in terms of the photon number density as follow

$$s = \frac{\pi^4}{45\zeta(3)} g_{*s}\, n_\gamma \simeq 1.80\, g_{*s}\, n_\gamma \quad . \tag{1.91}$$

From entropy conservation we can now obtain the scaling law relating the cosmic scale factor with the temperature; in fact from (1.78) and (1.89) we get

$$T \sim g_{*s}^{-1/3} R^{-1} \quad . \tag{1.92}$$

We stress that if g_{*s} depends on T, then the adiabatic invariant $RT = const.$ for pure expansion does not hold.

1.3.4 Decoupling

Non equilibrium phenomena are properly described by the Boltzmann equation for the phase space distribution functions of the given species involved in them. Such description is reported in appendix A. Here we make a very simple and general analysis of non equilibrium phenomena occurring during the evolution of the Universe.

A specie i is said to *decouple* at a temperature T_D^i (corresponding to a given R_D and time t_D) when it goes out of equilibrium with the background plasma. The conditions for this to occur will be considered in sect. 1.4. Of course no particle is ever truly decoupled since there are always some residual interactions with the bath, but it is a convenient assumption to consider that a specie decouples at a given temperature T_D^i.

Let us first consider species that are relativistic at decoupling ($m_i < T_D^i$) [6]. In this case the distribution at decoupling results to be the equilibrium one:

$$f_i(p, T_D^i) = \left(\exp\left\{\frac{E_i}{T_D^i}\right\} \pm 1\right)^{-1} \quad . \tag{1.93}$$

Subsequently the decoupled i particles will expand freely without interactions, hence their number in a comoving volume is conserved and their thermodynamical quantities are functions of the scale factor R alone. Although non interacting, after decoupling their phase space distribution will retain the equilibrium form as long as the particles remain relativistic, since from (1.6) we have

---

[6] For simplicity we consider only the non degenerate case

$$E_i(t_D) \;=\; E_i\left(\frac{R}{R_D}\right) \quad , \tag{1.94}$$

and thus for $t \geq t_D$

$$f_i(p, T_i \leq T_D^i) \;=\; \left(\exp\left\{\frac{E_i R}{T_D^i R_D}\right\} \pm 1\right)^{-1} \;=\; \left(\exp\left\{\frac{E_i}{T_i}\right\} \pm 1\right)^{-1} \quad . \tag{1.95}$$

This is because of the adiabatic invariant (for pure expansion)

$$T_i \;=\; T_D^i\left(\frac{R_D}{R}\right) \;\sim R^{-1} \quad . \tag{1.96}$$

Initially the temperature T_i exactly follows the photon temperature but, as the Universe cools below some mass thresholds, the corresponding massive particles will become non relativistic and annihilate. This will heat the photons and other interacting particles but not the decoupled i particles, so that T_i will drop below T and consequently n_i/n_γ will decrease below its value at decoupling.

For species that are non relativistic at decoupling ($m_i \gg T_D^i$), (1.93) continues to be valid and after decoupling the phase space distribution will again retain its equilibrium form, but now $E_i(t_D) \simeq p_D^2/2m_i$ and from (1.6) we have

$$E_i(t_D) \;=\; E_i\left(\frac{R}{R_D}\right)^2 \quad , \tag{1.97}$$

thus for $t \geq t_D$

$$f_i(p, T_i \leq T_D^i) \;=\; \left(\exp\left\{\frac{E_i R^2}{T_D^i R_D^2}\right\} \pm 1\right)^{-1} \;=\; \left(\exp\left\{\frac{E_i}{T_i}\right\} \pm 1\right)^{-1} \quad , \tag{1.98}$$

where

$$T_i \;=\; T_D^i\left(\frac{R_D}{R}\right)^2 \;\sim R^{-2} \quad . \tag{1.99}$$

From the discussion above it is then clear that ultrarelativistic and non relativistic species retain their equilibrium distribution after decoupling with temperatures varying as in (1.96) or (1.99). This is no longer true for species with intermediate energy at decoupling, $T_D^i \sim m_i$. In fact for these we have

$$\frac{E_i(t_D)}{T_D^i} \;=\; \frac{1}{T_D^i}\sqrt{p_D^2 + m_i^2} \;=\; \frac{1}{T_D^i}\sqrt{\left(\frac{R}{R_D}\right)^2 p^2 + m_i^2} \;\equiv\; \frac{E_i}{T_i} \quad , \tag{1.100}$$

which “defines” a momentum dependent temperature, indicating thus a non equilibrium distribution.

1.3.5 Time - temperature relationship

The useful relationship between the time t and the background (photon) temperature T in the radiation dominated era can be obtained straightforwardly by integrating the Friedmann-Lemaitre equations by means of entropy conservation. In fact,

$$t \; = \; \int_0^{R(t)} \frac{1}{H} \frac{dR}{R} \quad , \tag{1.101}$$

by using the Eq. (1.28) (neglecting the curvature term in the RD era) and (1.86), giving

$$H \; \simeq \; \sqrt{\frac{4\pi^3}{45 M_P^2}} \, g_*^{1/2} \, T^2 \quad , \tag{1.102}$$

and entropy conservation (1.78) with Eq. (1.89),

$$- \, 3 \, \frac{dR}{R} \; = \; 3 \, \frac{dT}{T} \; + \; \frac{dg_{*s}}{g_{*s}} \quad , \tag{1.103}$$

we find

$$t \; = \; - \sqrt{\frac{45 M_P^2}{4\pi^2}} \int_0^T g_*^{-1/2} \left(1 \; + \; \frac{1}{3} \, \frac{T}{g_{*s}} \, \frac{dg_{*s}}{dT} \right) \frac{dT}{T^3} \quad . \tag{1.104}$$

During the periods when both g_* and g_{*s} are approximately constant (i.e. away from phase transition and mass thresholds where relativistic degrees of freedom change) the relation (1.104) simplifies to

$$t \; \simeq \; 2.42 \, g_*^{-1/2} \left(\frac{1 \, MeV}{T} \right)^2 \; sec \tag{1.105}$$

or, quite approximately, $t(sec) \sim T^{-2}(MeV)$.

1.4 Thermal evolution of the Universe

The cosmological model of Friedmann-Lemaitre, as described in the previous sections, does not allow a Universe in thermal equilibrium since, in this case, the Universe itself would be stationary, which is not the case. However, sufficiently away from the Big Bang event, we can nevertheless approximate the evolution of the Universe as made of several subsequent phases of (different) thermal equilibrium with temperature T mainly varying as R^{-1}. Thermal equilibrium is realized if the reactions between the particles in the heat bath take place very rapidly compared with the expansion rate, set by H. Thus denoting with $\Gamma = n_i < \sigma v >$ the thermal average of the given scattering reaction rate (σ and v being the cross section and the particle velocity, respectively), the (approximate) condition for having equilibrium is given by [32]

$$\Gamma \gtrsim H \quad . \tag{1.106}$$

Of course the opposite condition $\Gamma \lesssim H$ is not a sufficient one for the exit from the equilibrium since, as we have seen, for example, a relativistic low interacting specie maintain its equilibrium distribution but with $T \sim R^{-1}$. Nevertheless the decoupling temperature T_D, as used above, is defined by

$$\Gamma(T_D) = H(T_D) \quad . \tag{1.107}$$

The correct way of proceeding is to solve the Boltzmann transport equations for the given specie (see Appendix A), but here we are interested in a semi-quantitative discussion, and the criteria above fit well.

The scattering rate depends on the particular interaction experienced by the particles, while (in the RD era) the expansion rate is approximately

$$H \sim \frac{T^2}{M_P} \quad . \tag{1.108}$$

For interactions mediated by massless gauge bosons (for example photons or $W^{\pm}$,Z^0 before the electroweak phase transition) there is no particular mass parameter, so that for reactions of the type $a + b \rightarrow c + d$ the cross section is approximately given by $< \sigma > \sim \alpha^2 T^{-2}$, α being a dimensionless coupling constant. Thus, for example, for relativistic particles in the radiation dominated era (and $n \sim T^3$) we have

$$\Gamma \sim \alpha^2 T \quad . \tag{1.109}$$

Hence for this type of interactions the decoupling temperature is set by $T_D \sim \alpha^2 M_P$ and for $T \lesssim \alpha^2 M_P$ equilibrium is established, while for $T \gtrsim \alpha^2 M_P$ the reaction rates take place slowly (they are *frozen out*).

For interactions mediated by gauge bosons with mass M_X we now have $< \sigma > \sim G_X^2 T^2 \sim \alpha^2 M_X^{-4} T^2$ and

$$\Gamma \sim \frac{\alpha^2 T^5}{M_X^4} \quad . \tag{1.110}$$

In this case the decoupling temperature results $T_D \sim (M_X^4/\alpha^2 M_P^2)^{1/3}$ and for temperature above this (but below M_X) equilibrium is maintained, while for $T \lesssim T_D$ the reactions are frozen out.

In practice, apart from the massless neutrinos (whose decoupling will be studied below), all particles in the Standard Model of elementary particles are strongly coupled to the thermal plasma (of $e^\pm, \gamma$) while they are relativistic. This is why we can reliably describe the evolution only in terms of the 'plasma' (photon) temperature T and neutrino temperature T_ν. Thus the thermal history of the Universe, as pictorially reported in table 1.2, can be fairly reconstructed reliably back to the Fermi scale but, with some cautions, also nearly up to the GUT scale. This happens because of the dilute RD plasma approximation, in which non relativistic particles of plasma are (forced) in equilibrium with the relativistic species with negligible abundances. Some uncertainties arise, however, when the ideal gas approximation breaks down, that is at phase transitions associated with symmetry breaking and at very high temperatures, where equilibrium is not achieved.

1.4.1 Neutrino decoupling

The above discussion can be interestingly illustrated by the example of the decoupling of (massless) neutrinos. They are maintained in equilibrium by reaction such as $\nu\overline{\nu} \to e^+e^-$, $\nu e \to \nu e$ and so on, whose averaged cross sections are of the order of $< \sigma > \sim G_F^2 T^2$, where G_F is the Fermi coupling constant. From (1.107), (1.108), (1.110) we then find the neutrino decoupling temperature

$$T_D^\nu \sim 1\, MeV \tag{1.111}$$

(a more careful estimate of the cross sections [33, 34] gives $T_D^{\nu_\mu,\nu_\tau} \simeq 3.5\, MeV$ and $T_D^{\nu_e} \simeq 2.3\, MeV$, the higher decoupling temperature of ν_μ, ν_τ depending on the fact that they interact only through weak neutral current, while for ν_e there is also a charged current contribution). Thus above $\sim 1\, MeV$ neutrinos are in equilibrium with the plasma of photons with $T_\nu = T$ and (from (1.56)) $n_\nu = (3/4) n_\gamma$, afterwards they decouple from the plasma and their temperature T_ν scales approximately as R^{-1}. Subsequently, as the temperature drops below $\sim 0.5\, MeV$, e^+ and e^- annihilate, heating the photons but not the decoupled neutrinos. In these three phases we have respectively

$$g_*^{(1)} \;=\; g_*(T \gtrsim T_D^\nu) \;=\; 2 \,+\, \frac{7}{8}(4 \,+\, 3{\times}2) \;=\; \frac{43}{4} \quad , \tag{1.112}$$

$$g_*^{(2)} \;=\; g_*(m_e \lesssim T \lesssim T_D^\nu) \;=\; 2 \,+\, \frac{7}{8}4 \;=\; \frac{11}{2} \quad , \tag{1.113}$$

$$g_*^{(3)} \;=\; g_*(T \lesssim m_e) \;=\; 2 \quad . \tag{1.114}$$

The evolution of the neutrino temperature through the period of $e^\pm$ annihilation can be easily computed by entropy conservation. Note that from (1.78) the entropy of each specie in equilibrium in the comoving volume is conserved but, in the present case, also the neutrino entropy after their decoupling is conserved since, after decoupling, the total neutrino number in the comoving volume does not change anymore (assuming stable neutrinos). Thus from the conservation of the total entropy $S = S_I + S_\nu$ and neutrino entropy S_ν, it follows that also the entropy S_I associated to the species still interacting [15], given approximately by (see (1.91), (1.89))

$$S_I \;\sim\; g_*\, N_\gamma \;\sim\; g_*\, R^3\, T^3 \quad , \tag{1.115}$$

is conserved, i.e.

$$S_I^{(2)} \;=\; S_I^{(3)} \quad , \tag{1.116}$$

implying, from (1.113), (1.114),

$$N_\gamma^{(3)} \;=\; \frac{11}{4}\, N_\gamma^{(2)} \quad , \tag{1.117}$$

$$(R\,T)^{(3)} \;=\; \left(\frac{11}{4}\right)^{\frac{1}{3}} (R\,T)^{(2)} \quad . \tag{1.118}$$

However, $(R\,T)^{(3)} = (R\,T_\nu)^{(2)} = const. = (R\,T_\nu)^{(3)}$ (since $T_\nu \sim R^{-1}$), for which, after $e^\pm$ annihilation

$$\frac{T}{T_\nu} \;\simeq\; \left(\frac{11}{4}\right)^{\frac{1}{3}} \quad . \tag{1.119}$$

Note that after $e^\pm$ annihilation there are no other relativistic species that can become non relativistic (altering the effective degrees of freedom) so that (1.119) is just the relation between the present values of γ and ν temperature, as well as (1.117) relates the present number of γ to that preceding $e^\pm$ annihilation. Furthermore, we also have from (1.117)

$$\left(\frac{n_\nu}{n_\gamma}\right)^{(3)} \;=\; \frac{4}{11}\left(\frac{n_\nu}{n_\gamma}\right)^{(2)} \;=\; \frac{4}{11} \times \frac{3}{4} \;=\; \frac{3}{11} \quad . \tag{1.120}$$

From this value of T till present days, neutrinos remain relativistic and therefore continue to retain their equilibrium distribution; hence the degrees of freedom characterizing the present energy density and entropy (γ + 3 ν) are given by

$$\begin{aligned} g_*^0 &= 2 + \frac{7}{8}\,(3{\times}2)\left(\frac{4}{11}\right)^{\frac{4}{3}} \simeq 3.36 && (1.121) \\ g_{*s}^0 &= 2 + \frac{7}{8}\,(3{\times}2)\left(\frac{4}{11}\right) = \frac{43}{11} && (1.122) \end{aligned}$$

from which we deduce, for example, ($T \simeq 2.73\,K$)

$$\begin{aligned} n_\gamma^0 &= \frac{2\zeta(3)}{\pi^2}\,T^3 \simeq 422\,cm^{-3} && (1.123) \\ s_\gamma^0 &= \frac{2\pi^2}{45}\,g_{*s}^0\,T^3 \simeq 2970\,cm^{-3} && (1.124) \\ \rho_R^0 &= \frac{\pi^2}{30}\,g_*^0\,T^4 \simeq 8.09{\times}10^{-34}\,g\,cm^{-3} && (1.125) \\ \Omega_R^0\,h_0^2 &\simeq 4.31{\times}10^{-5} \quad . && (1.126) \end{aligned}$$

The present quantities related to neutrinos are obtained from

$$\begin{aligned} n_\nu^0 &= \frac{3}{11}\,n_\gamma^0 && (1.127) \\ T_\nu^0 &\simeq 1.96\,K \quad . && (1.128) \end{aligned}$$

A more careful analysis of the T_ν - T relation is conducted in appendix B, where we report the generalization of Eq. (1.119).

Table 1.2: History of the Universe.

Time	Temperature	Event	Particle content
today	$T \simeq 2.73\,K$		γ + 3 decoupled ν
$t \sim 10^{17}\,s$	$T \sim 10^{-2}\,eV$	Galaxy formation	”
$t \sim 10^{13}\,s$	$T \sim 1\,eV$	Matter-Radiation decoupling Atom formation	”
$t \sim 10^{11}\,s$	$T \sim 10\,eV$	$\rho_{matter} \sim \rho_{radiation}$ Structure formation	”
$t \sim 10^{4}\,s$	$T \sim 10^{4}\,eV$	Planck spectrum established	”
	$T \sim m_e$		add $e^{\pm}$
$t \sim 1\,s$	$T \sim 1\,MeV$	Light element nucleosynthesis	”
	$T \sim 2 \div 3\,MeV$		νs become interacting
	$T \sim m_\mu$		add $\mu^{\pm}$
	$T \sim m_\pi$		add $\pi^{\pm}$, π^0
$t \sim 10^{-6}\,s$	$T \sim 150 \div 400\,MeV$	Quark-hadron transition	
	$T \sim m_s$		$\gamma, 3\nu, e^{\pm}, \mu^{\pm}$ $u, \overline{u}, d, \overline{d}, s, \overline{s}, gluons$
	$T \sim m_c$		add $c, \overline{c}$
	$T \sim m_\tau$		add $\tau^{\pm}$
	$T \sim m_b$		add $b, \overline{b}$
	$T \sim m_{W,Z}$		add $W^{\pm}, Z^0$
	$T \sim m_t$		add $t, \overline{t}$
$t \sim 10^{-11}\,s$	$T \sim 300\,GeV$	Electroweak phase transition	add H^0
$t \sim 10^{-34}\,s$	$T \sim 10^{15}\,GeV$	GUT symmetry breaking Inflation	add X, Y
$t \sim 10^{-43}\,s$	$T \sim 10^{19}\,GeV$	Quantum gravity	?

Chapter 2

Primordial Nucleosynthesis

2.1 Preliminaries

During about the first 20 minutes in the evolution of the Universe, conditions were favourable for the synthesis of (significant abundances of) light nuclides, such as D, ^3H, ^3He, ^4He, ^7Li, ... The onset of nuclear reactions which build up the light nuclei takes place slightly after the decoupling of the weak interactions (see table 1.2) which keep neutron and proton in chemical equilibrium. This is a necessary step since, as long as free nucleons are in equilibrium, the (equilibrium) abundances of all bound nuclei are quite negligible, due to the very high value of the entropy per nucleon ($s/n_N \sim 10^{10}$).

Introducing the subject, we will start with some definitions and comments. The number density n_A of a given nuclear specie (Z, A) has been defined in (1.48) and, since the specie is non relativistic, it is given by the expression (1.51):

$$n_A \simeq g_A \left(\frac{m_A T}{2\pi} \right)^{\frac{3}{2}} e^{-\frac{m_A - \mu_A}{T}} \quad . \tag{2.1}$$

The baryon number (density) n_B is the total number of nucleons (bound or free) in the comoving volume:

$$n_B = \sum_A A \, n_A \quad . \tag{2.2}$$

It is also useful to introduce the dimensionless parameter

$$\eta = \frac{n_B}{n_\gamma} \quad , \tag{2.3}$$

which measures the baryon to photon number ratio.

The mass fraction X_A of a given specie is instead defined as [1]

$$X_A = \frac{A n_A}{n_B} \tag{2.4}$$

and verifies the normalization condition

$$\sum_A X_A = 1 \quad . \tag{2.5}$$

Finally, the abundance Y_A of a nuclide relative to hydrogen is

$$Y_A = \frac{n_A}{n_H} \quad , \tag{2.6}$$

and, in terms of this, the mass fraction can be also expressed as

$$X_A = \frac{A Y_A}{\sum_A A Y_A} \quad . \tag{2.7}$$

In chemical equilibrium, the parameter μ_A in (2.1) is given by

$$\mu_A = Z\,\mu_p + (A - Z)\,\mu_n \quad , \tag{2.8}$$

where μ_p, μ_n are the proton and neutron chemical potential, respectively. In terms of the quantities of the constituent nucleons, the number density n_A can therefore be written as

$$n_A = g_A\,\frac{A^{\frac{3}{2}}}{2^A}\left(\frac{2\pi}{m_N T}\right)^{\frac{3}{2}(A-1)} n_p^Z\, n_n^{A-Z}\, e^{\frac{B_A}{T}} \quad , \tag{2.9}$$

where m_N is the nucleon mass and

$$B_A = Z\,m_p + (A - Z)\,m_n - m_A \tag{2.10}$$

is the binding energy of the given nuclear specie (Z, A). From (2.9) and (1.56) (applied to photons) we can then deduce the following formula for the mass fraction in terms of the nucleon quantities and the η parameter:

$$X_A = \left(\frac{\zeta(3)}{\sqrt{8\pi}}\right)^{A-1} \frac{g_A}{2}\,A^{\frac{5}{2}}\left(\frac{T}{m_N}\right)^{\frac{3}{2}(A-1)} \eta^{A-1}\,X_p^Z\,X_n^{A-Z}\,e^{\frac{B_A}{T}} \quad . \tag{2.11}$$

From (2.9) or (2.11) we then see that the greater is the binding energy of a given specie, the larger is its abundance (though, of course, this is not the only condition for having an appreciable amount of a nuclide). In table 2.1 we report the values of the binding energy of light nuclides relevant for nucleosynthesis.

---

[1] In many papers, the mass fraction for the primordial ^4He is usually denoted with Y.

Table 2.1: Binding energies (in KeV) of light nuclides (data taken from [35]).

n	0.0	^{11}B	76204.800 ± 0.421
p	0.0	^{11}C	73439.899 ± 0.952
D	2224.573 ± 0.002	^{12}B	79575.205 ± 1.400
^{3}H	8481.821 ± 0.004	^{12}C	92161.753 ± 0.014
^{3}He	7718.058 ± 0.002	^{12}N	74041.317 ± 1.000
^{4}He	28295.673 ± 0.005	^{13}C	97108.065 ± 0.016
^{6}Li	31994.564 ± 0.475	^{13}N	94105.267 ± 0.270
^{7}Li	39244.526 ± 0.473	^{14}C	105284.507 ± 0.019
^{7}Be	37600.358 ± 0.472	^{14}N	104658.628 ± 0.016
^{8}Li	41277.328 ± 0.488	^{14}O	98733.236 ± 0.076
^{8}B	37737.813 ± 1.107	^{15}N	115491.930 ± 0.019
^{9}Be	30258.837 ± 62.471	^{15}O	115955.627 ± 0.503
^{10}B	64750.700 ± 0.370	^{16}O	127619.336 ± 0.019

2.2 Observed primordial abundances

Primordial abundances of light elements are, in general, significantly altered by nuclear processing in stars; hence, the deduction of the primordial abundances from the ones observed today is very difficult and, in some sense, is always dependent by the chemical evolution model.

Primordial D is easily destroyed by (p, γ) reactions in stars where the temperature is greater than $\sim 6{\times}10^{5}\,{}^{o}K$; it can be, furthermore, converted in ^{3}He which is, however, also burned. Instead ^{4}He grows in abundance with time: throughout stellar evolution, a star becomes more and more enriched in ^{4}He and, through stellar mixing and mass loss, the interstellar gas can increase its content in ^{4}He. Finally, ^{7}Li is destroyed by nuclear reactions with protons in low mass stars, but it is nevertheless produced in supernovæ, red giant interiors, supermassive objects, etc.

We will shortly review the actual experimental situation for the light element abundances.

2.2.1 D

Deuterium present in stellar interior is destroyed by the energy-generating reactions; in fact, it has not been detected in any star . Nevertheless, there are accurate data from giant planets in the solar system [36] and from the local interstellar medium (ISM) [37].

Since there are no known astrophysical sources of D [38], a firm lower bound to the primordial abundance from the lowest observed one can be obtained

$$\frac{D}{H} > 1.1{\times}10^{-5} \quad . \tag{2.12}$$

Other estimates involve models of galactic chemical evolution to infer the pre-galactic abundance in D from those actually present in the ISM.

Deuterium has also been observed by many authors in the spectra of high red-shift quasar absorption systems (QAS) [39], [40], [41]. In principle these measurements would be capable of determining the primordial value of D/H. However, at present, this is not the case. In fact, while in several measurements a rather high value of $D/H \sim 2.0{\times}10^{-4}$ has been reported [39], for other observed QAS a significantly lower value ($\sim 3.4{\times}10^{-5}$) has been quoted [40], [41]. The present situation, then, does not lead to a conclusive value for D/H [41]; a "reasonable" bound from these observations is the following [42]:

$$\frac{D}{H} \gtrsim 2.5{\times}10^{-5} \quad . \tag{2.13}$$

2.2.2 ^3He

^3He is the product of incomplete H burning in stars comparable in mass to the Sun, but it is burned away in the interiors of heavier stars.

^3He has been detected in meteoritic extractions [43] as well as in several interstellar medium (ISM) [44] measurements of ^3He in galactic HII regions [2] and in planetary nebulae [45]. Observations show a wide dispersion which may be indicative of pollution or a bias [46], and large evolutionary uncertainties make very difficult to extrapolate the primordial abundance. However, noting that D is burnt in stars to ^3He a (fairly known) fraction of which survives stellar processing, a more reliable result can be obtained by considering the sum of D and ^3He and requiring that these two isotopes not be overabundant at the time of formation of the solar system [47]. This yields the limit

$$\frac{D + {}^3He}{H} \gtrsim 10^{-4} \quad . \tag{2.14}$$

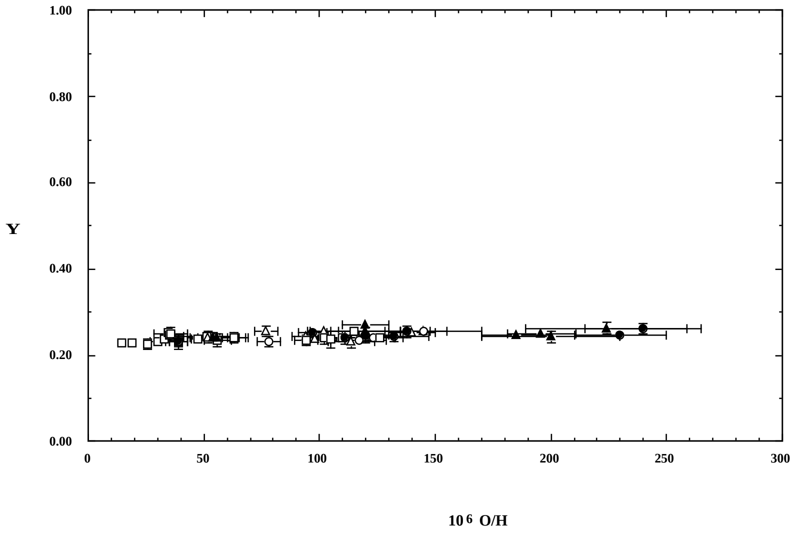

Figure 2.1: The ^4He (Y) vs oxygen (O/H) abundances in extragalactic HII regions (taken from Ref. [10]).

2.2.3 ^4He

The abundance of ^4He has been determined in a variety of astrophysical sources [48], [49], such as atmospheres of young and old stars, planetary nebulae, HII regions (galactic and extragalactic) and so on. The almost, quite amazing constancy (within a $\sim 20\%$ factor) of the observed ^4He abundance by mass of about 25 % in all these objects, as can be seen from Figure 2.1, points to an uniform origin, which is the primordial nucleosynthesis. However, although this abundance is measured with a much higher accuracy than for the other light elements, one has to be careful to extrapolate the primordial abundance from the today observed one because of stellar processing. In fact, stars generate their energy by burning hydrogen into helium and, at their death, they return this processed material to the ISM to be incorporated into subsequent generation of stars.

To determine the primordial abundance of ^4He, one must allow for the stellar helium component through its correlation with some other element which is made only in stars (such as N, O). The primordial value is then obtained with an extrapolation to zero metallicity. For this reason, it is better to concentrate on data from those regions least contaminated by the products of stellar evolution: the ^4He abundance is, in fact, best

---

[2] These are regions in which interstellar gas is heated and ionized by the radiation from hot young stars. In astrophysical notations AI means neutral A element, AII stands for A ionized once, and so on.

determined by observations of HeII → HeI recombination lines in extragalactic HII regions. Measuring both ${}^4He$ and O/H abundances, it has been found that the data are well fitted by a linear correlation [50] for $X_{{}^4He}$ ($\equiv Y$) versus O/H, and then the primordial value can be determined from the intercept of that relation. Moreover, the primordial ${}^4He$ abundance can also be determined by studying the correlation between $X_{{}^4He}$ and N/H (in almost all HII regions both O/H and N/H data are available). However, in this case, it is not still clear if a linear fit should be appropriate (at least in the situations in which N/H is not proportional to O/H) [50], [51], [52]. Nevertheless, the quoted difference between the intercepts of $X_{{}^4He}$ versus N/H and $X_{{}^4He}$ versus O/H is small ($\lesssim 0.003$).
At present, there are two different quoted abundances [48], [49]

$$X_{{}^4He} = 0.234 \pm 0.0054 \tag{2.15}$$

$$X_{{}^4He} = 0.243 \pm 0.003 \quad . \tag{2.16}$$

The Izotov et al. [49] result (2.5) is higher because of dropping the lowest metallicity galaxy from their sample due to its anomalously low HeI line intensities (which seems underlying stellar and interstellar absorption). Also, different ways to extract the primordial value of $X_{{}^4He}$ are employed. Although we do not enter into the details of the discussion for the quoted values, we limit ourselves to observe that the systematic error may be significantly larger than the ones included above [51]. In particular, the atomic physics inputs seem to be uncertain (regarding mainly the HeI line intensities) and more accurately known physical conditions in the HII regions are auspicable. This can be done by measuring several different line intensities.
We finally note that the error on the ${}^4He$ mass fraction is on the third significant digit, and consider the upper bound

$$X_{{}^4He} < 0.24 \quad , \tag{2.17}$$

as a reasonable one and

$$X_{{}^4He} < 0.25 \quad , \tag{2.18}$$

as a reliable bound [42].

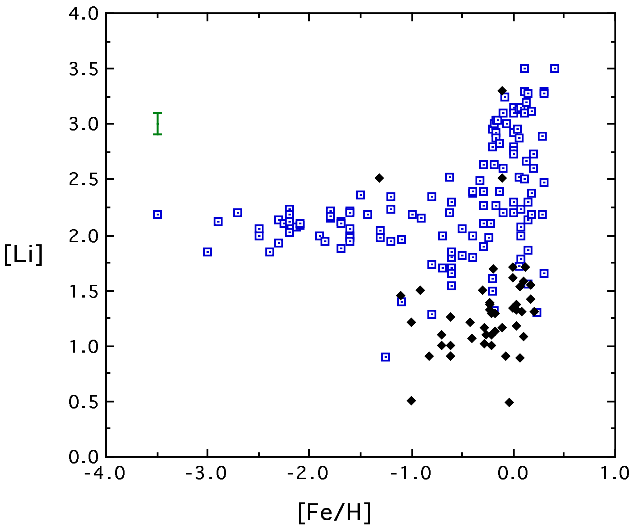

Figure 2.2: The ^7Li abundance in halo stars with $T_{surf} > 5500\,K$ as a function of metallicity. Here $[Li] = \log(^7Li/H) + 12$ and $[Fe/H] = (\log(Fe/H))/(\log(Fe/H)_\odot)$ (taken form Ref. [10]).

2.2.4 ^7Li

As a star evolves, its surface lithium is subject to destruction and dilution. In fact ^7Li, like D, is easily destroyed (at temperatures above $\sim 2{\times}10^6\,K$) by (p,α) reactions, so that only the lithium remaining on the stellar surface survives. This, however, will be further diluted through mixing of the outer layers with the interior. To avoid this, stars with a surface temperature $T > 5500\,K$ and a metallicity less than 1/20th solar are mainly observed, so that effects such as stellar convection may be not important.

^7Li is observed in the atmospheres of both very old stars (Population II) and young ones (Population I) [53], [54]. When we plot the ^7Li abundance as a function of metallicity (for stars with $T_{surf} > 5500\,K$) a plateau region is observed, as can be seen in Figure 2.2, indicating a primordial (or very close to it) value for the abundance.

The best estimate for the mean ^7Li abundance (including statistical uncertainties) is the following [54]:

$$\frac{^7Li}{H} = (1.6 \pm 0.1) \times 10^{-10} \quad . \tag{2.19}$$

However, we stress that ^7Li abundance determination is sensitive to several stellar parameters (surface temperature, metallicity and so on) and an important source of systematic error is due to the possibility that ^7Li has been depleted in stars from their

initial abundances. These uncertainties are limited by the observation of ^6Li [55] (with $^6Li/^7Li = 0.05{\pm}0.02$), a very fragile isotope; in fact standard stellar models predict that any depletion of ^7Li would be accompanied by a very severe depletion of ^6Li [56].
Finally, Li is also produced, along with Be and B, in cosmic ray spallation of C, N, O by p, α (and also by $\alpha - \alpha$ fusion). Hence abundances of Be and B have been served as a consistency check [57] on primordial Li, concluding that no more than 10 - 20 % of the ^7Li is due to cosmic ray nucleosynthesis.
Of course, for ^7Li the uncertainties are dominated by systematic effects.

Abundances of other elements have also been observed, such as those of the intermediate mass isotopes ^9Be, ^{10}B and ^{11}B. However, for these, large uncertainties are introduced, since it is believed that these isotopes are formed in cosmic ray nucleosynthesis. In fact, the observed abundances are far above the BBN predictions and a comparison between theory and experiments is extremely difficult.

2.3 Production of the light elements

Before going into the details of the primordial nucleosynthesis, in this section we will discuss (mainly qualitatively) the main features and results of Big Bang Nucleosynthesis.

2.3.1 $T \gtrsim 1\, MeV$ $(t \lesssim 1\, s)$

At sufficiently high temperatures, neutrons and protons are maintained both in kinetic [3] and chemical equilibrium by charged current weak interactions:

$$\nu_e + n \leftrightarrow e^- + p \tag{2.20}$$

$$e^+ + n \leftrightarrow p + \overline{\nu}_e \tag{2.21}$$

$$n \leftrightarrow p + e^- + \overline{\nu}_e \quad . \tag{2.22}$$

Because of chemical equilibrium, the following relation between the chemical potentials holds

$$\mu_n + \mu_\nu = \mu_p + \mu_e \quad . \tag{2.23}$$

---

[3] Kinetic equilibrium is maintained also and primarily by nuclear and electromagnetic elastic scattering reactions

The neutron to proton density ratio is then given by

$$\left(\frac{n_n}{n_p}\right)_{eq} = e^{-\frac{Q}{T}} e^{\frac{\mu_e - \mu_\nu}{T}} \tag{2.24}$$

(detailed balance), where $Q = m_n - m_p \simeq 1.29\,MeV$ is the difference between the neutron and proton mass. As discussed in sect. 1.3.1, the electron chemical potential is small compared to the temperature T in the region relevant for BBN. Furthermore, assuming zero neutrino chemical potential, we have then

$$\left(\frac{n_n}{n_p}\right)_{eq} \simeq e^{-\frac{Q}{T}} \quad . \tag{2.25}$$

The nucleons abundances track their values in equilibrium,

$$X_n(T) \simeq X_p(T) = \frac{1}{e^{\frac{Q}{T}} + 1} \quad , \tag{2.26}$$

as long as the rates for the reactions (2.20),(2.21),(2.22) decrease sufficiently and become comparable with the expansion rate H. This happens, as we have seen in sect. 1.4, at about $T \sim 1\,MeV$. At this time, neutrons "freeze out", i.e. go out of chemical equilibrium, and X_n (and X_p) relaxes to the final constant value

$$X_n^F \simeq X_p^F \simeq \frac{1}{e^{\frac{Q}{T_F}} + 1} \quad , \tag{2.27}$$

($T_F \sim 1\,MeV$ is the freeze out temperature) rather than following the exponential falling of (2.26). Since $Q/T_F \sim O(1)$, a substantial fraction of nucleons survives when chemical equilibrium between them is broken, while if T_F would be much lower than Q then $n_n \simeq 0$. The abundances of the other nuclides are very small for $T \gg 1\,MeV$, and can be calculated from (2.11). They become appreciable when the temperature goes down the binding energy per nucleon of the given specie, which is typically of the order of $1 \div 8\,MeV$. However, there are two facts that delay the onset of nucleosynthesis: the low binding energy of the first nuclide in the nucleosynthesis chain, deuterium, and the high number of photons (or high entropy) present at the nucleosynthesis era. In fact, for $T \lesssim 1 \div 8\,MeV$ deuterium (and hence the other nuclides to be formed from this) synthesis is energetically favoured, so the reaction $n + p \rightarrow D + \gamma$ takes place but, due to the high number of photons, the inverse reaction takes place as well and more efficiently than other reactions such as $n + D \rightarrow {}^3H + \gamma$ or $p + D \rightarrow {}^3He + \gamma$. Hence the abundances of these light elements are still very small for these temperatures (deuterium "bottleneck"). For reference, we report on the typical abundances of some light nuclei for $T \simeq 10\,MeV$, as calculated from (2.11) with $\eta \sim 10^{-9}$:

$$\begin{aligned}
X_n &\simeq X_p \simeq 0.5 \quad , && (2.28)\\
X_D &\simeq 6{\times}10^{-12} \quad , && (2.29)\\
X_{^3He} &\simeq 2{\times}10^{-23} \quad , && (2.30)\\
X_{^4He} &\simeq 2{\times}10^{-34} \quad , && (2.31)\\
X_{^{12}C} &\simeq 2{\times}10^{-126} \quad . && (2.32)
\end{aligned}$$

Instead, as neutrons freeze out, the n/p ratio is given by (2.25) with $T \simeq T_F$ ($n_n/n_p \simeq 1/6$) and for $T \sim 1\,MeV$ the abundances of light nuclides are

$$\begin{aligned}
X_n &\simeq \frac{1}{7} \quad , && (2.33)\\
X_p &\simeq \frac{6}{7} \quad , && (2.34)\\
X_D &\simeq 10^{-12} \quad , && (2.35)\\
X_{^3He} &\simeq 10^{-23} \quad , && (2.36)\\
X_{^4He} &\simeq 10^{-28} \quad , && (2.37)\\
X_{^{12}C} &\simeq 10^{-108} \quad . && (2.38)
\end{aligned}$$

2.3.2 $T \simeq 0.3 \div 0.1\,MeV$ $(t \simeq 1 \div 3\,min)$

As the temperature cools below $0.5 \div 0.3\,MeV$ the synthesis of complex nuclei becomes thermodynamically favourable. Thus, neutrons and protons react with each other to build up light nuclides through the following sequence of two-body reactions:

$$\begin{array}{lll}
p\,(n,\gamma)\,D & & \\
D\,(p,\gamma)\,^3He & D\,(D,n)\,^3He & D\,(D,p)\,^3H \\
^3H\,(D,n)\,^4He & ^3H\,(^4He,\gamma)\,^7Li & \\
^3He\,(n,p)\,^3H & ^3He\,(D,p)\,^4He & ^3He\,(^4He,\gamma)\,^7Be \\
^7Li\,(p.^4He)\,^4He & ^7Be\,(n,p)\,^7Li & \\
\ldots & & .
\end{array} \qquad (2.39)$$

(a complete list of nuclear reactions is reported in appendix C). The first reaction is, of course, crucial since deuterium has to be formed in appreciable amount, before the other reactions can start. In fact, many body interactions such as $2p + 2n \rightarrow^4 He$ are in general ineffective, due to the small number densities of nucleons. After deuterium, appreciable quantities of ^3H and ^3He may form. The synthesis of ^4He is, however, delayed until enough tritium has been built up, since the main process for making ^4He involves this hydrogen isotope.

Nearly all neutrons surviving down to freeze out are captured in ^4He because of its large binding energy per nucleon; its mass fraction is then approximately given by

$$X_{^4He} = \frac{4n_{^4He}}{n_B} \simeq \frac{4\,(n_n/2)}{n_n+n_p} = \frac{2(n_n/n_p)}{1+(n_n/n_p)} \quad . \tag{2.40}$$

For $T \simeq 0.1\,MeV$, the n/p ratio is about 1/7 (actually, it is a bit smaller than the freeze out value since neutrons have been depleted by β-decay), so that

$$X_{^4He} \simeq \frac{1}{4} \quad . \tag{2.41}$$

Heavier nuclei do not form in any significant quantity both because of absence of stable nuclei with $A = 5, 6$ which forbids nucleosynthesis through $(n,^4He)$, $(p,^4He)$ or $(^4He,^4He)$ reactions) and the large Coulomb barriers for reactions such as $^3H(^4He,\gamma)^7Li$ and $^3He(^4He,\gamma)^7Be$.

For $t \gtrsim 10^3\,s$ BBN is over, since the low temperature and low density in the Universe suppress nuclear reactions. Hence the most abundant nuclides with which we are left are hydrogen (p) and ^4He (incorporating almost all neutrons), followed by trace amounts of D, ^3He and ^7Li. Note that the ^3He abundance includes that of survived ^3H which subsequently β-decays and similarly the ^7Li abundance includes that of ^7Be.

Observe that the ^4He abundance, as approximately given by (2.41), is quite insensitive to the nucleon density (or η) present in the Universe, and almost only depends on the weak reaction rates determining neutron freeze out. This is not true for the other elements, for which the nucleon density directly determines the two-body nuclear reaction rates. It is expected that D and ^3He abundances decrease with increasing η, since for higher values of η we have a more efficient burning into ^4He. In fact, from (2.11), abundances increase with η so that BBN can start earlier when at higher temperature and the n/p ratio is larger. As far as ^7Li abundance, it is expected to decrease with increasing η when it is determined by the competition between $^4He(^3H,\gamma)^7Li$ and $^7Li(p,^4He)^3He$, while for sufficiently high η it starts increasing again with η due to larger production of ^7Be through $^4He(^3He,\gamma)^7Be(e^-,\nu_e)^7Li$.

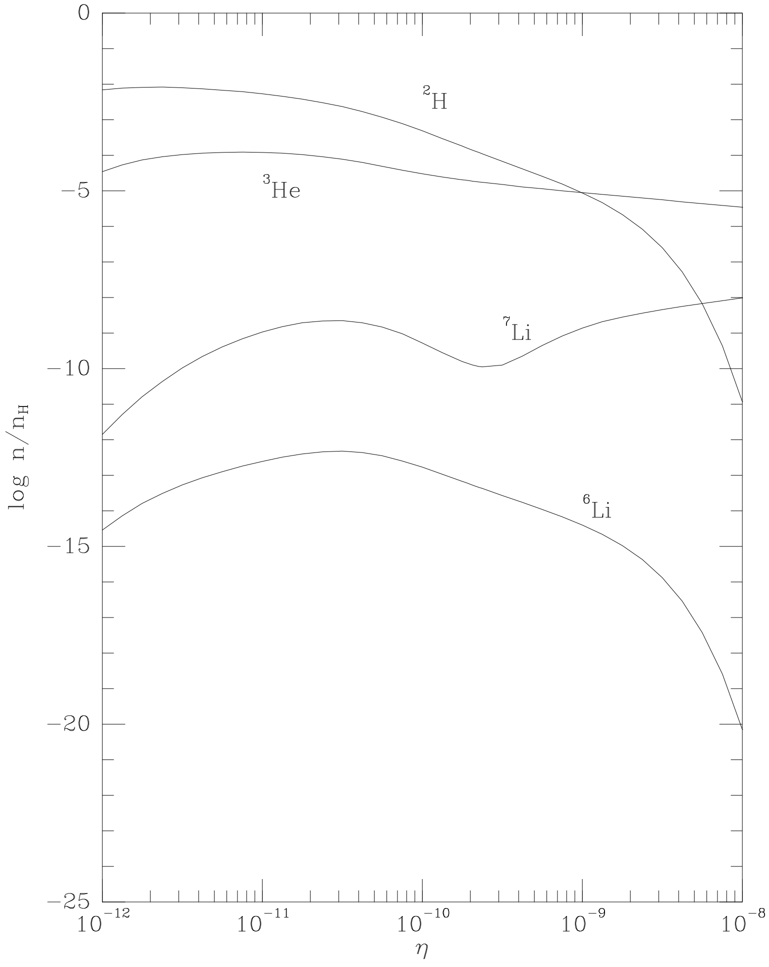

Figure 2.3: The light element abundances from big bang nucleosynthesis as a function of η (taken from Ref. [58]).

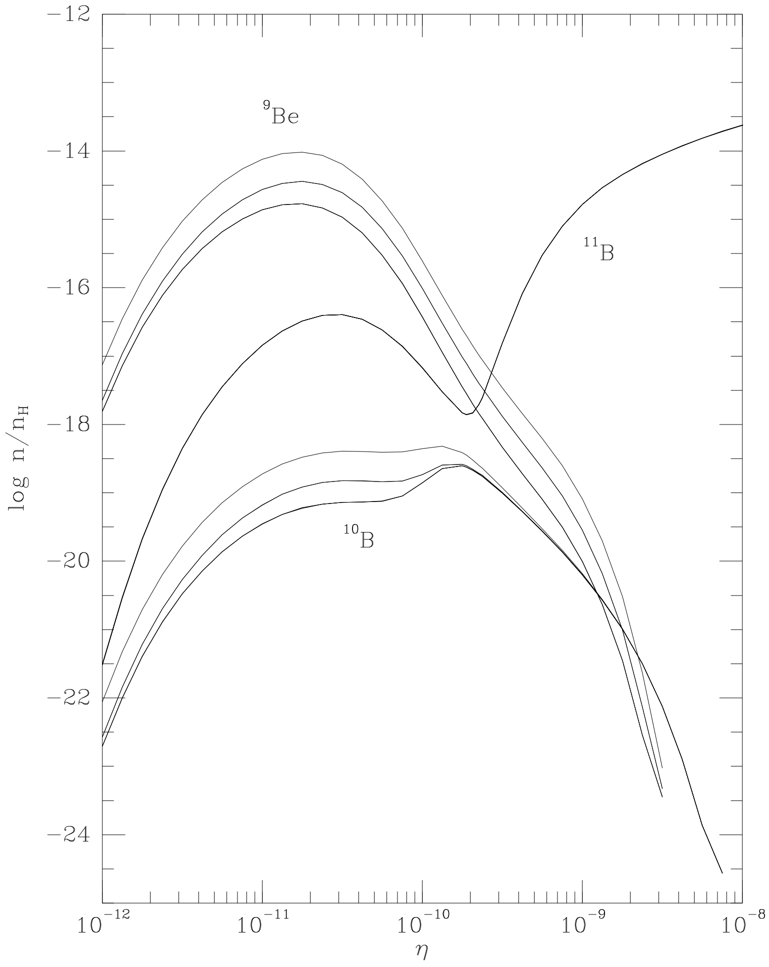

Figure 2.4: The intermediate mass element abundances from big bang nucleosynthesis as a function of η (taken from Ref. [58]).

In Figures 2.3, 2.4 we report [10] the predicted primordial abundances of some light elements versus the baryon to photon ratio η as calculated with the standard numerical code [59]. The discussed features come evident from these plots.

2.4 Calculation of the primordial abundances

In this section we will write down the equations governing the time evolution, during nucleosynthesis, of the abundances of the produced light elements.

The variables describing the Universe as a thermodynamic system during BBN are the following:

$$\begin{array}{l} R \\ T\,,\,T_\nu \\ \mu_e\,,\,\mu_\nu\,,\,\mu_n\,,\,\mu_p \\ Y_i \quad . \end{array} \tag{2.42}$$

The first is associated to the dynamical aspects of the system, i.e. expansion of the Universe, while the others describe the primordial plasma [4] of $e_\pm, \nu, n, p$ and Y_i are the nuclide abundances.

The relevant part of nucleosynthesis takes place after neutrino decoupling, so that the quantities describing the neutrino plasma evolve independently from the plasma in equilibrium and, for our purposes, may be disregarded. Hence, T_ν and μ_ν may be dropped from the list above.

Moreover, only two of the remaining three chemical potentials are independent, since the relation (2.23) holds at chemical equilibrium. The first independent variable we choose is the electron chemical potential or, equivalently, the parameter $\phi_e = \mu_e/T$. Instead, the second one, which is related to the nucleon chemical potential, is the total baryon number density n_B. Thus the independent variables we have to consider are the following

$$R\,,\,n_B\,,\,\phi_e\,,\,T\,,\,Y_i \quad , \tag{2.43}$$

for which it is necessary to write down the time evolution equations; however, let us note that in many cases is more convenient to follow the temperature evolution rather the time one, and this can be done once the relation between T and t is established [60, 61, 62, 59].

2.4.1 Equation for R

As seen in the previous chapter, the equation satisfied by the cosmic scale factor is the following:

$$\frac{1}{R}\frac{dR}{dt} = H \equiv \sqrt{\frac{8\pi}{3M_P^2}\,\rho - \frac{k}{R^2}} \quad , \tag{2.44}$$

where ρ is the total energy density. During the nucleosynthesis era, the curvature term k/R^2 is completely negligible, so that we can safely neglect its contribution to expansion.

---

[4] Note that it is explicitly assumed that species interacting electromagnetically or strongly are always in kinetic equilibrium, though chemical equilibrium may be not hold. For neutrinos, it is instead supposed that their decoupling is "instantaneous" (see below and chapter 6)

2.4.2 Equation for n_B

The total number N_B of baryons in the comoving volume is constant [5] and, assuming homogeneity, it is also independent of R. Hence the baryon number density $n_B = N_B/V$ varies as R^{-3}, so that

$$\frac{1}{n_B}\frac{dn_B}{dt} \;=\; -3\,\frac{1}{R}\frac{dR}{dt} \quad , \tag{2.45}$$

which is the equation for the evolution of n_B.

2.4.3 Equation for ϕ_e

The electron chemical potential (or ϕ_e) is fixed by the conservation of the electric charge and the total neutrality of the Universe [30]

$$n_{e^-} \;-\; n_{e^+} \;=\; n_p \quad , \tag{2.46}$$

neglecting the possible presence of antiprotons. The proton number density is

$$n_p \;=\; \sum_i Z_i\, n_i \;=\; n_B \sum_i Z_i\, Y_i \;\equiv\; n_B\, q_B \quad , \tag{2.47}$$

while, for $\phi_e \ll 1$, we have

$$\begin{aligned} n_{e^-} \;-\; n_{e^+} \;&\simeq\; \frac{2}{\pi^2}\,\phi_e\, T^3\, f(z) \quad , \\ f(z) \;&\equiv\; \int_0^\infty dx\, \frac{x^2\, e^\epsilon}{(e^\epsilon+1)^2} \quad , \end{aligned} \tag{2.48}$$

with $\epsilon = \sqrt{x^2+z^2}$ and $z = m_e/T$. From these we then obtain the equation for ϕ_e:

$$\phi_e \;\simeq\; \frac{\pi^2}{2}\,\frac{n_B\, q_B}{T^3\, f(z)} \quad , \tag{2.49}$$

with $q_B \equiv \sum_i Z_i Y_i$ defined in (2.47).

2.4.4 Equation for T

The important equation relating temperature with time is deduced from energy conservation, which gives

$$\frac{d}{dt}(\rho V) \;+\; \mathrm{p}\,\frac{dV}{dt} \;=\; 0 \quad , \tag{2.50}$$

---

[5] At the energy scales relevant for BBN there are no baryon number violating processes.

where $V \sim R^3$ is the comoving volume and ρ, p are the total energy density and pressure of the particles involved, namely:

$$\rho \;=\; \rho_\gamma \,+\, \rho_e \,+\, \rho_B \quad , \tag{2.51}$$

$$\mathrm{p} \;=\; \mathrm{p}_\gamma \,+\, \mathrm{p}_e \,+\, \mathrm{p}_B \quad . \tag{2.52}$$

(assuming that neutrinos are completely decoupled [6]) The photon contributions $\rho_\gamma, \mathrm{p}_\gamma$ depend only on the temperature and are given by equations (1.57), (1.58), while $\rho_e = \rho_{e^-} + \rho_{e^+}$, $\mathrm{p}_e = \mathrm{p}_{e^-} + \mathrm{p}_{e^+}$ depend in general on both T and ϕ_e:

$$\rho_\gamma \;=\; \frac{\pi^2}{15} T^4 \qquad\qquad \mathrm{p}_\gamma \;=\; \frac{1}{3}\,\rho_\gamma \tag{2.53}$$

$$\rho_e \;\simeq\; \frac{2}{\pi^2} T^4\, g(z) \;+\; O(\phi_e^2) \qquad\qquad \mathrm{p}_e \;\simeq\; \frac{2}{3\pi^2} T^4\, h(z) \;+\; O(\phi_e^2) \tag{2.54}$$

$$g(z) \;\equiv\; \int_0^\infty dx\, \frac{x^2\,\epsilon}{e^\epsilon + 1} \qquad\qquad h(z) \;\equiv\; \int_0^\infty dx\, \frac{x^4}{\epsilon}\, \frac{1}{e^\epsilon + 1} \quad . \tag{2.55}$$

The baryon terms can be written, in the non relativistic approximation, as (see (1.52), (1.53))

$$\begin{aligned} \rho_B \;&=\; \sum_i \rho_i \;\simeq \sum_i \left(m_i n_i \,+\, \frac{3}{2} T\, n_i \right) \;= \\ &=\; M_u\, n_B \left(1 \,+\, \sum_i \left(\frac{\Delta m_i}{M_u} \,+\, \frac{3}{2}\, \frac{T}{M_u} \right) Y_i \right) \end{aligned} \tag{2.56}$$

$$\mathrm{p}_B \;=\; \sum_i \mathrm{p}_i \;\simeq \sum_i T\, n_i \;=\; T\, n_B \sum_i Y_i \quad , \tag{2.57}$$

where M_u is the atomic mass unit (referred to ^{12}C) while Δm_i is the mass excess for the nuclide i (mass excesses for the light nuclides relevant for BBN are reported in appendix D).

From (2.50) after some simple algebra we arrive at the formal equation for T

$$\frac{dT}{dt} \;=\; -\,3 \frac{1}{R}\, \frac{dR}{dt}\, (\rho \,+\, \mathrm{p}) \left(\frac{d\rho}{dT} \right)^{-1} \quad . \tag{2.58}$$

First of all, let us note that the energy density derivative with respect to T has to be evaluated along the time direction, that is

$$\frac{d\rho}{dT} \;=\; \left(\frac{dT}{dt} \right)^{-1} \frac{d\rho}{dt} \;=\; \left(\frac{dT}{dt} \right)^{-1} \left(\frac{d\rho_\gamma}{dt} \,+\, \frac{d\rho_e}{dt} \,+\, \frac{d\rho_B}{dt} \right) \tag{2.59}$$

---

[6] In this approximation, neutrino plasma energy is separately conserved,

$$
\begin{aligned}
\frac{d\rho_\gamma}{dt} &= \frac{d\rho_\gamma}{dT}\frac{dT}{dt} \\
\frac{d\rho_e}{dt} &= \left(\frac{\partial\rho_e}{\partial T} + \frac{\partial\rho_e}{\partial\phi_e}\frac{\partial\phi_e}{\partial T}\right)\frac{dT}{dt} + \left(\frac{\partial\rho_e}{\partial\phi_e}\frac{\partial\phi_e}{\partial n_B}\frac{dn_B}{dt} + \frac{\partial\rho_e}{\partial\phi_e}\frac{\partial\phi_e}{\partial q_B}\frac{dq_B}{dt}\right) \\
\frac{d\rho_B}{dt} &\simeq \rho_B\left(-3\,\frac{1}{R}\frac{dR}{dt} + \frac{3}{2}\frac{1}{M_u}\frac{dT}{dt}\sum_i Y_i + \sum_i Y_i + \sum_i\left(\frac{\Delta m_i}{M_u} + \frac{3}{2}\frac{T}{M_u}\right)\frac{dY_i}{dt}\right) \quad .
\end{aligned}
$$

Hence we have

$$
\begin{aligned}
\frac{d\rho}{dT} &= \left(\frac{\partial\rho_e}{\partial T} + \frac{\partial\rho_e}{\partial\phi_e}\frac{\partial\phi_e}{\partial T} + \frac{d\rho_\gamma}{dT} + \frac{3}{2}\frac{1}{M_u}\rho_B\sum_i Y_i\right) + \\
&- 3\,\frac{1}{R}\frac{dR}{dt}\left(\frac{dT}{dt}\right)^{-1}\left\{\rho_B\left(1 - \left(3\,\frac{1}{R}\frac{dR}{dt}\right)^{-1}\sum_i\left(\frac{\Delta m_i}{M_u} + \frac{3}{2}\frac{T}{M_u}\right)\frac{dY_i}{dt}\right) + \right. \\
&- \left.\left(3\,\frac{1}{R}\frac{dR}{dt}\right)^{-1}\left(\frac{\partial\rho_e}{\partial\phi_e}\frac{\partial\phi_e}{\partial n_B}\frac{dn_B}{dt} + \frac{\partial\rho_e}{\partial\phi_e}\frac{\partial\phi_e}{\partial q_B}\frac{dq_B}{dt}\right)\right\}
\end{aligned}
$$

and substituting Eq. (2.58), solving with respect to dT/dt, we find

$$
\begin{aligned}
\frac{dT}{dt} &= -\left\{3\,\frac{1}{R}\frac{dR}{dt}\left(\rho_\gamma + \rho_e + \mathrm{p}_\gamma + \mathrm{p}_e + \mathrm{p}_B\right) + \right. \\
&+ \left.\frac{\partial\rho_e}{\partial\phi_e}\frac{\partial\phi_e}{\partial n_B}\frac{dn_B}{dt} + \frac{\partial\rho_e}{\partial\phi_e}\frac{\partial\phi_e}{\partial q_B}\frac{dq_B}{dt} + \sum_i\left(\frac{\Delta m_i}{M_u} + \frac{3}{2}\frac{T}{M_u}\right)\frac{dY_i}{dt}\right\} \cdot \\
&\cdot \left\{\frac{\partial\rho_e}{\partial T} + \frac{\partial\rho_e}{\partial\phi_e}\frac{\partial\phi_e}{\partial T} + \frac{d\rho_\gamma}{dT} + \frac{3}{2}\frac{1}{M_u}\rho_B\sum_i Y_i\right\}^{-1} \quad . \qquad (2.60)
\end{aligned}
$$

This is the equation relating temperature with time we looked for. Note that it is now written in terms of known quantities, once Eqs. (2.44) and (2.45) are taken into account.

2.4.5 Equations for Y_i

The change in time of the abundance Y_i of a given nuclide i is driven by the rates for the nucleon reactions producing or destroying it which we will consider to be of the form

$$
i + j \longleftrightarrow k + l \quad . \qquad (2.61)
$$

If $\Gamma_{ij\to kl}$ is the reaction rate for the direct process and $\Gamma_{kl\to ij}$ that for the inverse one, the time evolution of Y_i is given by the following equation:

$$
\frac{dY_i}{dt} = \Gamma_{kl\to ij}\,Y_l\,Y_k - \Gamma_{ij\to kl}\,Y_i\,Y_j \quad . \qquad (2.62)
$$

In general, one can consider also more complex reactions, in which more than one nuclide for each specie is present:

$$
N_i\,(i) + N_j\,(j) \longleftrightarrow N_k\,(k) + N_l\,(l) \quad , \qquad (2.63)
$$

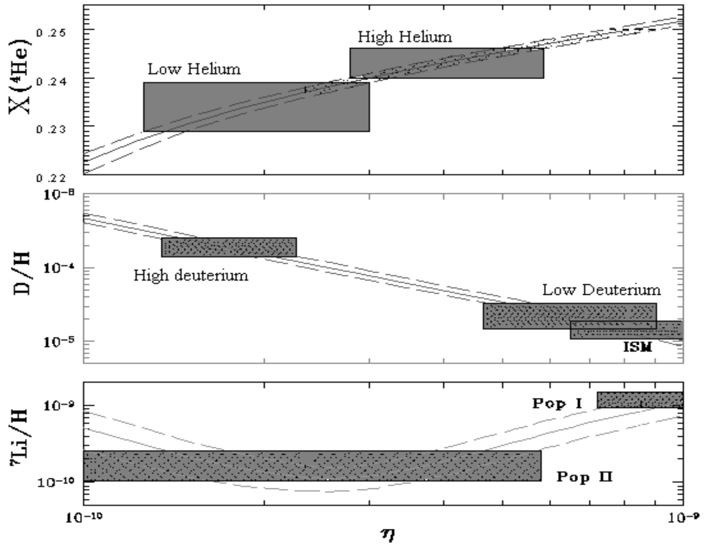

Figure 2.5: ^4He mass fraction and D, ^7Li abundances predicted in the standard BBN scenario. Also shown are the observed values of these isotopes (adapted from Ref. [7]).

where N_a is the (integer) number of a given nuclide taking part to the considered reaction. In this case the evolution equations are of the following general form:

$$\frac{dY_i}{dt} = \sum_{j,k,l} N_i \left(\Gamma_{kl \to ij} \frac{Y_l^{N_l} \, Y_k^{N_k}}{N_l! \, N_k!} - \Gamma_{ij \to kl} \frac{Y_i^{N_i} \, Y_j^{N_j}}{N_i! \, N_j!} \right) \quad . \tag{2.64}$$

The complete nuclear reaction network used in BBN calculations is reported in appendix C.

2.5 Theory versus observations. Constraints from BBN

We can now compare the inferred bounds on the abundances of light elements discussed in section 2.2 with their values computed within the standard BBN scenario.

The two conflicting ^4He mass fraction results reflect into the QSO determinations of deuterium abundance, and two different sets of measurements mutually incompatible

$$X_{^4He} = 0.234 \pm 0.0054 \quad , \qquad D/H = (1.9 \pm 0.4) \cdot 10^{-4} \tag{2.65}$$

$$X_{^4He} = 0.243 \pm 0.003 \quad , \qquad D/H = (3.40 \pm 0.25) \cdot 10^{-5} \tag{2.66}$$

arise. Obviously, large helium mass fractions require low values for deuterium abundance and vice versa. The situation is well illustrated in Figure 2.5 where both theoretical predictions and experimental observations are reported; from this the ranges of the η parameter corresponding to the different sets of data (2.65), (2.66) can be directly read off. However, a very recent (re-)analysis [10] of observational data has superseded the discussed dichotomy, and a unique range for η emerges, as can be seen from Figure 1. Nevertheless, adopting the reliable bounds of Eqs. (2.13), (2.18), (2.19) we can derive the conservative limit on η [7]

$$4.1 \times 10^{-11} < \eta < 9.1 \times 10^{-10} \quad , \tag{2.67}$$

overwhelming all the quoted difficulties in abundance determinations. These values of η translate into the following range for the nucleon density (normalized to the critical density)

$$0.0015 < \Omega_B h^2 < 0.033 \quad , \tag{2.68}$$

which is then an independent estimate of the baryon content of the Universe. Confronting with Eq. (1.36), it seems evident that non baryonic (dark) matter exists in the Universe. For an account of dark matter problems, see for example [63].

Having established the consistency of standard BBN, we can use it to constrain new physics beyond the Standard Model of elementary particles. Here we don't perform an exhaustive analysis of these constraints, which is far from the scope of this thesis and for which we remind to excellent reviews (such as [7]); our aim is to show how precise BBN results can be used to extract important informations on particle physics.

Limits on this are mostly sensistive to the bounds imposed on the ^4He abundance, which is predominantly determined by the neutron to proton ratio at freeze out. This is determined by the competition between the weak interaction rates and the expansion rate of the Universe, according to Eq. (1.107). The presence of additional neutrino flavours (or any other relativistic particle species) at the time of BBN increases the overall energy density and hence the expansion rate, leading to a larger value of T_F, n/p and ultimately $X_{^4He}$. The dependence of $X_{^4He}$ on the effective number N_ν of neutrinos can be parametrized as follows [10]:

$$X_{^4He} = 0.2262 + 0.0131 \, (N_\nu - 3) + 0.0135 \ln \left(\frac{\eta}{10^{-10}} \right) \tag{2.69}$$

(this fit holds near the central value of (2.67)). Note the weak logarithmic dependence of $X_{^4He}$ on the η parameter. By requiring that all constraints on elemental yields be simultaneously satisfied, a Monte Carlo analysis has given the following conservative limit on N_ν [42]

$$N_\nu \ \leq \ 3.75 \ + \ 78 \ (X_{^4He}^{max} \ - \ 0.24) \quad . \tag{2.70}$$

A number of other constraints on known or hypothetical particles, both relativistic and non relativistic at the time of BBN, as well as limits on the strength of new forces, can be deduced. These also have important implications for the problem of dark matter in the Universe. While these constraints are much more stringent than the ones obtained in laboratory experiments, pointing out the relevance of BBN studies, they are (particle physics) model dependent and cannot be discussed here. We remind to the recent reviews [10, 7] and references therein.

Chapter 3

The Born rates for $n \leftrightarrow p$ reactions

The initial conditions for the primordial nucleosynthesis are settled out by the ratio of the relative abundances of neutrons and protons. When BBN is starting, the primordial plasma consists of nucleons, electrons, positrons, neutrinos, antineutrinos and photons in thermal equilibrium. The relative abundance of neutrons and protons is determined by the following charged-current weak interactions:

$$(a) \quad \nu_e \, + n \, \rightarrow \, e^- \, + p \qquad , \qquad (b) \quad e^- \, + p \, \rightarrow \, \nu_e \, + n \tag{3.1}$$

$$(c) \quad e^+ \, + n \, \rightarrow \, \overline{\nu}_e \, + p \qquad , \qquad (d) \quad \overline{\nu}_e \, + p \, \rightarrow \, e^+ \, + n \tag{3.2}$$

$$(e) \quad n \, \rightarrow \, p + e^- \, + \overline{\nu}_e \qquad , \qquad (f) \quad p + e^- \, + \overline{\nu}_e \, \rightarrow \, n \tag{3.3}$$

In this chapter, the leading contribution for the rates (per nucleon and per time) for these six reactions is calculated and the relevant approximations are particularly pointed out.

For a generic process in (3.1), (3.2), (3.3) , the reaction rate can be written in the form

$$d\Gamma(i \rightarrow f) \, = \, \sum_{\text{spins}} |M|^2 \, (2\pi)^4 \, \delta^4 \left(\sum_\alpha \mathrm{p}_\alpha \right) \, d\Phi \quad , \tag{3.4}$$

where $|M|^2$ is the squared matrix element, which has to be summed over all spin degrees of freedom. The δ-function gives the energy-momentum conservation, $\mathrm{p}_a \, = \, (E_a, \mathbf{p_a})$ being the 4-momenta of the particles entering in the process (each p_a is intended with a positive sign if the particles involved in the reaction is in and with a negative sign if it is out). The quantity $d\Phi \, = \, \prod_a d\Phi_a$ is the phase space factor for the given reaction. Since the processes (3.1), (3.2), (3.3) occur in a thermal bath, the phase space factor associated with each initial (Fermi) particle is

$$d\Phi_a \, = \, \frac{d^3\mathbf{p_a}}{(2\pi)^3} \, \frac{1}{2E_a} \, F_a \quad , \tag{3.5}$$

while for final (Fermi) particles we have

$$d\Phi_a \,=\, \frac{d^3\mathbf{p_a}}{(2\pi)^3}\,\frac{1}{2E_a}\,(1\,-\,F_a) \quad , \tag{3.6}$$

where F_a is the phase-space density of the a-th particle at temperature T, which takes the thermal equilibrium value (in the rest frame of the thermal radiation) given by the Fermi function

$$F_a(E_a) \,=\, \frac{1}{e^{\frac{E_a}{T_a}}\,+\,1} \tag{3.7}$$

only for those species actually in equilibrium. Note that in writing (3.4) we have assumed that n_a does not depend on spin, so that the summation over this degree of freedom is limited to $|M|^2$.

The quantity of interest in BBN is the reaction rate per incident nucleon, so that Γ in (3.4) has to be divided by the number density

$$n_b \,=\, 2\int \frac{d^3\mathbf{p_b}}{(2\pi)^3}\,F_b \tag{3.8}$$

of the incident nucleon (say b). Assuming that $\sum_{\text{spins}} |M|^2$ does not depend on the initial nucleon momentum (this assumption, which is justified in the infinite nucleon mass approximation, will be discussed later), the net effect on the reaction rate is the following

$$d\Gamma(i\to f) \,=\, \frac{1}{2}\sum_{\text{spins}} |M|^2\,(2\pi)^4\,\delta^4\left(\sum_{\alpha} \mathrm{p}_\alpha\right)\prod_{a\neq b} d\Phi_a\,\frac{1}{2M_b} \tag{3.9}$$

(from now on, we indicate with Γ the reaction rate per incident nucleon). Furthermore, since at the epoch of BBN the baryon density is very low ($\eta \sim 10^{-9}$), we can also neglect the occupation number of the final nucleon (say c), so the final expression for $\Gamma(i\to f)$ to be considered is

$$d\Gamma(i\to f) \,=\, \frac{1}{2}\sum_{\text{spins}} |M|^2\,(2\pi)^4\,\delta^4\left(\sum_{\alpha} \mathrm{p}_\alpha\right)\left(\prod_{leptons} d\Phi_a\right)\frac{d^3\mathbf{p_c}}{(2\pi)^3}\,\frac{1}{2M_b}\,\frac{1}{2M_c} \quad . \tag{3.10}$$

We now proceed to explicitly calculate the reaction rates for the processes in (3.1), (3.2), (3.3) in the Born approximation.

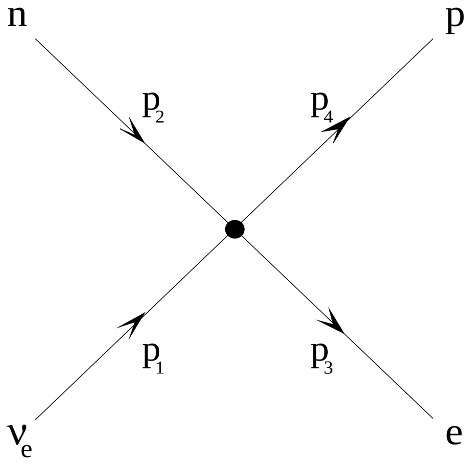

Figure 3.1: The Feynman diagram for the reaction $\nu_e\ +\ n\ \rightarrow\ e^-\ +\ p$.

3.1 The reaction $\nu_e\ +\ n\ \rightarrow\ e^-\ +\ p$ and the other processes

Let us start with considering the direct reaction in (3.1); in the Born approximation the Feynman diagram for this process is given in Figure 3.1. The amplitude is

$$M\ =\ \frac{G_F}{\sqrt{2}}\,\overline{u}_p(\mathrm{p}_4)\gamma_\mu(C_V - C_A\gamma_5)u_n(\mathrm{p}_2)\overline{u}_e(\mathrm{p}_3)\gamma^\mu(1-\gamma_5)u_\nu(\mathrm{p}_1)\quad , \tag{3.11}$$

where G_F is the Fermi coupling constant and C_V, C_A are the vector and axial coupling of the nucleon. In the neutron rest frame (which, in the limit $m_N \to \infty$, coincides with the plasma rest frame), neglecting proton motion ($\mathbf{p_4} \sim \mathbf{0}$, $E_4 \sim M_4$), we then have

$$\sum_{\text{spins}} |M|^2\ =\ 32G_F^2\, M_2M_4\, \left(\left({C_V}^2 + 3{C_A}^2\right) E_1E_3\ +\ \left({C_V}^2 - {C_A}^2\right) p_2p_3\cos\,\theta_{e\nu}\right) \tag{3.12}$$

(hereafter $p_\alpha \equiv |\mathbf{p}_\alpha|$)¿ In $\Gamma(\nu_e\ + n \rightarrow e^- + p)$, after integration over angles, the last term does not contribute, thus we can disregard it, and obtain the well known result

$$\sum_{\text{spins}} |M|^2\ =\ 32\,G_F^2\,\left({C_V}^2 + 3{C_A}^2\right)\,M_2M_4E_1E_3\quad . \tag{3.13}$$

The reaction rate in (3.10) for the present process then takes the form

$$\begin{aligned} d\Gamma(\nu_e + n \to e^- + p) &= \frac{1}{2}\,32\,G_F^2\,\left({C_V}^2 + 3{C_A}^2\right)\,M_2 M_4 E_1 E_3 \,\cdot \\ &\cdot\quad (2\pi)^4\,\delta^4(p_1 + p_2 - p_3 - p_4)\,\frac{1}{2M_2}\frac{1}{2M_4}\frac{1}{2E_1}\frac{1}{2E_3}\,\cdot \\ &\cdot\quad \frac{d^3\mathbf{p_1}}{(2\pi)^3}\frac{d^3\mathbf{p_3}}{(2\pi)^3}\frac{d^3\mathbf{p_4}}{(2\pi)^3}\,F_\nu(p_1)\,(1 - F_e(p_3)) \end{aligned} \tag{3.14}$$

(we have distinguished the neutrino Fermi function from that of electrons since, in general, neutrino temperature T_ν is different from the $e^\pm, \gamma$ bath temperature T, as discussed in the previous chapter). The integration over the proton 3-momentum can be eliminated by using $\delta^3(\mathbf{p_1} + \mathbf{p_2} - \mathbf{p_3} - \mathbf{p_4})$. From the isotropy of space, also the integration over the incident neutrino solid angle $\int d\Omega_{\nu_e}$ can be easily performed, leading to an overall factor 4π:

$$d\Gamma(\nu_e + n \to e^- + p) = \frac{2G_F^2\left({C_V}^2 + 3{C_A}^2\right)}{(2\pi)^4}\,\delta(E_1 - Q)\,p_1^2 dp_1\,p_3^2 dp_3\,d\Omega_3\,F_\nu(p_1)\,(1 - F_e(p_3)) \quad , \tag{3.15}$$

where $Q = M_4 - M_2 + E_3$. The energy δ-function can be used to perform the integration in dp_1, assuming massless (or almost massless) neutrinos, i.e. $E_1 \sim |\mathbf{p_1}|$. Finally, also the integration over the electron angles $\int d\Omega_3$ is easily performed since the differential rate does not depend (in the present approximations) on these quantities. We are then left with the following result;

$$\Gamma(\nu_e + n \to e^- + p) = \frac{G_F^2\left({C_V}^2 + 3{C_A}^2\right)}{2\pi^3}\int dp_3\,p_3^2\,Q^2\,\theta(Q)\,F_\nu(Q)\,(1 - F_e(p_3)) \quad . \tag{3.16}$$

The integration limits are imposed by the condition $Q \geq 0$; in the present case we have $p_3 \in \left[\sqrt{\Delta^2 - m^2}, +\infty\right)$, with $\Delta = M_2 - M_4$ (in the following, with Δ we always denote the neutron - proton mass difference).

For the other five processes in (3.1), (3.2), (3.3) one simply has to observe that the form of $\sum_{\text{spins}} |M|^2$ in (3.13) remains unchanged due to crossing symmetry. Then in the final result (3.16) we have just to replace Q (which is determined by the energy conservation for each reaction) and the thermal factors (which depend on the initial and final lepton states for each process). In Table 3.1 we report the values for Q and the thermal factors for each reaction in (3.1), (3.2), (3.3) , using the same notation adopted for $\nu_e + n \to e^- + p$ (i.e. $1 = \nu_e$ or $\overline{\nu}_e$, $2 = n$, $3 = e^-$ or e^+, $4 = p$). The Born rates for each reaction in (3.1), (3.2),

Table 3.1: The Q parameter and thermal factors for the reactions in (3.1), (3.2), (3.3) .

Reactions	Q	Thermal factors
$\nu_e\, n \rightarrow e^-\, p$	$-\Delta + E_3$	$F_\nu(Q)\,(1 - F_e(E_3))$
$e^-\, p \rightarrow \nu_e\, n$	$-\Delta + E_3$	$F_e(E_3)\,(1 - F_\nu(Q))$
$e^+\, n \rightarrow \overline{\nu}_e\, p$	$\Delta + E_3$	$F_e(E_3)\,(1 - F_\nu(Q))$
$\overline{\nu}_e\, p \rightarrow e^+\, n$	$\Delta + E_3$	$F_\nu(Q)\,(1 - F_e(E_3))$
$n \rightarrow p\, e^-\, \overline{\nu}_e$	$\Delta - E_3$	$(1 - F_\nu(Q))\,(1 - F_e(E_3))$
$p\, e^-\, \overline{\nu}_e \rightarrow n$	$\Delta - E_3$	$F_\nu(Q)\, F_e(E_3)$

(3.3) , as functions of photon temperature in the range relevant for nucleosynthesis, are plotted in Figure 3.2. The relation between neutrino and photon temperature we adopt is reported in the Appendix B.

3.2 Radiative electromagnetic corrections: the neutron lifetime

The reaction rates for the six weak processes in (3.1), (3.2), (3.3) are proportional to the quantity

$$G_F^2 \left({C_V}^2 + 3{C_A}^2 \right) = G_V^2 \left(1 + 3\frac{{C_A}^2}{{C_V}^2} \right) \quad , \tag{3.17}$$

as it can be seen from Eq. (3.16), for example. The value of G_F^2 is very well known from the measurements of the muon decay rate [18], while G_V^2 is obtained from the observations of $0^+ \rightarrow 0^+$ nuclear β decays after applying radiative and isospin-mixing corrections [18]. Instead, the empirical value of the ratio C_A/C_V is deduced, for example, from experiments measuring the angular distribution of decay products of polarized neutrons [18]. It is very common in the literature on BBN (see for example [4]) to rewrite the effective coupling constant in (3.17) in terms of the neutron lifetime (free neutron decay in vacuum) since, as it can be immediately deduced from (3.16) and Table 3.1 dropping out the thermal factors, it is given by the following relation

$$\tau_n^{-1} = \frac{G_F^2 \left({C_V}^2 + 3{C_A}^2 \right)}{2\pi^3} m_e^5 \int_1^{\frac{\Delta}{m_e}} d\epsilon\, \epsilon \left(\epsilon - \frac{\Delta}{m_e} \right)^2 \left(\epsilon^2 - 1 \right)^{\frac{1}{2}} \quad , \tag{3.18}$$

where m_e is the electron mass.

Rewriting the reaction rates in terms of the neutron lifetime, it is then customary to

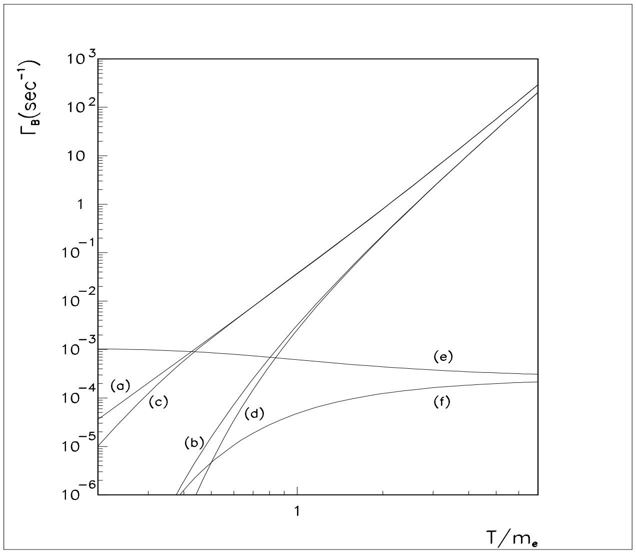

Figure 3.2: The Born rates Γ_B versus photon temperature divided by electron mass m_e. Hereafter reaction labels are the same as in (3.1), (3.2), (3.3) .

substitute τ_n with its experimental value. This way of reasoning does not bring to accurate BBN theoretical predictions at a certain degree of approximation, but introduces an uncertainty in the BBN calculations due to the experimental uncertainty on the neutron lifetime. This procedure is usually adopted to circumvent the problem of an accurate estimation of radiative (electromagnetic) corrections to G_V which is, nevertheless, a very important one. To give an idea of the relevance of this problem, it suffices to observe that if we calculate the neutron lifetime from the tree level formula (3.18) (not containing radiative corrections), inserting the value of G_V and C_A/C_V reported in [18], we obtain for τ_n the value $\sim 961\,s$ which is not at all consistent with the experimental value $886.7 \pm 1.9\,s$: we need a correction factor of about 8 %.

This simple exercise shows that the inclusion of radiative corrections is a very important step, which we are going to discuss.

Let us consider order α corrections to the neutron lifetime (α is the fine structure constant). These can be separated into "outer" corrections, involving the nucleon as a whole, and "inner" corrections, depending on nucleon structure. Obviously, inner corrections are sensible to the details of the strong interactions inside the nucleon, while it can be shown

[64] that outer corrections, at least up to terms of order α, are independent of these.

The main Feynman diagrams contributing to order α corrections to neutron lifetime are sketched in Figure 3.3. The electromagnetic interactions of the proton are through its charge and magnetic moment, while those of the neutron are only through its magnetic moment. All diagrams reported in Figure 3.3 are of order α but the ones involving magnetic moment interactions of the nucleons are suppressed with respect to the others by the inverse of nucleon mass. Notice that since we use the value of G_F as measured from muon decay, we have also to consider radiative corrections for the muon decay rate (at the same order in α). The relevant diagrams are similar to those pictured in Figure 3.3, but with n, p replaced by μ, ν_μ ; obviously for muon decay there are only outer corrections, since we deal with pointlike particles. In the following we consistently take into account also order α corrections to muon decay and report the global correction factor for the neutron decay rate.

The outer correction to the (non integrated) decay rate can be written as

$$\frac{\alpha}{2\pi}\, g(E, E_m) \quad , \tag{3.19}$$

where $g(E, E_m)$ is a function of electron energy E and end-point energy E_m, reported in [64]. This function, which is the same for electron and positron capture, describes the deviations from the allowed electron spectrum arising from the radiative corrections of order α [1]. It increases the decay probability for neutron β decay (and then decreases neutron lifetime) by about 1.5 %.

Inner corrections are much more difficult to handle, since they strongly depend on nucleon structure. In general, one can follow two different approaches. On one side one can directly consider radiative corrections to the effective nucleon weak current $\overline{u}_p \gamma_\mu (1 - \frac{C_A}{C_V}\gamma_5) u_n$ [65] while on the other side, one can study corrections for the weak quark current $\overline{q}\gamma_\mu(1-\gamma_5)q$ and then translate the quark-based description to hadronic description [66]. Here we adopt the second point of view, and report the results obtained by Marciano and Sirlin [66]

$$\frac{\alpha}{2\pi}\left(4\,\ln\frac{M_Z}{M_P} + \ln\frac{M_P}{M_A} + 2C + A_g\right) \quad . \tag{3.20}$$

---

[1] It is common to substitute the function $g(E, E_m)$ in (3.19) with its mean value $\overline{g}(E_m)$ obtained averaging over the allowed electron spectrum. However, since we will consider not only neutron decay but also the other five reactions in (3.1), (3.2), (3.3) , we do not employ this approximation.

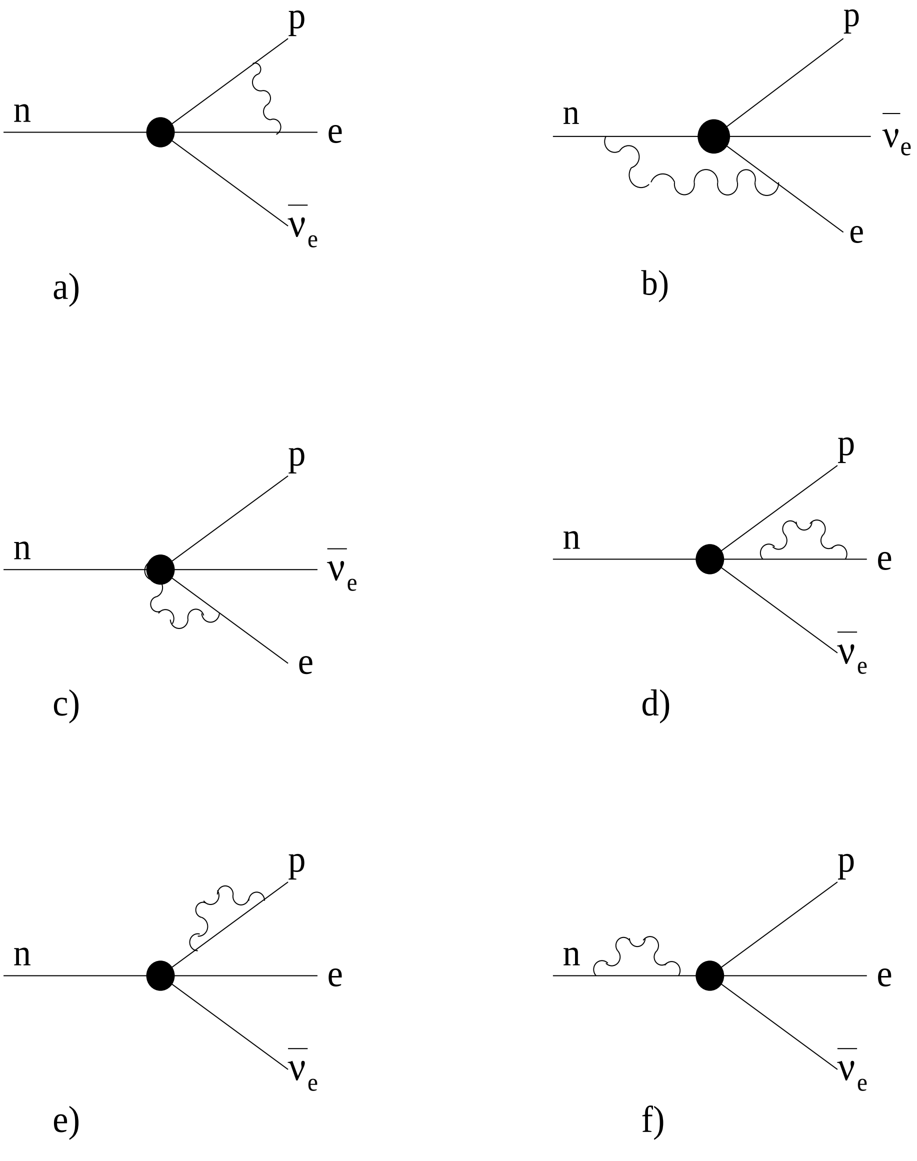

Figure 3.3: The Feynman diagrams for order α radiative corrections to neutron decay.

The first term represent the dominant model-independent short-distance contribution (M_P is the proton mass, while M_Z is the Z boson mass). The second and third terms are axial-current induced contributions, where M_A is a low energy cutoff applied to the short-distance part of the γW box diagram and $2C$ is the remaining long-distance (low energy) correction. These terms depend on the details of the strong interaction structure and are the main sources of uncertainty in the radiative corrections. The allowed range for the cutoff M_A is $400 \div 1600\, MeV$, while $C = 3C_A \cdot 0.266 \cdot (\mu_p + \mu_n)$, $\mu_p + \mu_n \simeq 0.88$ being the nucleon isoscalar magnetic moment. We then have

$$\frac{\alpha}{2\pi}\left(\ln\frac{M_P}{M_A} + 2C\right) \simeq 0.0012 \pm 0.0018 \quad . \tag{3.21}$$

The last term in (3.20) is a perturbative QCD correction whose calculation is rather reliable and gives

$$A_g \simeq -0.34 \quad . \tag{3.22}$$

Let us observe that the largest correction comes from the first term in (3.20). Thus, it seems appropriate to approximate the effects of higher orders by summing all leading-logarithmic corrections of the type $\alpha^n \ln^n M_Z$ ($n = 1, 2, 3, ...$) via a renormalization group analysis. This has been done in [67]; the corrected rate then acquires the factor

$$\mathcal{G}(E) = \left(1 + \frac{\alpha}{2\pi}\left(\ln\frac{M_P}{M_A} + 2C\right) + \frac{\alpha(M_P)}{2\pi}\left(g(E, E_m) + A_g\right)\right) S(M_P, M_Z) \quad . \tag{3.23}$$

where $\alpha(\mu)$ is the QED running coupling constant defined in the $\overline{MS}$ scheme satisfying the equation

$$\mu\frac{d}{d\mu}\,\alpha(\mu) \simeq b_0(\mu)\,\alpha^2(\mu) \quad , \tag{3.24}$$

with

$$b_0(\mu) = \frac{2}{2\pi}\sum_f Q_f^2\,\theta(\mu - m_f) - \frac{7}{2\pi}\,\theta(\mu - M_W) \quad . \tag{3.25}$$

The sum runs over all elementary fermions with mass m_f and charge Q_f, M_W is the W boson mass. The short-distance enhancement factor $S(M_P, M_Z)$ is given by [67], [66] [2]

$$S(M_P, M_Z) = \left(\frac{\alpha(m_c)}{\alpha(M_p)}\right)^{\frac{3}{4}} \left(\frac{\alpha(m_\tau)}{\alpha(m_c)}\right)^{\frac{9}{16}} \left(\frac{\alpha(m_b)}{\alpha(m_\tau)}\right)^{\frac{9}{19}} \left(\frac{\alpha(M_W)}{\alpha(m_b)}\right)^{\frac{9}{20}} \left(\frac{\alpha(M_Z)}{\alpha(M_W)}\right)^{\frac{36}{17}} \quad . \tag{3.26}$$

---

[2] The expression reported in [66] is here corrected allowing the (now observed) top quark mass to be higher than the W, Z boson masses

Table 3.2: QED running coupling constant for several energy scales.

$\alpha^{-1}(M_W)$	$=$	$\alpha^{-1}(M_Z) + \frac{17}{18\pi} \ln \frac{M_Z}{M_W}$	$\simeq$	127.94
$\alpha^{-1}(m_b)$	$=$	$\alpha^{-1}(M_W) + \frac{40}{9\pi} \ln \frac{M_W}{m_b}$	$\simeq$	132.08
$\alpha^{-1}(m_\tau)$	$=$	$\alpha^{-1}(m_b) + \frac{38}{9\pi} \ln \frac{m_b}{m_\tau}$	$\simeq$	133.27
$\alpha^{-1}(m_c)$	$=$	$\alpha^{-1}(m_\tau) + \frac{32}{9\pi} \ln \frac{m_\tau}{m_c}$	$\simeq$	133.62
$\alpha^{-1}(M_p)$	$=$	$\alpha^{-1}(m_c) + \frac{8}{3\pi} \ln \frac{m_c}{M_p}$	$\simeq$	133.90

In the $\overline{MS}$ scheme one has $\alpha^{-1}(M_Z) \simeq 127.90$ [18]. The running coupling constants at different scales are reported in Table 3.2 where we use the *central* values for the quark masses as quoted in [18]. From this one easily finds

$$S(M_P, M_Z) \simeq 1.02254 \quad . \tag{3.27}$$

The radiative corrections considered here, which are described by the factor in (3.23), are not, however, the only corrections to be taken into account for the neutron decay (they contribute for about 4 % to the lifetime, against the required global correction of about 8 %). The remaining leading corrections are usually viewed as corrections to the phase space factor [68], namely to the integrand function in (3.18) since they are (electron) energy dependent. We will express the contribution to the phase space factor as multiplicative (energy dependent) terms to the integrand function.

Let us first examine the correction due to the distortion of the outgoing electron wave by the Coulomb field of the proton. This can be calculated by solving the Dirac equation for an electron under the influence of a spatially finite proton charge distribution of radius $R \simeq 1\, fm$; the wave function is then evaluated at the centre of the proton. The correction factor is then given by [68]

$$\mathcal{F}(E)\, \mathcal{L}(E) \simeq \left(1 + \alpha\pi \frac{E}{\sqrt{E^2 - m_e^2}}\right) \left(1 - \alpha\, R\, E \left(\frac{m_e^2}{2E^2} + 1\right)\right) \quad . \tag{3.28}$$

Note that the first term in (3.28) is usually denoted as the Fermi function for the Coulomb scattering.

Another relevant correction comes from the fact that neither the electron wavefunction evaluated at the centre of the proton through $\mathcal{F}(E)\, \mathcal{L}(E)$) nor the (anti-)neutrino one are constant through the proton volume. Thus the decay rate has to be found by an appropriate convolution of the electron, (anti-)neutrino and proton wavefunctions through the proton volume. This brings to the following correction factor [68]

$$\mathcal{C} \simeq 1 + c_0 + \frac{c_1}{E} + c_2\, E + c_3\, E^2 \quad , \tag{3.29}$$

$$\begin{aligned}
c_0 &= \frac{1}{5}\left(R^2\, m_e^2 \left(1 - \frac{2}{3}B -, \frac{E_m^2}{m_e^2}\right) - \alpha\, B\, R\, E_m\right) \quad , \\
c_1 &= \frac{2B}{15}\, R^2\, m_e^2\, E_m \quad , \\
c_2 &= \frac{1}{5}\,(3 - B)\, R\, \left(\frac{2}{3}\, R\, E_m - \alpha\right) \quad , \\
c_3 &= \frac{2}{15}\,(3 - B)\, R^2 \quad , \\
B &= \frac{{C_V}^2 - {C_A}^2}{\left({C_V}^2 + 3{C_A}^2\right)} \quad .
\end{aligned}$$

Finally, there are also small corrections related to the fact that the outgoing proton is not at rest, since it has a finite mass. This type of effect will be considered in detail in the following chapter. Here, we only want to point out that if the proton recoils, then the Coulomb field that distorts the electron wave comes from a moving source. The correction associated to this effect is contained in the factor [68]

$$\mathcal{Q}(E) \simeq 1 - \frac{\alpha\, \pi\, m_e^2}{M_p\, \sqrt{E^2 - m_e^2}} \left(1 + B\, \frac{E_m - E}{3E}\right) \quad . \tag{3.30}$$

From previous results, the neutron lifetime corrected at order α against electromagnetic interactions reads

$$\begin{aligned}
\tau_n^{-1} &= \frac{G_F^2\left({C_V}^2 + 3{C_A}^2\right)}{2\pi^3} \int_{m_e}^{\Delta} dE\, E\, (E - \Delta)^2 \left(E^2 - m_e^2\right)^{\frac{1}{2}} \cdot \\
&\quad \cdot\ \mathcal{G}(E)\, \mathcal{F}(E)\, \mathcal{L}(E)\, \mathcal{C}(E)\, \mathcal{Q}(E) \quad ,
\end{aligned} \tag{3.31}$$

where $\mathcal{G}(E)$ is the correction function in (3.23) and the other terms are reported in (3.28) - (3.30). Concerning the relevance of the different corrections just considered, a comment is in turn. For seek of completeness we have reported an exhaustive description of all corrections at order α, but as clearly appears from the explicit expressions of (3.23)-(3.30), the main contributions come from (3.23) and $\mathcal{F}(E)$ term in (3.28). All other contributions, contained in $\mathcal{L}(E)$, $\mathcal{C}(E)$ and $\mathcal{Q}(E)$, are in fact much smaller and thus they can be safely neglected, since they are suppressed by a factors of the order Δ/Λ_{QCD}. Actually the α^2

contributions coming from radiative and Coulomb effects are even larger, or of the same order of magnitude, than these terms, so they should be included for consistency if $\mathcal{L}(E)$, $\mathcal{C}(E)$ and $\mathcal{Q}(E)$ are taken into account [68]. For the level of accuracy of our analysis it will be sufficient to include $\mathcal{F}(E)$ and $\mathcal{G}(E)$ at order α only.

Evaluating numerically the integral in (3.31) we then obtain for the neutron lifetime the value [3] $893.8\,s$ which is now quite compatible with the experimental value. Note that the theoretical prediction can be further refined (leading to a slightly better agreement with the experiments) by considering other small effects (again of order α) such as magnetic moment (normal and anomalous) interactions, residual average proton polarization due to parity non-conservation and so on. While these effects are briefly discussed in [68], for our purposes we do not consider them, since their contributions are energy independent and then account only for an overall factor.

3.3 Results for the reaction rates

The analysis of radiative corrections for β-decay shows that their contribution to the rates for the processes in (3.1), (3.2), (3.3), relevant for BBN, is expected to be as large as few percent. To reach accuracy of the order of one percent in rate evaluations it is therefore necessary to correct Born rates for both radiative and Coulomb effects. This last contribution, however, is only present when both electron and proton are present in the initial or final state, since it can be viewed as the electromagnetic rescattering of the two charged particles. In this way it is straightforward to show that no Coulomb corrections $\mathcal{F}(E)$ are present for the channels $e^+ + n \leftrightarrow \overline{\nu}_e + p$. The results reported in (3.23), (3.28) can be applied to the general formula for the decay rates (3.10) by rewriting the dependence on the electron spectrum end-point E_m in terms of neutrino energy. In fact, with the same notation of Figure 3.1 we have that $E_m = E_1 + E_3$. Then, in general the correction factors depend on both the electron energy E_3 and neutrino energy E_1, which are both integration variables.

Indicating with $d\Gamma_B$ the uncorrected decay rate in (3.10), the corrected one is given

---

[3] For completeness we have included also the corrections coming from the finite nucleon mass changing the squared matrix element, which are considered in the next chapter. However, these corrections are very small.

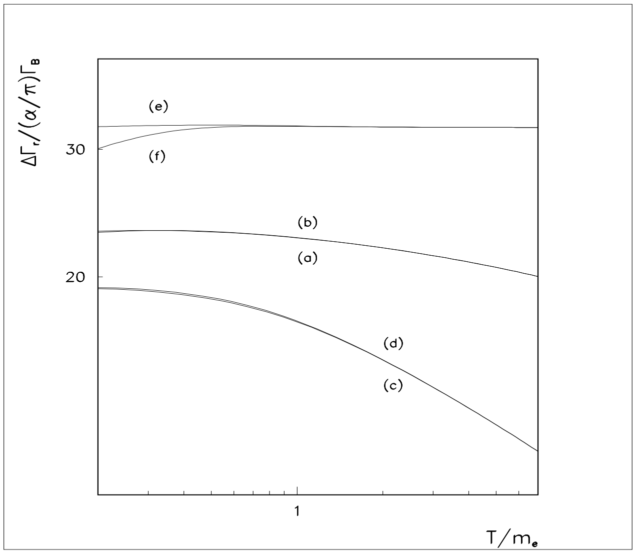

Figure 3.4: Radiative corrections to the Born rates for the processes in (3.1), (3.2), (3.3) .

by

$$d\Gamma_r \simeq \mathcal{G}(E_1, E_3)\, \mathcal{F}(E_3)\, d\Gamma_B \quad , \tag{3.32}$$

where the factors are the same ones reported in (3.23), (3.28) but with E_m substituted by $E_1 + E_3$, and the factor $\mathcal{F}(E_3)$ does not apply to reactions (c), (d).

Equipped with the corrected formula in (3.32), we may now numerically evaluate the Born rates for the reactions in (3.1), (3.2), (3.3) . In Figure 3.4 we show the relative difference between the Born rates and the radiatively corrected ones, namely the quantity

$$\Delta\Gamma_r = \frac{\Gamma_r - \Gamma_B}{(\alpha/\pi)\, \Gamma_B} \quad . \tag{3.33}$$

Note that at sufficiently high temperatures the corrections for a given process and the inverse one coincide. Apart from the β-decay reactions, whose corrections are practically constant with temperature, for the scattering reactions the considered radiative corrections are relevant especially at low temperatures.

In our BBN calculations reported in chapter 6 we have also included an overall rescaling factor τ_n^{th}/τ_n^{exp} for the reaction rates allowing the theoretical prediction for the neutron lifetime to be fully compatible with the experimental value. This is a standard procedure, which allows to overcome the problem of a precise determination of the coupling constant for weak interactions involved in BBN, expressing this overall factor in terms of the experimental value of neutron lifetime. We stress, however, that it is worth rescaling the rate only after all known corrections have been included, since this increases the accuracy of the prediction. In this way the ansatz that the residual correction be an overall factor and not, as it is reasonable to expect, a function of leptons energies, may introduce errors less than 1%. Although not included in Figure 3.4 (it would cause a trivial overall shift of the curves), we have also rescaled the corrected rates in (3.32) by the factor

$$1 + \delta_\tau \equiv \frac{\tau_n^{th}}{\tau_n^{exp}} \simeq 1.008 \quad , \tag{3.34}$$

representing an energy independent constant correction which should be included to reproduce the experimental value for neutron lifetime at zero temperature and density.

Chapter 4

Finite nucleon mass corrections

In this chapter we calculate the corrections to the Born rates for the $n \leftrightarrow p$ reactions (3.1), (3.2), (3.3) induced by relaxing the assumption of infinite mass nucleons [69]. Such an assumption was made (implicitly or explicitly) in several points of the calculations done in the previous chapter, which will be now subject to critical examination.

The main effect of considering finite values for the nucleon masses are due to a non vanishing nucleon velocity (and then recoil effect) and to the presence to effective extra nucleon interactions such as weak magnetism.

Recoil effects have been neglected during the calculation of Born rates in the evaluation of the spin summed squared matrix element (Eq. (3.12) is valid only for fixed nucleons) and in the calculation of phase space integrals. The last point (kinematical changes) comes out from the fact that a finite nucleon velocity modifies the energy-momentum conservation relations and then the phase space for the given process changes. In particular, both the statistical distributions (Fermi functions) and the integration limits change with respect to the Born case (note also that Eq. (3.9) is valid only if one neglects recoil effect in $\sum_{\text{spins}} |M|^2$). The most practical implication of considering recoil effects is that it is no more possible to write the reaction rate as a one-dimensional integral, as in Eq. (3.16).

However, recoil effects are not the only ones involved in the finite nucleon mass corrections. Up to the same order of approximation we have also to consider modifications of the effective nucleon weak current due to weak magnetism, and, in general, to interaction terms due to the scalar and pseudoscalar couplings of the nucleons.

In the following section we firstly calculate the dynamical changes in the squared matrix element induced by weak magnetism, scalar and pseudoscalar interactions. Then, in the subsequent section, we will examine kinematical changes induced in the phase space structure of the reaction rates. At first order in T/M_N these two corrections can be treated independently.

4.1 Corrections to the transition amplitude

For definiteness let us consider the process shown in Figure (3.1). At first order in $1/M_N$, the transition amplitude can be written as

$$M = \frac{G_F}{\sqrt{2}}\,\overline{u}_p(p_4)O_\mu u_n(p_2)\,\overline{u}_e(p_3)\gamma^\mu(1-\gamma_5)u_\nu(p_1) \quad , \tag{4.1}$$

where the effective nucleon-nucleon weak coupling is given in general by [70]

$$O_\mu = \gamma_\mu(C_V - C_A\gamma_5) + i\,\frac{f_2}{M_N}\,\sigma_{\mu\nu}\,q^\nu + f_3\,q_\mu + f_{ps}\,\gamma_5\,q_\mu \quad . \tag{4.2}$$

Here q_μ denotes the momentum transfer to the final nucleon and f_2, f_3, f_{ps} are the anomalous weak charged-current magnetic moment, scalar and pseudoscalar couplings of the nucleon, respectively [71]. In general, the couplings C_V, C_A, f_2, f_3, f_{ps} are form-factors, which all depend on q^2. However, at the relevant energy scales for the considered processes, this q^2-dependence can be neglected, being of higher order than $1/M_N$.

With some algebra, one can evaluate the squared modulus of (4.1) summed over all spins. It is very useful, for references to the other processes, to write the resultant expression in terms of the relativistic invariants s, t [1]. With the same notation of section (3.1) we obtain the result reported in appendix E. The expression in (E.1) holds for all the six processes in (3.1), (3.2), (3.3) .

Let us note that in the formula (E.1) we have retained only the leading terms, namely those corresponding to first order in the couplings f_2, f_3 and f_{ps}. Aa a further simplification we can drop out all the terms coming from scalar and pseudoscalar interactions, which are indeed very weak (in the following we then use $f_3 = f_{ps} = 0$)

In Figure 4.1 we plot the "zero temperature" cumulative corrections, i.e. the corrections to the transition amplitude considered here plus the radiative QED corrections evaluated in the previous chapter; for the process $\nu_e + n \to e^- + p$ we have $\Delta\Gamma_R = \Gamma_R - \Gamma_B$

---

[1] The third invariant u has been eliminated through the relation $u = -s - t + M_1^2 + M_2^2 + M_3^2 + M_4^2$ which follows from energy-momentum conservation.

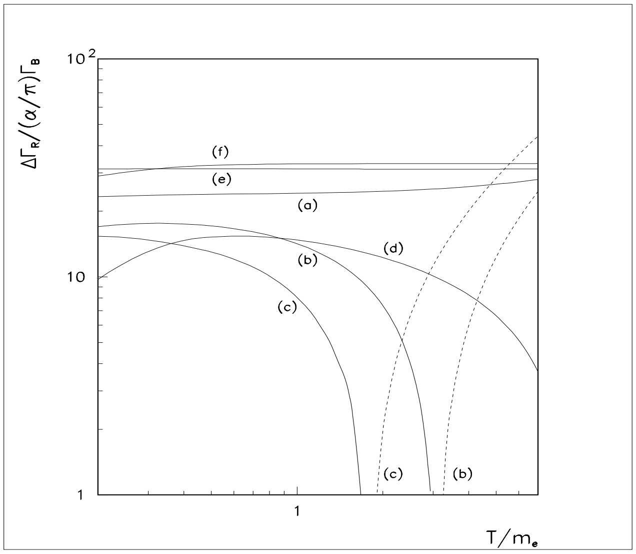

Figure 4.1: “Zero temperature” radiative corrections to the Born rates for the processes in (3.1), (3.2), (3.3) (see text). We use the same notations of chapter 3.

with

$$\begin{aligned}\Gamma_R(\nu_e + n \to e^- + p) &= \frac{1+\delta_\tau}{128\pi^3 M_n}\int_0^\infty dE_1 \int_{E_{inf}}^{E_{sup}} dE_3 \sum_{\text{spins}} |M|^2(E_1,E_3) \\ &\times \; \mathcal{G}(E_1,E_3)\;\mathcal{F}(E_3)\;F_\nu(E_1)\;[1-F_e(E_3)] \quad , \qquad (4.3)\end{aligned}$$

where

$$E_{inf} = \frac{\Big[(M_n+E_1)(M_n^2-M_p^2+m_e^2+2E_1M_n) - 2E_1\xi\Big]}{2M_n(M_n+2E_1)} \quad , \qquad (4.4)$$

$$E_{sup} = \frac{\Big[(M_n+E_1)(M_n^2-M_p^2+m_e^2+2E_1M_n) + 2E_1\xi\Big]}{2M_n(M_n+2E_1)} \quad , \qquad (4.5)$$

$$\xi = \frac{1}{2}\sqrt{\Big[M_n^2-M_p^2-m_e^2+2E_1M_n\Big]^2 - 4m_e^2M_p^2} \quad . \qquad (4.6)$$

The reason for this name is that in the limit of zero temperature these corrections do not vanish, differently from what occurs to the other corrections considered in this thesis. Note that the constant shift correction $\pi\delta_\tau/\alpha$ (see Eq. (3.34)) has been subtracted in order to show the pure radiative and Coulomb effects and finite mass corrections. As we will see, these corrections turn to be the most relevant ones for the Born rates.

4.2 Kinematical corrections

Apart from the dynamical corrections to the squared matrix element calculated in the previous section, there are also other corrections to the reaction rates which are of kinematical nature, arising properly from the finite nucleon velocity. While dynamical corrections are due to the fact that for a slightly moving nucleon the collision probability is higher than for a fixed one, kinematical corrections involve changes in the energy carried off by leptons due to nucleon motion.

It is important to note that the reaction rates (per incident nucleon) intervening in the Boltzmann equations for the calculations of the elemental abundances have to be evaluated in the reference frame of the comoving volume (radiation rest frame).

For definiteness let us consider the reaction $\nu_e + n \rightarrow e^- + p$ whose exact expression for the rate is given by

$$\Gamma(\nu_e + n \rightarrow e^- + p) = \frac{1}{n} \int \frac{d^3\mathbf{p_2}}{(2\pi)^3} \frac{1}{2E_2} F_n(E_2) \left\{ \int \frac{d^3\mathbf{p_4}}{(2\pi)^3} \frac{1}{2E_4} \frac{d^3\mathbf{p_1}}{(2\pi)^3} \frac{1}{2E_1} \frac{d^3\mathbf{p_3}}{(2\pi)^3} \frac{1}{2E_3} \right.$$
$$\left. (2\pi)^4 \, \delta^4(p_1 + p_2 - p_3 - p_4) \sum_{\text{spins}} |M|^2 \right\} F_\nu(E_1) \, (1 - F_e(E_3)) \quad (4.7)$$

(as already discussed, we approximate $1 - F_p(E_4) \simeq 1$), where

$$n = 2 \int \frac{d^3\mathbf{p_2}}{(2\pi)^3} F_n(E_2) \qquad (4.8)$$

is the incident neutron number density. All the quantities in (4.7) are evaluated in the comoving volume reference frame; we denote with a prime the corresponding values in the neutron rest frame (in the infinite nucleon mass limit the two reference frames coincide). If the neutron motion lies along the z-axis, we have

$$\begin{pmatrix} E_2 \\ p_{2z} \end{pmatrix} = \Lambda \begin{pmatrix} E_2' \\ p_{2z}' \end{pmatrix} = \begin{pmatrix} \gamma & \gamma\, u \\ \gamma\, u & \gamma \end{pmatrix} \begin{pmatrix} M_2 \\ 0 \end{pmatrix} \quad , \qquad (4.9)$$

where $u = p_{2z}/M_2$ is the neutron velocity and

$$\gamma = \frac{1}{\sqrt{1 - u^2}} \simeq 1 + \frac{v^2}{2} = 1 + \frac{p_{2z}^2}{2M_2^2} \quad , \qquad (4.10)$$

$$\gamma\, u = \frac{u}{\sqrt{1 - u^2}} \simeq u = \frac{p_{2z}}{M_2} \quad . \qquad (4.11)$$

For the leptons we then obtain

$$\begin{pmatrix} E_{1,3} \\ p_{1,3}^n \end{pmatrix} = \Lambda \begin{pmatrix} E_{1,3}' \\ p_{1,3}^{n\,\prime} \end{pmatrix} = \begin{pmatrix} 1 + \frac{p_{2z}^2}{2M_2^2} & \frac{p_{2z}}{M_2} \\ \frac{p_{2z}}{M_2} & 1 + \frac{p_{2z}^2}{2M_2^2} \end{pmatrix} \begin{pmatrix} E_{1,3}' \\ p_{1,3}^{n\,\prime} \end{pmatrix} \quad , \qquad (4.12)$$

where $p^n_{1,3}$ is the lepton momentum component along neutron motion. In general for the lepton energies we can write

$$E_{1,3} \; \simeq \; E'_{1,3} \, + \, \frac{\mathbf{p_2}\cdot\mathbf{p_{1,3}}}{M_2} \, + \, \frac{\mathbf{p_2}^{\mathbf{2}}}{2M_2^2} \, E'_{1,3} \quad , \tag{4.13}$$

Now, let us note that even if Γ in (4.7) has to be evaluated in the comoving volume reference frame, the quantity in {...} is a Lorentz invariant which takes the same value in any reference frame. We choose to evaluate this quantity in the nucleon rest frame. In this way, the kinematical corrections involve only the quantities outside the braces [2]. The correction to the phase space term is then easily calculated

$$\begin{aligned}
\delta\left(F_\nu\,(1\,-\,F_e)\right) \;&=\; F_\nu(E_1)\;(1\,-\,F(E_3))\;-\;F_\nu(E'_1)\;(1\,-\,F(E'_3))\;\simeq \\
&\simeq\; F_\nu(E'_1)\;(1\,-\,F(E'_3))\left\{\frac{\mathbf{p_2}\cdot\mathbf{p_3}}{M_2\,T}\,F(E'_3)\;-\;\frac{\mathbf{p_2}\cdot\mathbf{p_1}}{M_2\,T_\nu}\;(1\,-\,F_\nu(E'_1))\;+\right.\\
&-\;\frac{1}{2}\left(\frac{\mathbf{p_2}\cdot\mathbf{p_3}}{M_2\,T}\right)^2\;F(E'_3)\;(1\,-\,2F(E'_3))\;+\\
&-\;\frac{\mathbf{p_2}\cdot\mathbf{p_3}\;\mathbf{p_2}\cdot\mathbf{p_1}}{M_2^2\,T\,T_\nu}\,F(E'_3)\;(1\,-\,F_\nu(E'_1))\;+\\
&-\;\frac{1}{2}\left(\frac{\mathbf{p_2}\cdot\mathbf{p_1}}{M_2\,T}\right)^2\;(1\,-\,F_\nu(E'_1))\;(1\,-\,2F_\nu(E'_1))\;+\\
&\left.+\;\frac{\mathbf{p_2}^{\mathbf{2}}}{2M_2^2T}\,E'_3\,F(E'_3)\;-\;\frac{\mathbf{p_2}^{\mathbf{2}}}{2M_2^2T}\,E'_1\;(1\,-\,F_\nu(E'_1))\right\} \quad .
\end{aligned} \tag{4.14}$$

It is here appropriate to approximate the neutron distribution function with a Boltzmann function

$$F_n(E_2) \;=\; \frac{1}{e^{\frac{E_2}{T}}\,+\,1} \;\simeq\; e^{-\frac{E_2}{T}} \;\simeq\; e^{-\frac{M_2}{T}}\,e^{-\frac{\mathbf{p_2}^{\mathbf{2}}}{2M_2T}} \quad , \tag{4.15}$$

thus the correction to the rate for the considered reaction is

$$\begin{aligned}
\delta\Gamma\;(\,\nu_e\;n\rightarrow e^-\,p)\;\simeq\;\frac{1}{n}\int\frac{d^3\mathbf{p_2}}{(2\pi)^3}\,\frac{1}{2E_2}\,e^{-\frac{M_2}{T}}\,e^{-\frac{\mathbf{p_2}^{\mathbf{2}}}{2M_2T}}\left\{\int\frac{d^3\mathbf{p_4}}{(2\pi)^3}\,\frac{1}{2E_4}\,\frac{d^3\mathbf{p_1}}{(2\pi)^3}\,\frac{1}{2E_1}\right.\\
\left.\frac{d^3\mathbf{p_3}}{(2\pi)^3}\,\frac{1}{2E_3}\,(2\pi)^4\,\delta^4(p_1+p_2-p_3-p_4)\sum_{\text{spins}}|M|^2\right\}\,\delta\left(F_\nu\,(1\,-\,F_e)\right) \quad .
\end{aligned} \tag{4.16}$$

Since the expression in {...} does not depend on neutron momentum (see the above discussion), it is very convenient to perform first the integration over this quantity. First order terms in (4.14) do not contribute, since

---

[2] Note that even if the quantity in {...} is an invariant, nevertheless the integration limits, in general, change their values allowing changes in the phase space due to neutron motion. However, we only want to calculate the leading kinematical correction contribution, thus we have to consider only corrections coming from the terms outside braces, while the quantities inside them (including the integration limits) have to be calculated in the infinite nucleon mass approximation.

$$\int \frac{d^3\mathbf{p_2}}{(2\pi)^3}\,\frac{1}{2M_2}\,e^{-\frac{M_2}{T}}\,e^{-\frac{\mathbf{p_2}^{\mathbf{2}}}{2M_2T}}\,p_{2i} \;=\; 0 \quad , \tag{4.17}$$

for symmetry reasons. Instead for second order terms we have

$$\begin{aligned} \frac{1}{n}\int \frac{d^3\mathbf{p_2}}{(2\pi)^3}\,\frac{1}{2M_2}\;\; e^{-\frac{M_2}{T}}\,e^{-\frac{\mathbf{p_2}^{\mathbf{2}}}{2M_2T}}\,p_{2i}\,p_{2j} \;\simeq\; \frac{\int \frac{d^3\mathbf{p_2}}{(2\pi)^3}\,\frac{p_{2i}\,p_{2j}}{2M_2}\,e^{-\frac{\mathbf{p_2}^{\mathbf{2}}}{2M_2T}}}{2\,\int \frac{d^3\mathbf{p_2}}{(2\pi)^3}\,e^{-\frac{\mathbf{p_2}^{\mathbf{2}}}{2M_2T}}} \;= \\ =\;\; \frac{1}{2}\,\delta_{ij}\,\frac{\int \frac{d^3\mathbf{p_2}}{(2\pi)^3}\,\frac{p_{2i}^2}{2M_2}\,e^{-\frac{\mathbf{p_2}^{\mathbf{2}}}{2M_2T}}}{2\,\int \frac{d^3\mathbf{p_2}}{(2\pi)^3}\,e^{-\frac{\mathbf{p_2}^{\mathbf{2}}}{2M_2T}}} \;=\; \frac{T}{4}\,\delta_{ij} \quad , \end{aligned} \tag{4.18}$$

hence Eq. (4.16) now becomes

$$\begin{aligned} \delta\Gamma(\nu_e\; n \to e^-\, p) \;\;\simeq\;\; & \int \frac{d^3\mathbf{p_4}}{(2\pi)^3}\,\frac{1}{2E_4}\,\frac{d^3\mathbf{p_1}}{(2\pi)^3}\,\frac{1}{2E_1}\,\frac{d^3\mathbf{p_3}}{(2\pi)^3}\,\frac{1}{2E_3}\,\cdot \\ & \cdot\;\; (2\pi)^4\,\delta^4(p_1+p_2-p_3-p_4)\,\sum_{\text{spins}} |M|^2\;\delta\Phi \quad , \end{aligned} \tag{4.19}$$

with

$$\begin{aligned} \delta\Phi \;\;=\;\; & \frac{T}{4M_2^2}\left(-\frac{1}{2}\,\frac{\mathbf{p_3}^{\mathbf{2}}}{T^2}\,F(E_3')\;(1\,-\,2F(E_3'))\;-\;\frac{\mathbf{p_1'}\!\cdot\!\mathbf{p_3'}}{TT_\nu}\,F(E_3')\;(1\,-\,F_\nu(E_1'))\;+\right. \\ & +\;\frac{1}{2}\,\frac{\mathbf{p_1}^{\mathbf{2}}}{T_\nu^2}\;(1\,-\,F_\nu(E_1'))\;(1\,-\,2F_\nu(E_1'))\;+\;\frac{3}{2}\,\frac{E_3'}{T}\,F(E_3')\;+ \\ & \left.-\;\frac{3}{2}\,\frac{E_1'}{T_\nu}\;(1\,-\,F_\nu(E_1'))\right) \quad , \end{aligned} \tag{4.20}$$

and $\sum_{\text{spins}} |M|^2$ is given by the expression in (3.12). As in section (3.1), the integration over the proton 3-momentum can be eliminated by using the $\delta^3(\mathbf{p_1}\,+\,\mathbf{p_2}\,-\,\mathbf{p_3}\,-\,\mathbf{p_4})$, whereas the neutrino energy integration (for approximatively massless neutrinos) through the energy δ-function. Also integration over angles can be analytically performed (only the one over electron-neutrino angle is now non trivial). The result is

$$\begin{aligned} \Delta\Gamma_K(\nu_e\; n \to e^-\, p) \;\;=\;\; & \frac{G_F^2(c_V^2+3c_A^2)}{2\pi^3}\left(\frac{T}{2M_n}\right)\int dp_3\; p_3^2\, Q^2\, \theta(Q)\, F_\nu(Q)\;(1-F(E_3))\,\cdot \\ \cdot\;\; & \left[\frac{Q^2}{T_\nu^2}(1-F_\nu(Q))(1-2F_\nu(Q)) - \frac{p_3^2}{T^2}F(E_3)(1-2F(E_3)) + \right. \\ +\;\; & 3\frac{E_3}{T}F(E_3) - 3\frac{Q}{T_\nu}(1-F_\nu(Q)) - 3\;+ \\ +\;\; & \left.\left(\frac{c_A^2-c_V^2}{c_V^2+3c_A^2}\right)\left(\frac{2p_3^2Q}{3TT_\nu E_3}\right)F(E_3)(1-F_\nu(Q))\right] \quad , \end{aligned} \tag{4.21}$$

where we have used the same notation of section (3.1). The above expression for $\Delta\Gamma_K(\nu_e + n \rightarrow e^- + p)$ cannot be extended to all reactions of (3.1), (3.2), (3.3) by simply using the substitution rules of Table 3.1. This is due to the different form of the statistical factors involved in the corresponding expressions of (4.7). However, it is easy to find that the factor in square brackets must be replaced as follows. First of all, note that for the reaction $\overline{\nu}_e + p \rightarrow e^+ + n$ this factor is the same as in (4.21). Differently, for $e^- + p \rightarrow \nu_e + n$ and $e^+ + n \rightarrow \overline{\nu}_e + p$, one has

$$\begin{aligned} \Bigg[& -3 - \frac{Q^2}{T_\nu^2} F_\nu(Q)\left[1 - 2F_\nu(Q)\right] + \frac{{p_3}^2}{T^2}\left[1 - F(E_3)\right]\left[1 - 2F(E_3)\right] + 3\frac{Q}{T_\nu} F_\nu(Q) \\ & -3\frac{E_3}{T}\left[1 - F(E_3)\right] + \left(\frac{{C_A}^2 - {C_V}^2}{\left({C_V}^2 + 3{C_A}^2\right)}\right)\left(\frac{2{p_3}^2 Q}{3TT_\nu E_3}\right) F_\nu(Q)\left[1 - F(E_3)\right] \Bigg] \quad , \end{aligned} \tag{4.22}$$

while for $n \rightarrow e^- + \overline{\nu}_e + p$

$$\begin{aligned} \Bigg[& -3 - \frac{Q^2}{T_\nu^2} F_\nu(Q)\left[1 - 2F_\nu(Q)\right] - \frac{{p_3}^2}{T^2} F(E_3)\left[1 - 2F(E_3)\right] + 3\frac{q}{T_\nu} F_\nu(Q) \\ + \quad & 3\frac{E_3}{T} F(E_3) - \left(\frac{{C_A}^2 - {C_V}^2}{\left({C_V}^2 + 3{C_A}^2\right)}\right)\left(\frac{2{p_3}^2 Q}{3TT_\nu E_3}\right) F(E_3) F_\nu(Q) \Bigg] \quad . \end{aligned} \tag{4.23}$$

Finally for $e^- + \overline{\nu}_e + p \rightarrow n$

$$\begin{aligned} \Bigg[& -3 + \frac{Q^2}{T_\nu^2}\left[1 - F_\nu(Q)\right]\left[1 - 2F_\nu(Q)\right] + \frac{{p_3}^2}{T^2}\left[1 - F(E_3)\right]\left[1 - 2F(E_3)\right] - 3\frac{Q}{T_\nu}\left[1 - F_\nu(Q)\right] \\ - \quad & 3\frac{E_3}{T}\left[1 - F(E_3)\right] - \left(\frac{{C_A}^2 - {C_V}^2}{\left({C_V}^2 + 3{C_A}^2\right)}\right)\left(\frac{2{p_3}^2 Q}{3TT_\nu E_3}\right)\left[1 - F(E_3)\right]\left[1 - F_\nu(Q)\right] \Bigg] \quad . \end{aligned} \tag{4.24}$$

We report the results in Figure 4.2 in the form of the ratio $\Delta\Gamma_K/(\alpha/\pi)\Gamma_B$ for comparison with the other corrections which are of order α. Note that in the entire temperature range relevant for nucleosynthesis the dominant corrections are positive and apply to the scattering reactions (b), (d).

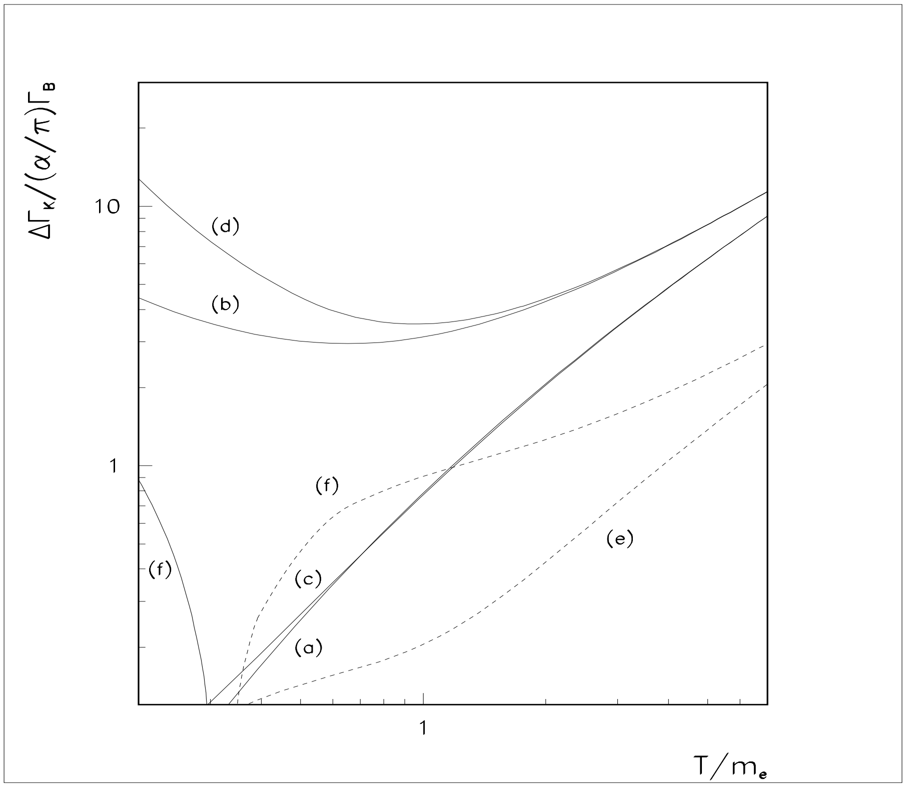

Figure 4.2: The ratio $\Delta\Gamma_K/(\alpha/\pi)\Gamma_B$. Dashed lines correspond to negative values and labels refer to reactions in (3.1), (3.2), (3.3) .

Chapter 5

QED thermal radiative corrections

The reaction rates for the processes in (3.1), (3.2), (3.3) strongly depend whether they take place in vacuum or in a heat bath at given temperature T. The most important contribution comes from the density of states in the integration over phase space. This has been already taken into account in the previous chapters for the calculation of the rates in the Born approximation and of the finite nucleon mass corrections. However, there are also a number of effects [33], [72] - [84] induced by a $T \neq 0$ background which have to be considered; they are usually referred to as thermal radiative corrections.

Since the temperature range of interest for BBN is around $1\, MeV$, the most significative thermal radiative corrections to the processes in (3.1), (3.2), (3.3) arise in the context of QED. First of all, if the particles entering in the given process propagate in a heat bath, they in general acquire an effective thermal mass induced by coherent interactions with the medium (in particular with the photons in the bath). The Feynman diagrams to be considered in this case are reported in Figure 5.1 for the process (3.1).
Moreover, wavefunction renormalization caused by $T \neq 0$ background has to be taken into account as well. Finally, there are vertex corrections mediated by the exchange of a photon in the bath; they are sketched in Figure 5.2. These corrections contain infrared divergences, which have to be eliminated via the inclusion of corrections coming from the spontaneous and induced emission and absorption of thermal photons, as described by the diagrams in Figure 5.3.

All these effects will be here considered at order α. While we have to evaluate the square of the diagrams in Figure 5.3, for the mass shift and vertex corrections only the interference of the diagrams in Figure 5.1 and 5.2 with the Born graph in Figure 3.1 will

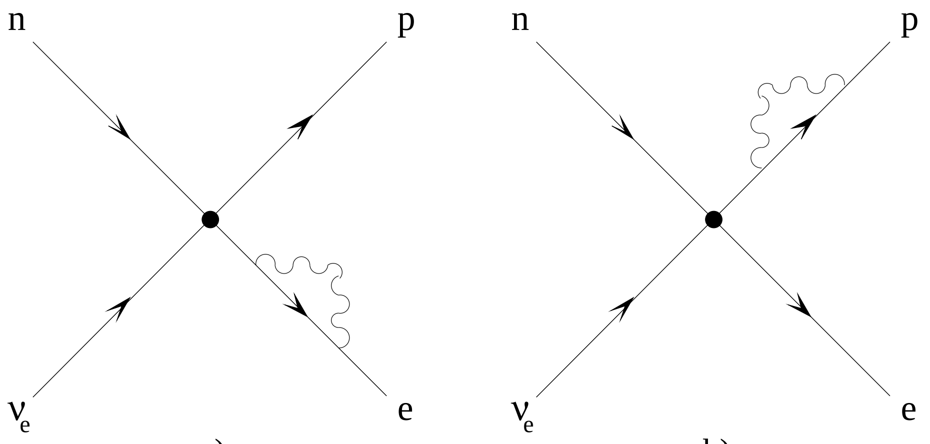

a) b)

Figure 5.1: The Feynman diagrams for mass shift and wavefunction renormalization for the process in (3.1).

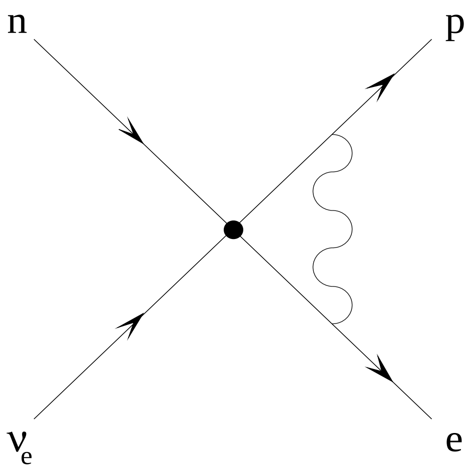

Figure 5.2: The Feynman diagram for vertex correction for the process in (3.1).

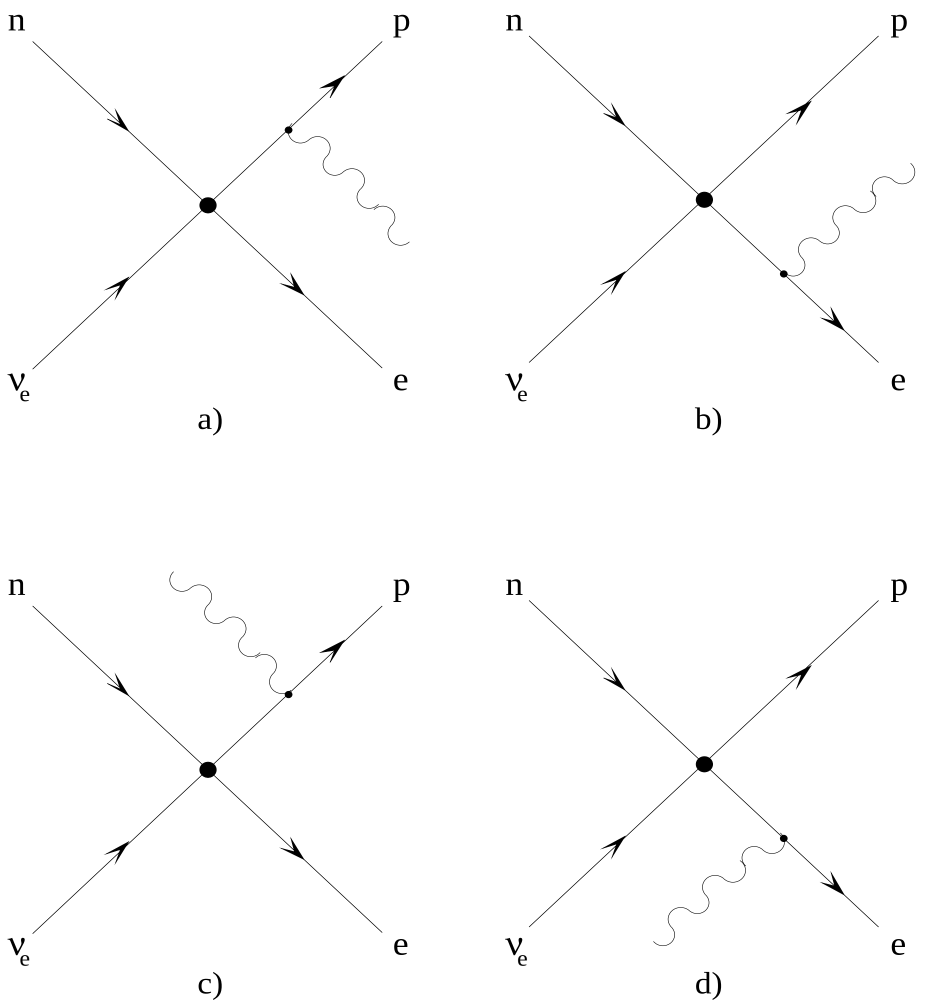

Figure 5.3: Photon emission and absorption diagrams for the process in (3.1).

give contribution of order α. Note that we have considered only electromagnetic interactions of electrons and protons interacting with the particles in the plasma through their electric charge; this gives indeed the main contribution to the effect we are considering. Moreover, since these effects already contribute as corrections to the Born rates, they will be calculated in the infinite nucleon mass approximation. In particular we will adopt the nucleon rest frame.

Finally, the modified dispersion relation for $e^{\pm}$ and photons also call for corrections to the thermodynamic quantities (energy density, pressure and so on) [85] calculated in chapter 1, which are relevant for the BBN itself.

All these effects will be considered in this chapter; in particular in the following four sections we focus on the thermal radiative corrections to the Born rates for the reactions in (3.1), (3.2), (3.3) , while in the last section we consider finite temperature QED corrections to the relevant thermodynamic quantities. Note, however, that since we are looking only for the main contributions coming from these radiative corrections, we can safely assume, throughout this chapter, a negligible electron chemical potential, which is usually, in fact, a small quantity.

Our calculations will be carried out in the framework of the real time formalism (RTF) [86] of the finite temperature and density quantum field theory [87, 88], an account of which is given in appendix F.

5.1 Mass shift correction

Due to interactions with the particles in the plasma, an electron (or a proton [1]) acquires an effective mass depending on the temperature of the bath. Therefore, the mass parameter entering in the expressions for the decay rates should be substituted with its effective value, which has been explicitly calculated in the appendix F.

We focus on the reaction $\nu_e + n \rightarrow e^- + p$ (see Figure 5.1), whose Born rate is given in Eq. (3.16); in this expression, according to (F.33) (see appendix F), we have to substitute

---

[1] Since electrons and protons, at a first approximation, have equal electromagnetic interactions, the self-energy terms for these two particles are equal. However, the mass shift correction for protons is much less important than that for electrons because of their large (vacuum) mass. We are only interested in leading terms and so we disregard proton mass shift corrections.

$E_3 \rightarrow E_3 + \mu$ and, correspondingly,

$$Q \rightarrow Q + \mu \quad , \tag{5.1}$$

in all quantities appearing in (3.16). With the same notation of the appendix F, the parameter μ is given by

$$\mu = \frac{\alpha}{\pi} \left\{ \frac{\pi^2}{3} \frac{T^2}{E_3} + \frac{2}{E_3} \int_0^\infty dk \, \frac{k}{E} F(E) + \frac{m_e^2}{2E_3 p_3} \int_0^\infty dk \frac{k}{E} F(E) \, (\log A - \log B) \right\} \tag{5.2}$$

with $E \equiv \sqrt{k^2 + m_e^2}$, $E_3 \equiv \sqrt{p_3^2 + m_e^2}$ and A, B are reported in (F.26). The mass shift correction we then obtain is

$$\begin{aligned} \Delta\Gamma_M \, (\nu_e + n \rightarrow e^- + p) &= \frac{G_F^2 \left({C_V}^2 + 3{C_A}^2 \right)}{2\pi^3} \int dp_3 \, p_3^2 \, \theta(Q) \cdot \\ &\cdot \left\{ (Q+\mu)^2 \, F_\nu(Q+\mu) \, (1 - F(E_3+\mu)) - Q^2 \, F_\nu(Q) \, (1 - F(E_3)) \right\} \quad , \end{aligned} \tag{5.3}$$

Expanding in the variable μ, at first order in α we finally get

$$\begin{aligned} \Delta\Gamma_M(\nu_e \, n \rightarrow e^- \, p) &= \frac{G_F^2 \left({C_V}^2 + 3{C_A}^2 \right)}{2\pi^3} \cdot \int dp_3 \, p_3^2 \, Q^2 \, \mu \, \theta(Q) \, F_\nu(Q) \, (1 - F(E_3)) \cdot \\ &\cdot \left(\frac{2}{Q} + \frac{F(E_3)}{T} - \frac{F_\nu(-Q)}{T_\nu} \right) \end{aligned} \tag{5.4}$$

Similar expressions for the other reactions in (3.1), (3.2), (3.3) can be easily found by using the substitutions of Table 3.1 and replacing the factor

$$\left(\frac{2}{Q} + \frac{F(E_3)}{T} - \frac{F_\nu(-Q)}{T_\nu} \right) \quad , \tag{5.5}$$

in the above expression as follows. This factor applies to the reaction $\overline{\nu}_e + p \rightarrow e^+ + n$ as well. For $e^- + p \rightarrow \nu_e + n$ and $e^+ + n \rightarrow \overline{\nu}_e + p$, we have instead

$$\left(\frac{2}{Q} - \frac{1 - F(E_3)}{T} + \frac{F_\nu(Q)}{T_\nu} \right) \quad , \tag{5.6}$$

while for $n \rightarrow e^- + \overline{\nu}_e + p$

$$\left(-\frac{2}{Q} + \frac{F(E_3)}{T} - \frac{F_\nu(Q)}{T_\nu} \right) \quad , \tag{5.7}$$

and $e^- + \overline{\nu}_e + p \rightarrow n$

$$\left(-\frac{2}{Q} - \frac{1 - F(E_3)}{T} + \frac{1 - F_\nu(Q)}{T_\nu} \right) \quad . \tag{5.8}$$

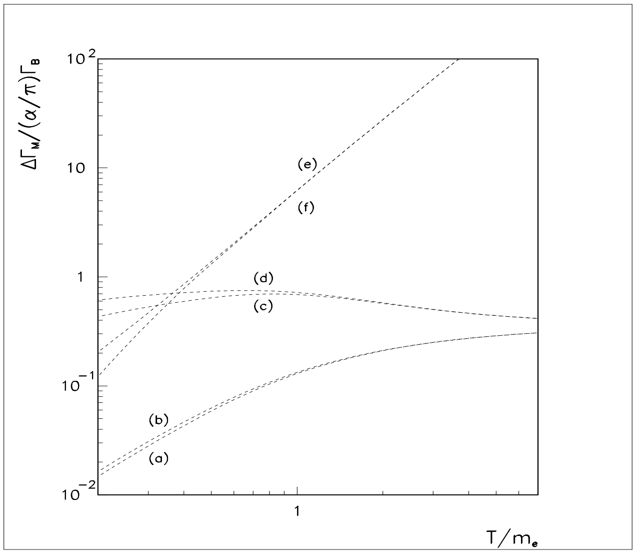

Figure 5.4: The ratio $\Delta\Gamma_M/(\alpha/\pi)\Gamma_B$. Dashed lines correspond to negative values and labels refer to reactions in (3.1), (3.2), (3.3) .

In Figure 5.4 the ratio $\Delta\Gamma_M/(\alpha/\pi)\Gamma_B$ is reported as a function of the (photon) temperature T for the six reactions in (3.1), (3.2), (3.3) . Note that mass shift corrections are negative for all these reactions and decreasing (in absolute value) with decreasing T for (a), (b), (e), (f) while they are almost constant for (c), (d) in the temperature range relevant for nucleosynthesis.

5.2 Wavefunction renormalization correction

The same diagrams in Figure 5.1 leading to mass shift corrections also contribute to wavefunction renormalization corrections. For definiteness we consider in detail the reaction (3.1). As studied in appendix F, the amplitude is again given by (3.11), but when we compute $\sum_{\text{spins}} |M|^2$ we have to replace the projectors $\Lambda_0^{\pm}$ with the renormalized ones, according to (F.34). With the same notation of chapter 3 we obtain the following expression for the correction to the decay rate:

$$\Delta\Gamma_W(\nu_e + n \to e^- + p) = \frac{G_F^2 \left({C_V}^2 + 3{C_A}^2\right)}{2\pi^3} \int dp_3\, p_3^2\, Q^2\, \theta(Q)\lambda\, F_\nu(Q)\,(1 - F(p_3)) \quad (5.9)$$

where the parameter λ is reported in the appendix F. Note that, in the non-relativistic limit for the nucleons, which we here adopt, the second term in (F.42) contribute to the correction $\Delta\Gamma_W$ with a term which vanishes after the angular integration is performed. From relations (F.9)-(F.11) it is easy to show that

$$\lambda \;=\; \frac{1}{\omega}\left\{-\,\left(\hat{T}_u^B \,+\, \hat{T}_u^F\right) \,+\, \left(\hat{T}_p^{B\prime} \,+\, \hat{T}_p^{F\prime}\right) \,+\, m_e\,\left(\hat{c}_B' \,+\, \hat{c}_F'\right)\right\} \tag{5.10}$$

The quantities $\hat{T}_u^B$, $\hat{T}_u^F$ can be immediately read off by Eqs. (F.15), (F.18) by substituting $p_0 = E_3$. Furthermore $T_p^{B\prime}$, $T_p^{F\prime}$, c_B', c_F' may be calculated by differentiating Eqs. (F.14), (F.17), (F.16), (F.19) with respect to p_0 prior the integration in dx is performed. After some algebra, the final result is

$$\begin{aligned}\lambda \;&=\; \frac{2\alpha}{\pi}\int dk\,\frac{B(k)}{k} \,-\, \frac{\alpha\,\pi\,T^2}{6\,E_3\,p_3}\,\ln\frac{E_3\,+\,p_3}{E_3\,-\,p_3} \,+ \\ &-\; \frac{\alpha}{2\pi\,E_3\,p_5}\int dk\,\frac{k}{E}\,F(E)\,\left((E_3\,+\,E)\,\ln A \,-\, (E_3\,-\,E)\,\ln B\right) \,+ \\ &-\; \frac{2\alpha}{\pi}\int dk\,\frac{k^2}{E}\,\frac{1}{p_3^2-k^2}\,F(E)\end{aligned} \tag{5.11}$$

Note that the first term in (5.11) is infrared divergent. This term, together with another similar divergent one coming from considering vertex corrections (see the following section), is cancelled by an opposite term provided by the photon and emission rate discussed in section 5.4. The collinear divergence still present in (F.38) for $p_3 = k$, together with a similar contribution from the vertex correction is also compensated by bremsstrählung diagrams.

The extension of (5.9) to the other processes in (3.1), (3.2), (3.3) can be straightforwardly obtained by using Table 3.1.

The results for $\Delta\Gamma_W/(\alpha/\pi)\Gamma_B$ are plotted in Figure 5.5. Also these corrections are negative for all the six reactions in (3.1), (3.2), (3.3) , and are monotonically decreasing with decreasing T.

5.3 Vertex correction

The vertex correction to the Born rate for the process $\nu_e \,+\, n \,\to\, e^- \,+\, p$ is given by the diagram in Figure 5.2, whose amplitude is

$$\begin{aligned}M_V \;&=\; i\,\frac{G_F}{\sqrt{2}}\int\frac{d^4k}{(2\pi)^4}\,\overline{u}_p(p_4)\,(ie\gamma^\rho)\,S_p(p_4+k)\,\gamma^\mu(C_V - C_A\gamma_5)\,u_n(p_2)\,\times \\ &\times\;\; iD_{\rho\sigma}(k)\,\overline{u}_e(p_3)\,(ie\gamma^\sigma)\,S_e(p_3-k)\,\gamma_\mu(1-\gamma_5)\,u_{\nu_e}(p_1) \quad ,\end{aligned} \tag{5.12}$$

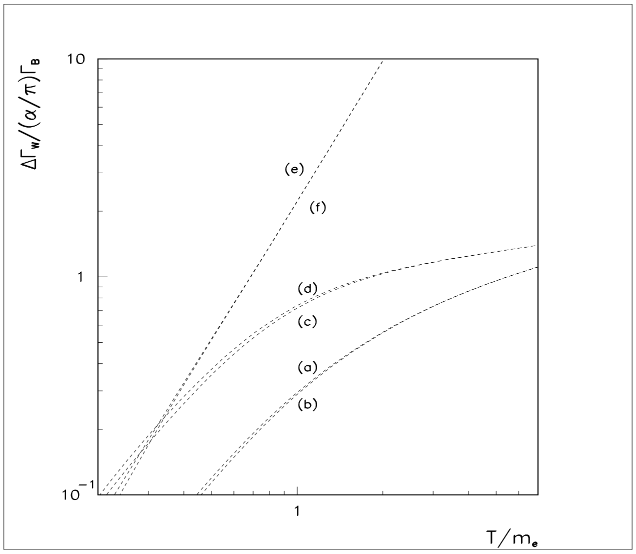

Figure 5.5: The ratio $\Delta\Gamma_W/(\alpha/\pi)\Gamma_B$. Dashed lines correspond to negative values and labels refer to reactions in (3.1), (3.2), (3.3) .

where S_F $(F = e, p)$ and $D_{\rho\sigma}$ are the real time formalism fermion and photon propagators respectively, reported in the Appendix F. After some algebra, and using the Dirac equation for the proton, M_V can be cast in the form

$$M_V \;=\; \frac{i\,G_F\,e^2}{\sqrt{2}\,(2\pi)^3}\left\{I_1\,A_\mu\,B^\mu \;+\; \frac{1}{2}\,I_2^{\rho\lambda}\,A^\mu\,B_{\rho\lambda\mu} \;+\; \frac{1}{2}\,I_3^{\rho\lambda}\,A_{\rho\lambda\mu}\,B^\mu \;+\; \frac{1}{4}\,I_4{}^{\lambda}{}_{\sigma}\,A^{\rho\sigma\mu}\,B_{\rho\lambda\mu}\right\} \tag{5.13}$$

where

$$\begin{aligned}
A^\mu &= \overline{u}_p\,\gamma^\mu(C_V - C_A\gamma_5)\,u_n \quad , \\
A^{\rho\sigma\mu} &= \overline{u}_p\,\gamma^\rho\,\gamma^\sigma\,\gamma^\mu(C_V - C_A\gamma_5)\,u_n \quad , \\
B^\mu &= \overline{u}_e\,\gamma^\mu(1-\gamma_5)\,u_{\nu_e} \quad , \\
B^{\rho\sigma\mu} &= \overline{u}_e\,\gamma^\rho\,\gamma^\sigma\,\gamma^\mu(1-\gamma_5)\,u_{\nu_e} \quad ,
\end{aligned}$$

and

$$\begin{aligned}
I_1 &= -p_4{\cdot}p_3\int d^4k\left(\frac{\delta(k^2)}{p_4{\cdot}k\,p_3{\cdot}k}B(k_0) + \frac{4\delta(k^2-m_e^2)\,F(k_0)}{(k+p_3)^2\,((p_4+p_3+k)^2-M^2)}\right) \quad , \\
I_2^{\rho\lambda} &= 4p_4^\rho\int d^4k\,\frac{\delta(k^2-m_e^2)\,F(k_0)\,(p_3+k)^\lambda}{(k+p_3)^2\,((p_4+p_3+k)^2-M^2)} \quad ,
\end{aligned}$$

$$
\begin{aligned}
I_3^{\rho\lambda} &= -4 p_3\!/\rho \int d^4k \, \frac{\delta(k^2 - m_e^2)\, F(k_0)\, (p_3 + k)^\lambda}{(k+p_3)^2\, ((p_4 + p_3 + k)^2 - M^2)} \quad , \\
I_4^{\lambda\sigma} &= \int d^4k \left(\frac{\delta(k^2)\, k^\lambda\, k^\sigma}{p_4{\cdot}k\, p_3{\cdot}k} B(k_0) \; + \; \frac{4\delta(k^2 - m_e^2)\, F(k_0)\, (p_3 + k)^\lambda\, (p_3 + k)^\sigma}{(k+p_3)^2\, ((p_4 + p_3 + k)^2 - M^2)} \right) \quad .
\end{aligned}
$$

The order α vertex correction to the Born rate is provided by the interference term of the diagram in Figure 5.2 with the tree level diagram in Figure 3.1,

$$
M_V\, M_B^* \; + \; M_V^*\, M_B \quad , \tag{5.14}
$$

where M_B is the Born expression (3.11)

$$
M_B \; = \; i\, \frac{G_F}{\sqrt{2}}\, A_\mu\, B^\mu \quad . \tag{5.15}
$$

After some lengthy calculations, the final result for the vertex correction we obtain is

$$
\begin{aligned}
\Delta\Gamma_V(\nu_e + n \to e^- + p) &= \frac{G_F^2(\left({C_V}^2 + 3{C_A}^2\right))}{2\pi^3}\, \frac{\alpha}{\pi} \int_0^\infty dp_3 \; p_3 \int_0^\infty \; dk \; k \; Q^2 \; \theta(Q) \\
\times F_\nu(Q) \;\; [1 - F(E_3)] \;\; \frac{F(E)}{E} & \left\{ \frac{E}{E_3 + E} \log A + \frac{E}{E_3 - E} \log B - \frac{2kp_3}{p_3^2 - k^2} \right\} . \quad .
\end{aligned} \tag{5.16}
$$

Note that we have only reported the non infrared divergent part (as for $\Delta\Gamma_W$, the infrared one comes from the Bose terms only, and will be cancelled by the bremsstrählung contribution) [2].

The expression in (5.16) is extended to the other processes in (3.1), (3.2), (3.3) by using the Table 3.1, and the plot for these corrections is reported in Figure 5.6. Note that for the scattering reactions (a), (b), (c), (d) the vertex corrections are positive in the relevant temperature range, while for (e), (f) the dominant contribution is negative.

5.4 Photon emission and absorption

In the primordial plasma, in which an electromagnetic component is present, spontaneous and induced photon emission as well as photon absorption take place, so that when considering a given process such as the one corresponding to the diagram in Figure 3.1, the bremsstrählung processes depicted by the diagrams in Figures 5.3 must be included as well. These also cancel the infrared divergences due to the radiative diagrams of Figure

---

[2] Note that the result for the vertex correction quoted in [72] as Eq. (11) has a missing factor $1/E$.

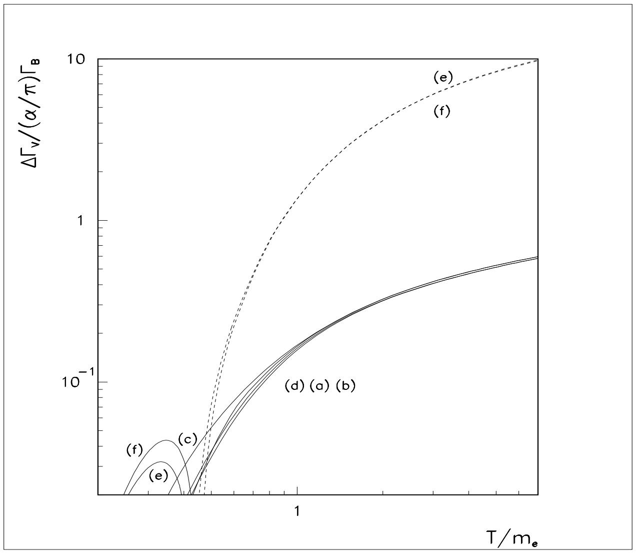

Figure 5.6: The ratio $\Delta\Gamma_V/(\alpha/\pi)\Gamma_B$. Dashed lines correspond to negative values and labels refer to reactions in (3.1), (3.2), (3.3) .

5.1, 5.2 corresponding to wavefunction and vertex renormalizations.

The matrix element for the emission processes in Figures 5.3 is the following:

$$\begin{aligned} M^e_\gamma &= \frac{i\,G_F}{\sqrt{2}}\,\{\overline{u}_p(p_4)\,\gamma^\mu(C_V - C_A\gamma_5)\,u_n(p_2)\,\overline{u}_e(p_3)\,(ie\gamma^\alpha)\,S_e(p_3+k)\,\gamma_\mu(1-\gamma_5)\,u_{\nu_e}(p_1) + \\ &- \overline{u}_p(p_4)\,(ie\gamma^\alpha)\,S_p(p_4+k)\,\gamma^\mu(C_V - C_A\gamma_5)\,u_n(p_2)\,\overline{u}_e(p_3)\,\gamma^\mu(1-\gamma_5)\,u_{\nu_e}(p_1)\}\,\epsilon^\alpha_\lambda(k) \end{aligned}$$

while a similar expression, M^a_γ, holds for the absorption processes. In order to simplify the compuatation of the spin summed squared matrix element, one can subtract from the beginning the infrared divergent terms coming from the propagators. They are all proportional to the Born $\sum_{\text{spins}}|M|^2$ and will cancel the divergences in $\Delta\Gamma_W$ and $\Delta\Gamma_V$. Note also that, for kinematical reasons, only the $T=0$ part in the propagators contribute to the amplitude.

After some extensive calculations, we obtain the following finite contribution to the rate $\Delta\Gamma_\gamma = \Delta\Gamma^e_\gamma + \Delta\Gamma^a_\gamma$

$$\Delta\Gamma_\gamma(\nu_e + n \to e^- + p) = \frac{G_F^2(\left({C_V}^2 + 3{C_A}^2\right))}{2\pi^3}\frac{\alpha}{\pi}\int_0^\infty dp_3\int_0^\infty dk\,\frac{p_3^2}{E_3}\,B(k)$$

$$\times\;[1-F(E_3)]\,\left\{-\left[\frac{2E_3}{k} - \frac{E_3^2}{kp_3}\log\left(\frac{E_3+p_3}{E_3-p_3}\right)\right]\left[\widetilde{Q}^2_+ + \widetilde{Q}^2_- - 2\widetilde{Q}^2\right]\right.$$

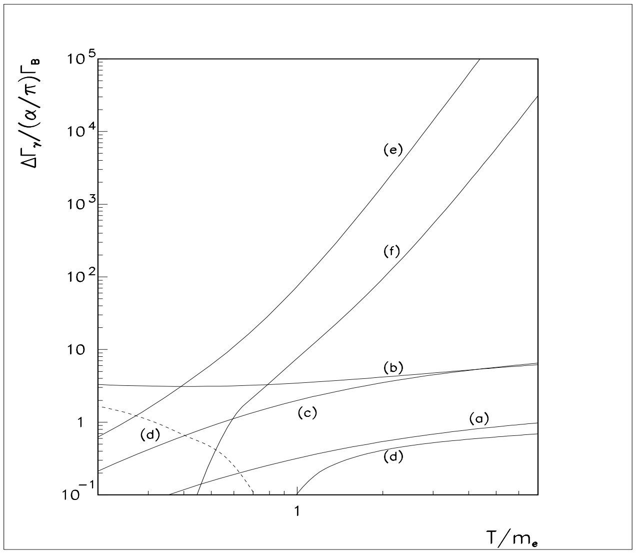

Figure 5.7: The ratio $\Delta\Gamma_\gamma/(\alpha/\pi)\Gamma_B$. Dashed lines correspond to negative values and labels refer to reactions in (3.1), (3.2), (3.3) .

$$- \left[2\xi - \frac{E_3}{p_3}\log\left(\frac{E_3+p_3}{E_3-p_3}\right)\right]\left[\widetilde{Q}_+^2 - \widetilde{Q}_-^2\right] + \frac{k}{2p_3}\log\left(\frac{E_3+p_3}{E_3-p_3}\right)\left[\widetilde{Q}_+^2 + \widetilde{Q}_-^2\right]\Bigg\}, \tag{5.17}$$

where $\widetilde{Q}_\pm^2 \equiv (Q\pm k)^2 F_\nu(Q\pm k)\ \theta(Q\pm k)$, $\widetilde{Q}^2 \equiv Q^2 F_\nu(Q)\ \theta(Q)$ and $S = 1$ [3].

For the other processes in (3.1), (3.2), (3.3) we have to use the Table 3.1 and set $\xi = 1$ for $\nu_e + n \leftrightarrow e^- + p$ and $n \leftrightarrow e^- + \overline{\nu}_e + p$, and $\xi = 0$ for $e^+ + n \leftrightarrow \overline{\nu}_e + p$.

The results for $\Delta\Gamma_\gamma/(\alpha/\pi)\Gamma_B$ are reported in Figure 5.7. It is easy to realize, from this figure, that photon emission and absorption contribution to the thermal radiative corrections for neutron decay and the inverse process is the dominant one (and positive) in the temperature range relevant for nucleosynthesis. This is simply understood since the inclusion of the process $\gamma + n \rightarrow e^- + \overline{\nu}_e + p$ greatly increases the neutron decay rates, otherwise strongly suppressed by phase space.

---

[3] Also here we must note that our result corrects Eq. (13) in Ref. [72] for the photon emission and absorption correction previously calculated.

5.5 Corrections to the equation of state

The temperature dependent effective mass of electrons and positrons in the primordial plasma affects the calculations of the thermodynamic quantities like particle number density, energy density, pressure and entropy, which directly enter in the evolution equations for the light element abundances (see section 2.4), as well as in the weak decay rates as discussed in section 5.1. In addition, also the induced effective photon mass has to be taken into account. The modified dispersion relations of $e^{\pm}$, γ have been calculated in appendix F, and they must be used (instead of the vacuum dispersion relations) in the evaluations of the quantities in (1.48)-(1.50).

The relevant quantities to be considered are the $e^{\pm}$, γ energy densities, entering in Eqs. (2.44) and (2.60), and pressure, which enter directly in the Eq. (2.60) for entropy density. Corrections to electron and positron number densities are also present in general, but, since in the electric charge conservation equation (2.46) only their difference is relevant, this results into a correction to the electron chemical potential. This is, generally, a small quantity and the corrections to it can be usually neglected.

The order α corrections to the photon energy density and pressure are easily calculated by inserting Eq. (F.57) in the Eqs. (1.49), (1.50) specialized to photons; with simple manipulations we obtain

$$\delta\rho_\gamma \simeq T^2 \frac{\alpha}{\pi} \int_0^\infty dp \, \frac{p^2}{E} \, F_e(E) \quad , \tag{5.18}$$

$$\delta \mathrm{p}_\gamma \simeq -\frac{1}{3} \, \delta\rho_\gamma \quad . \tag{5.19}$$

The expressions for order α corrections to $e^{\pm}$ energy density and pressure are deduced by substituting Eq. (F.33) into (1.49), (1.50) specialized to $e^{\pm}$; we found ($\rho_e = \rho_{e^-} + \rho_{e^+}$, $\mathrm{p}_e = \mathrm{p}_{e^-} + \mathrm{p}_{e^+}$)

$$\delta\rho_e \simeq \frac{2}{\pi^2} \int_0^\infty dp \, p^2 \, \mu \left(1 - \frac{E}{T} \, F_e(-E) \right) F_e(E) \quad , \tag{5.20}$$

$$\delta \mathrm{p}_e \simeq \frac{2}{3\pi^2} \int_0^\infty dp \, \frac{p^4}{E^2} \, \mu \left(1 + \frac{E}{T} \, F_e(-E) \right) F_e(E) \tag{5.21}$$

($E = \sqrt{p^2 + m_e^2}$).

The corrections to the energy density and pressure of the electromagnetic plasma ($\delta\rho = (30/\pi^2 T^4)(\delta r_\gamma + \delta\rho_e)$, $(90/\pi^2 T^4)(\delta \mathrm{p} = \delta p_\gamma + \delta \mathrm{p}_e)$) are plotted in Figure 5.8. As we can

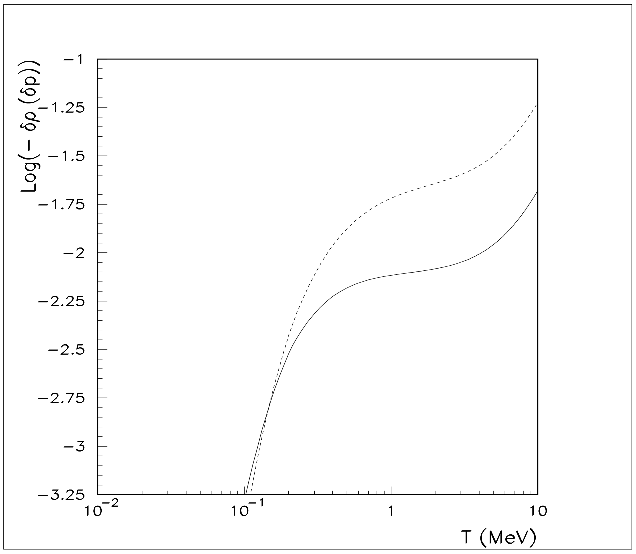

Figure 5.8: Radiative corrections to the energy density (solid line) and pressure (dashed line) of the electromagnetic component of the primordial plasma.

see, its contribution is of the same order of magnitude of the other thermal radiative corrections.

As briefly mentioned above, corrections to the energy densities directly influence the expansion rate of the Universe (see Eq. (2.44)) and eventually the primordial abundances through a change in the freeze out temperature. Moreover corrections to ρ and p also translate into corrections to the entropy density according to relation (1.79). On one side, this traduces into a modification of the time-temperature relation or, to be more specific, of the evolution equation for T (2.60). On the other side, the entropy of the $e^{\pm}$ plasma is transferred to photons when $e^{\pm}$ pairs disappear, while neutrinos do not benefit of this entropy releasing since at this epoch they are decoupled. Hence, this changes the neutrino-to-photon temperature ratio, which directly affects the weak rates. We have also calculated this effect, but we found that the modification of T_ν/T is quite negligible in the range relevant for BBN, much smaller than the precision of our goal.

Chapter 6

Calculations of Big Bang Nucleosynthesis. Results

In this thesis we have studied in details the fundamental processes underlying primordial nucleosynthesis and performed a complete analysis of the physical approximations that may be used as well as of corrections which should be included to reach the 1% reliability of the estimates. The relevance of this study and, in particular, of the precise determination of the primordial light element abundances, has been already pointed out in the Introduction. In this final chapter we summarize the main results obtained, give the accurate prediction for ^4He and outline the basic ingredients of forthcoming numerical code computing light element abundances, which is currently in progress.

6.1 Primordial nucleosynthesis: cosmology and particle physics inputs

As discussed in chapter 2, big bang nucleosynthesis is the result of two competing factors: nuclear and subnuclear processes between the particles in the primordial plasma, whose effect is to keep the species in thermal equilibrium, and the expansion of the Universe, which tends to hinder this equilibrium. It is then clear that the physics involved runs over cosmology (and, in particular, thermodynamics in the expanding Universe) and particle physics. Here we mainly summarize the basic inputs for studying primordial nucleosynthesis as well as the physical assumptions and approximations we used.

Standard cosmology is based on the observed homogeneity and isotropy of the Universe. These directly lead to the cosmological equations (1.28), (1.29) in the approximation of the Universe as a perfect fluid, to which must be added the equation of state (1.30) for the matter fields present in the Universe must be added. Primordial nucleosynthesis takes place when the curvature term k/R^2 in (1.28) is completely negligible, so that it is usually dropped out from the subsequent considerations.

From the cosmological equations, the energy conservation law (1.27) follows, as well as entropy conservation (1.78) for species in kinetic equilibrium. The total energy density and pressure, for species in equilibrium, are given by (1.84), (1.85). From these it follows that non relativistic matter (primarily baryons) gives a small contribution to the evolution in the RD era (in which BBN takes place), since its energy density is exponentially suppressed. This approximation will be used in several occasions.

The approach and the departure from thermal equilibrium is fully described by the Boltzmann transport equations, which involve the interaction rates of the particles present in the plasma. It is found that when a ultrarelativistic or non relativistic specie is completely decoupled from the heat bath, its distribution has the same form as that of an equilibrium one, but with a temperature parameter scaling, as the Universe expands, according to Eqs. (1.96) or (1.99). For such decoupled species, entropy is then separately conserved.

Further ingredients come from particle physics; let us focus on the nucleosynthesis era, when the relevant particles present in the plasma are photons, neutrinos, electrons and positrons, baryons. Photons and $e^{\pm}$ pairs form the background electromagnetic plasma, and their equilibrium is established by electromagnetic interactions. Baryons are maintained in kinetic equilibrium by electromagnetic and strong nuclear interactions, while neutrinos by weak interaction processes only. Chemical equilibrium in the electromagnetic component of the plasma is established by the annihilation reactions $e^+e^- \to \gamma\,\gamma$, while the weak reactions in (3.1), (3.2), (3.3) are responsible for the nuclear chemical equilibrium. Departure from chemical equilibrium happens as follows. The electron neutrino decoupling temperature is calculated to be $T_D^{\nu_e} \simeq 2.3\,MeV$, while for $\nu_\mu\,,\nu_\tau$ we have $T_D^{\nu_\mu\,,\nu_\tau} \simeq 3.5\,MeV$. In nucleosynthesis calculations it is assumed that neutrinos are completely decoupled from the background plasma before e^+e^- annihilations. Neutrino decoupling, however, occurs very close to e^+e^- annihilation, so that some residual interaction with the thermal plasma can cause the neutrinos to be slightly heated by the resultant entropy release. Careful studies have been conducted on this subject [89, 33], demonstrating that neutrino decoupling is *not* an instantaneous process. Hence, the spectrum of the decoupled neutrinos deviates slightly from the Fermi-Dirac form, causing the effective neutrino temperature to increase with momentum. However this increase accounts for only 0.7 % (even at relatively high momenta), justifying the usual approximation of instantaneous decoupling. Furthermore, the electron chemical potential, which is constrained by electric charge conservation, as well as the baryon chemical potential, is usually supposed to be a small quantity. This assumption is practically justified a posteriori. Instead, the neutrino chemical potentials are unconstrained, but they are set to zero in the standard nucleosynthesis scenario. Note that a non zero chemical potential for electron neutrinos can alter neutron-proton equilibrium, as well as increase the expansion rate of the Universe, while chemical potentials for other neutrino types can only speed up the expansion. In general, the lowering of the n/p ratio at freeze out may be compensated for by the net speed up of the expansion rate, although exotic models exist in which large lepton numbers can be generated (see [7] and references therein) [1].

There are no further assumptions and approximations regarding thermodynamics.

Electromagnetic and weak interaction reactions between elementary particles are *calculated* in the framework of the electroweak Standard Model. In particular, the crucial (for nucleosynthesis) weak processes in (3.1), (3.2), (3.3) have been here evaluated as follows. Born approximation is used as the reference for the reaction rates: it is based on tree level calculations of the probability amplitude in the infinite nucleon mass limit. We have then relaxed these assumptions. Firstly we reported the relevant zero temperature QED radiative and Coulomb corrections to the weak rates and then considered finite nucleon mass effects, namely weak magnetism, phase space modification and kinematical corrections due to the thermal motion of the initial nucleon in the comoving reference frame. The results for these corrections are plotted in Figures 4.1 , 4.2. Furthermore, we have also studied in details thermal radiative corrections, explicitly induced by the finite density of the plasma. In particular, we have calculated electron effective mass and wavefunction renormalization effects, vertex corrections and thermal photon emission and absorption processes, and the obtained results are reported in Figures 5.4, 5.5, 5.6, 5.7. With reference to the above mentioned Figures, the results for each reaction channel can be summarized as follows.

---

[1] These models are, however, constrained by BBN itself, since the introduction of non vanishing chemical potentials for neutrinos can substantially modify abundance predictions, destroying the agreement between theory and observations. In practice, allowed neutrino degeneracy cannot significantly altet the standard BBN model.

(a) $\nu_e + n \rightarrow e^- + p$

For the crucial BBN temperature range, $0.1\ MeV \leq T \leq 3.5\ MeV$, the two main corrections to the Born rate come from zero temperature radiative and kinetic terms. The contribution $\Delta\Gamma_R$ is weakly depending on T and represents the dominant term, though for large temperature the kinetic correction $\Delta\Gamma_K$ starts contributing significantly. The two combined contributions correct the Born rate for a factor $6 \div 9\%$, whilst thermal radiative ones are of the order of 1%.

(b) $e^- + p \rightarrow \nu_e + n$

For this channel radiative corrections are dominant at low temperature, while the kinetic ones give a quite relevant effect in whole BBN temperature range and correct the Born rate for a factor varying from 1% at low T up to 3% for $T = 3 \div 4\ MeV$. The radiative contribution is quite rapidly decreasing with temperature, reaching large negative values. This leads to a partial cancellation between $\Delta\Gamma_R$ and $\Delta\Gamma_K$. Thermal corrections are dominated by bremsstrählung contribution $\Delta\Gamma_\gamma$ and can be as large as 2% of Γ_B for large temperature.

(c) $e^+ + n \rightarrow \overline{\nu}_e + p$

For this process the radiative corrections have a behaviour quite similar to channel (b), though they are even more rapidly decreasing with temperature. This again leads to a partial cancellation between $\Delta\Gamma_R$ and the positive monotonically increasing $\Delta\Gamma_K$. Thermal corrections are again mainly provided by photon emission/absorption and monotonically increase with temperature up to a factor 2% of the corresponding Born rate.

(d) $\overline{\nu}_e + p \rightarrow e^+ + n$

The radiative and kinetic corrections sum up to a factor of about 5% of the Born rate. Actually the opposite behaviour of $\Delta\Gamma_R$ and $\Delta\Gamma_K$ conspires to give an almost constant total correction in the whole interesting temperature range. Thermal effects are quite small, contributing for less than 0.5%.

(e) $n \rightarrow e^- + \overline{\nu}_e + p$

For the neutron decay the radiative corrections are practically constant and give the leading effect for small temperature, $T \leq m_e$. For larger T the thermal photon emission/absorption processes rapidly become dominating over all other correction terms with a relative ratio to the Born rate as large as 10^4. However, this large correction is weakly contributing to total $n \rightarrow p$ rate, since in the temperature range $T > m_e$ the scattering processes (a)-(d) are largely dominant over decay and inverse decay.

(f) $e^- + \overline{\nu}_e + p \rightarrow n$

Same considerations of the direct process (e) hold for inverse neutron decay. As for the direct channel, the kinetic contribution is negative down to temperatures of the order $T \sim 0.2\ MeV$. The contribution of $|\Delta\Gamma_K|$ is however negligible for both processes, smaller than 1%.

All results are summarized in Figure 6.1, where we have shown the total relative corrections in percent. For the processes (a) and (d) the correction is almost constant over the entire considered range for T, and of the order of $6 \div 10\%$ and $5 \div 6\%$, respectively. The positive kinetic contribution soften the deep decreasing of the radiative terms for channels (b) and (c). Finally the large effect of thermal bremsstrählung for neutron decay and inverse process (e) and (f) is particularly evident. The cumulative "zero temperature", kinematical and thermal radiative corrections to the $n \rightarrow p$ and $p \rightarrow n$ rates are instead reported in Figures 6.2, 6.3, 6.4. We have shown the total rates $\Gamma(n \rightarrow p)$ and $\Gamma(p \rightarrow n)$ in Figure 6.5, while the total relative correction $\Delta\Gamma/\Gamma_B \equiv (\Gamma - \Gamma_B)/\Gamma_B$, in percent, are plotted in Figure 6.6. The whole correction $\Delta\Gamma$ for $n \leftrightarrow p$ turn out to be a positive decreasing function over the whole temperature range relevant for BBN. The main contribution at low temperature for both total rates comes from the radiative corrections, while for $T > 2 \div 3\ MeV$ kinetic contribution starts dominating. This is particularly evident by looking at Figures 6.2 and 6.3. While for radiative corrections the effect on $n \rightarrow p$ total rate is larger than on the $p \rightarrow n$ one, $\Delta\Gamma_K$ shows an opposite behaviour. The competition of these two corrections is then responsible for the presence of the inversion points in Figure 6.6 at $T \simeq 0.15\ MeV$ and $T \simeq 2\ MeV$. Finally, the order of magnitude

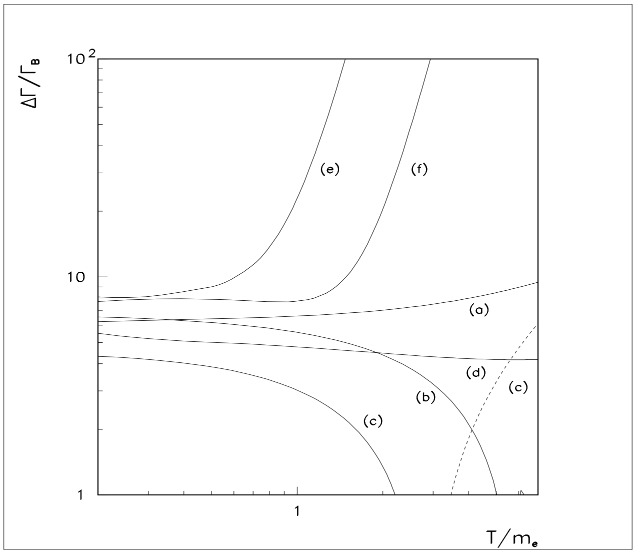

Figure 6.1: The total relative correction to the Born rates, in percent, are shown for the six processes in (3.1), (3.2), (3.3) .

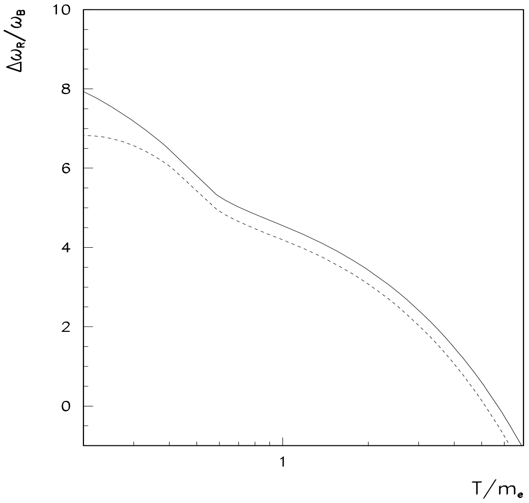

Figure 6.2: The zero temperature radiative corrections, for $n \to p$ (solid line) and $p \to n$ (dashed line) processes. Finite mass contributions coming from phase space integration and weak magnetism are also included. The result is expressed in percent.

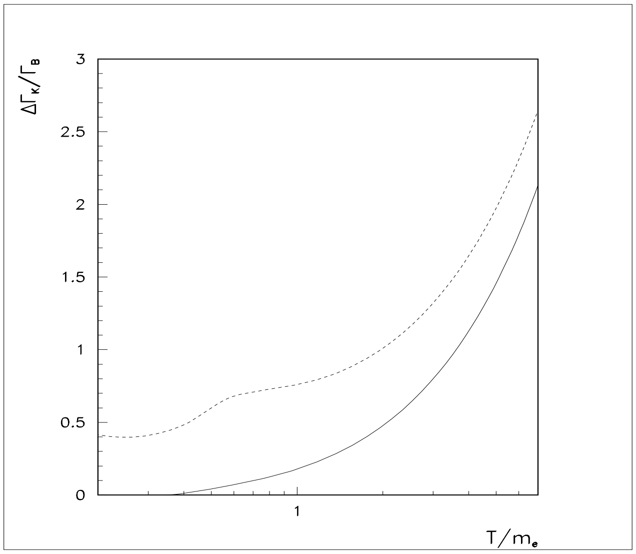

Figure 6.3: The kinematical contributions to the $n \to p$ (solid line) and $p \to n$ (dashed line) processes, normalized to the Born rates, in percent.

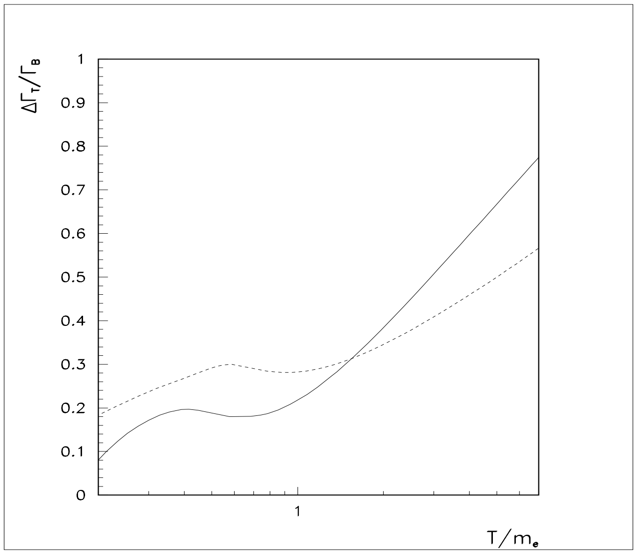

Figure 6.4: The whole thermal radiative corrections to the $n \to p$ (solid line) and $p \to n$ (dashed line) processes, expressed in percent.

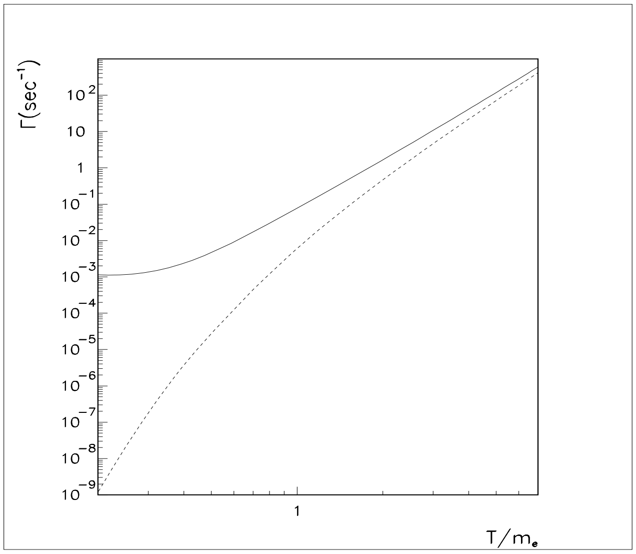

Figure 6.5: The total rates $\Gamma(n \rightarrow p)$ (solid line) and $\Gamma(p \rightarrow n)$ (dashed line), including all radiative, finite mass and thermal corrections.

of the pure thermal radiative corrections

$$\Delta\Gamma_T \equiv \Delta\Gamma_M + \Delta\Gamma_W + \Delta\Gamma_V + \Delta\Gamma_\gamma \quad , \tag{6.1}$$

is sensibly smaller, but nevertheless they may contribute for a factor $0.2 \div 0.4\%$ at the freeze-out temperature $T \sim 1\ MeV$. We have performed a fit of the numerical results for $\Gamma(n \rightarrow p)$ and $\Gamma(p \rightarrow n)$. The fitting expressions are the following

$$\Gamma(n \rightarrow p) \;=\; \frac{1}{\tau_n^{exp}} \sum_{l=0}^{8} a_l \left(\frac{T}{m_e}\right)^l \quad , \tag{6.2}$$

$$\Gamma(p \rightarrow n) \;=\; \frac{1}{\tau_n^{exp}} \exp\left(-\frac{q\ m_e}{T}\right) \sum_{l=1}^{10} b_l \left(\frac{T}{m_e}\right)^l \quad , \tag{6.3}$$

where for $n \rightarrow p$

$$a_0 = 1 \;\; ; \;\; a_1 = -0.0135609 \;\; ; \;\; a_2 = 1.227825 \;\; ; \;\; a_3 = -19.344104 \;\; ;$$

$$a_4 = 85.9281797 \;\; ; \;\; a_5 = -11.221606 \;\; ; \;\; a_6 = 14.4804529 \;\; ; \;\; a_7 = -3.082314 \;\; ;$$

$$a_8 = 0.357466 \;\; ; \;\; a_9 = -0.0200726 \;\; ; \;\; a_{10} = 0.10049{\cdot}10^{-3} \;\; ; \;\; a_{11} = 0.488642{\cdot}10^{-4} \;\; ;$$

$$a_{12} = -0.237462{\cdot}10^{-5} \;\; , \;\; a_{13} = 0.359274{\cdot}10^{-7} \tag{6.4}$$

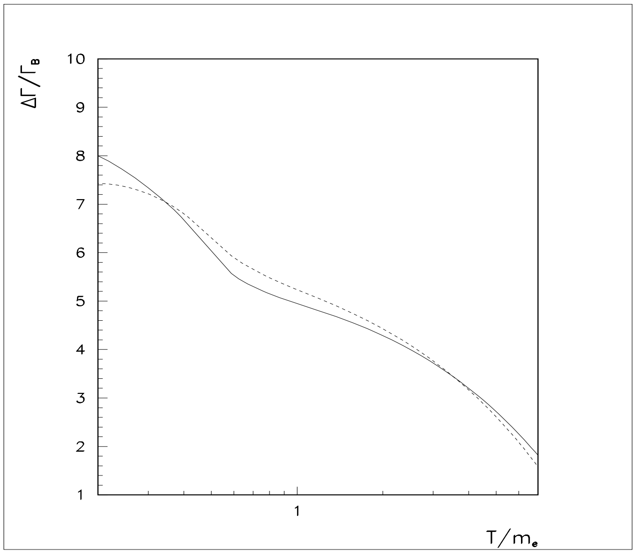

Figure 6.6: The total relative corrections $\Delta\Gamma/\Gamma_B$ for the $n \to p$ (solid line) and $p \to n$ (dashed line) processes, expressed in percent.

while for $p \to n$

$$\begin{gathered} b_1 = 20.884200 \;\; ; \;\; b_2 = -71.802238 \;\; ; \;\; b_3 = 118.853956 \;\; ; \;\; b_4 = -11.564594 \;\; ; \\ b_5 = 45.057913 \;\; ; \;\; b_6 = -3.316009 \;\; ; \;\; b_7 = 0.2744236 \;\; ; \;\; b_8 = -0.75654 \cdot 10^{-2} \;\; ; \\ b_9 = -0.37916 \cdot 10^{-3} \;\; ; \;\; b_{10} = 0.201124 \cdot 10^{-4} \;\; ; \;\; b_{11} = 0.791665 \cdot 10^{-6} \;\; ; \\ b_{12} = -0.640452 \cdot 10^{-7} \;\; ; \;\; b_{13} = 0.104891 \cdot 10^{-8} \;\; ; \;\; q = 2.90377 \;\; . \end{gathered} \tag{6.5}$$

The fit has been obtained requiring that the fitting functions differ by less than 0.1% from the numerical values.

Finally, note that mass shift radiative corrections affect not only the weak interaction reaction rates but also the energy density and pressure of $e^{\pm}$ and photons in the Universe. We have considered the corrections to these quantities as well, and the results are reported in Figure 5.8

Last but not least, we have to consider the strong nuclear processes intervening in primordial nucleosynthesis. Unfortunately, there is no very reliable theoretical computation for the interested nuclear reaction rates, so the strategy adopted is quite different: experimental data on the processes involved are used. However, a certain degree of uncertainty is introduced in this way, mainly due to the fact that the typical energies of the reactions taking place during BBN are quite different (too much low) from the available experimental ones, so that it is necessary to take some extrapolations. Moreover, a suitable thermal averaging of the measured cross sections (usually made with a Boltzmann distribution) is required:

$$< \sigma v > = \sqrt{\frac{8}{\pi M T^3}} \int dE \, \sigma(E) \, E \, e^{-E/T} \tag{6.6}$$

(M is the reduced mass).All this conspires to produce uncertainties in the obtained reaction rates as large as 10%. Fortunately, the impact of these on the predictions for light element abundances is extremely low [90]. This happens because, as we have already stressed, the crucial reactions for nucleosynthesis are those fixing the n/p ratio at freeze out (especially for ^4He abundance), and such reactions are very well theoretically evaluated, as discussed in this thesis. All the sources of uncertainties in primordial nucleosynthesis predictions are, however, currently well controlled by both MonteCarlo [91] simulations and semi-analytical analysis [90].

6.2 Prediction on the ^4He abundance

The conditions for BBN to take place were reached when the temperature in the Universe was in the range $10 \div 0.1 \, MeV$. Primordial nucleosynthesis is, in fact, the final outcome of the decoupling of the weak interactions which keep neutron and proton in thermal equilibrium and, shortly after, of the onset of nuclear reactions which start producing light nuclear species. At temperature $T >> 1 \; MeV$ the neutron to proton ratio is order unity and starts decreasing exponentially when the temperature reaches the value of their mass difference. As the temperature decreases, however, weak interactions are no longer fast enough to maintain equilibrium and a substantial final neutron fraction survives down to the phase of nucleosynthesis. All neutrons become practically bound in ^4He nuclei, due to the high binding energy per nucleon, which therefore represent the dominant products of BBN. While the ^4He mass fraction is weakly depending on the baryon to photon ratio η, it is strongly dependent on the neutron fraction at the nucleon freeze-out. An accurate theoretical prediction for the helium abundance, as well as for the other light nuclei produced during BBN, will be the subject of the next section; it can be obtained by using the standard BBN numerical code suitably modified to take into account all the corrections considered in this thesis. Here we report on the results for the expected variation of the surviving neutron fraction X_n induced by the whole effects $\Delta\Gamma(n \leftrightarrow p)$. This allows for a simple estimate of the corresponding variation of $X_{^4He}$; the baseline value for this quantity obtained with the standard BBN code without the inclusion of any correction is [12]

$$X^0_{^4He} \; = \; 0.2411 \quad . \tag{6.7}$$

The neutron fraction is determined by the differential equation

$$\frac{dX_n}{dT} = \frac{dt}{dT} \left[\Gamma(p \to n)(1 - X_n) - \Gamma(n \to p) X_n \right] \quad . \tag{6.8}$$

Writing $X_n = X^0_n + \delta X_n$, where δX_n is the correction induced by $\Delta\Gamma$, we have at first order

$$\begin{aligned} \frac{dX^0_n}{dT} &= \frac{dt}{dT} \left[\Gamma_B(p \to n)(1 - X^0_n) - \Gamma_B(n \to p) X^0_n \right] \quad , & (6.9) \\ \frac{d}{dT} \delta X_n &= -\frac{dt}{dT} \left[\left(\Gamma_B(p \to n) + \Gamma_B(n \to p) \right) \delta X_n - \Delta\Gamma(p \to n) \right. \\ &+ \left. \left(\Delta\Gamma(p \to n) + \Delta\Gamma(n \to p) \right) X^0_n \right] \quad . & (6.10) \end{aligned}$$

Notice that the zeroth order abundance X^0_n has been defined as the one obtained by the Born amplitudes rescaled by the *constant* factor 961/886.7, which provides at tree level the correct prediction for neutron lifetime (see our discussion in section 3). The Born rates $\Gamma_B(p \leftrightarrow n)$ in (6.9),(6.10) are therefore rescaled by the same factor. Equations (6.9),(6.10) have been numerically solved using our fitting function for $\Gamma(n \leftrightarrow p)$ and a similar one for $\Gamma_B(n \leftrightarrow p)$, which we do not report for brevity. We found for the asymptotic abundance $\delta X_n \simeq 0.0024$, with a relative change, in percent, $\delta X_n / X^0_n = 1.6\%$.

These results allows for a simple estimation of corrections to ^4He mass fraction by means of the formula (2.40)

$$X_{^4He} \; \simeq \; 2\, X_n(t_{ns}) \quad . \tag{6.11}$$

Note that $X_n(t_{ns})$ is evaluated at the time when nucleosynthesis begins, $t_{ns} \simeq 180\, s$; actually, by this time the neutron abundance surviving at freeze out has been depleted by β-decay to

$$X_n(t_{ns}) \; \simeq \; X^0_N \, e^{-t_{ns}/\tau_n} \quad , \tag{6.12}$$

where τ_n is the neutron lifetime. Hence the corrections to ^4He mass fraction can be evaluated from

$$\delta X_{^4He} \simeq 2\,\delta X_n\, e^{-t_{ns}/\tau_n} \quad . \tag{6.13}$$

and using the results for δX_n we find

$$\delta X_{^4He} \simeq 0.004 \qquad\qquad \frac{\delta X_{^4He}}{X_{^4He}} \simeq 1.6\,\% \quad . \tag{6.14}$$

The total correction, as mentioned in the previous section, is largely dominated by "zero temperature" radiative and finite nucleon mass corrections, which give a *positive* contribution to $X_{^4He}$.

6.3 Building the BBN code

In this section we finally describe the way the primordial abundances of light nuclei can be numerically evaluated and discuss how to build of a BBN code [59] - [62]. Such a code follows the evolution of these abundances, and primarily tracks p, n, D, T, ^3He, ^4He, ^6Li, ^7Li and ^7Be. The initial temperature can be chosen to be, for example, $T = 10\,MeV$, and hence for the initial abundances we can take the nuclear statistical equilibrium values (2.11):

$$X_A = \left(\frac{\zeta(3)}{\sqrt{8\pi}}\right)^{A-1} \frac{g_A}{2}\, A^{\frac{5}{2}} \left(\frac{T}{m_N}\right)^{\frac{3}{2}(A-1)} \eta^{A-1}\, X_p^Z\, X_n^{A-Z}\, e^{\frac{B_A}{T}} \tag{6.15}$$

(hereafter we use the same notation of chapter 2). In fact, at temperatures $\gtrsim 1\,MeV$, the nuclear rates are sufficiently high to keep all abundances at their equilibrium values. It is usually made the reasonable assumption that the elements are always maintained in kinetic equilibrium by electromagnetic and strong interactions, while this may be not true for chemical equilibrium; then the coefficients in the nuclear rates depend only on η and T.

The set of evolution equations relevant for nucleosynthesis, which is the main body of the BBN code, has been deduced in chapter 2. Here, we report these equations for completeness:

$$\frac{1}{R}\frac{dR}{dt} \simeq \sqrt{\frac{8\pi}{3M_P^2}}\,\left[\rho_\gamma + \rho_e + \rho_\nu + \rho_B\right]^{1/2} \tag{6.16}$$

$$\frac{1}{n_B}\frac{dn_B}{dt} = -3\,\frac{1}{R}\frac{dR}{dt} \tag{6.17}$$

$$\phi_e \simeq \frac{\pi^2}{2}\,\frac{n_B\, q_B}{T^3\, f(z)} \tag{6.18}$$

$$\begin{aligned}\frac{dT}{dt} &= -\left[3\frac{1}{R}\frac{dR}{dt}\left(\rho_\gamma + \mathrm{p}_\gamma + \rho_e + \mathrm{p}_e + \Theta(T-T_D)\left(\rho_\nu + \mathrm{p}_\nu\right) + \mathrm{p}_B\right)\right.\\ &+ \left.\frac{\partial\rho_e}{\partial\phi_e}\left(\sum_j \frac{\partial\phi_e}{\partial Y_j}\frac{dY_j}{dt} - 3\,\frac{1}{R}\frac{dR}{dt}\,n_B\,\frac{\partial\phi_e}{\partial n_B}\right) + n_B\sum_j\left(\Delta M_j + \frac{3}{2}T\right)\frac{dY_j}{dt}\right]\\ &\times \left[\frac{\partial\rho_e}{\partial T} + \frac{\partial\rho_e}{\partial\phi_e}\frac{\partial\phi_e}{\partial T} + \frac{d\rho_\gamma}{dT} + \Theta(T-T_D)\,\frac{d\rho_\nu}{dT} + \frac{3}{2}n_B\sum_j Y_j\right]^{-1} \end{aligned} \tag{6.19}$$

$$\frac{dY_i}{dt} = \sum_{j,k,l} N_i\left(\Gamma_{kl\to ij}\,\frac{Y_l^{N_l}\,Y_k^{N_k}}{N_l!\,N_k!} - \Gamma_{ij\to kl}\,\frac{Y_i^{N_i}\,Y_j^{N_j}}{N_i!\,N_j!}\right) \equiv \Gamma_i(Y_j) \quad . \tag{6.20}$$

As already mentioned, this set of equations does not include the evolution equations for neutrinos. Here, however, we have explicited the effect of not decoupled neutrinos on the involved quantities by means of the theta-function $\Theta(T-T_D)$, T_D being the decoupling temperature. The relevant thermodynamic quantities can be read off by Eqs. (2.51)-(2.57), while q_B is the baryon electric charge, as defined by equation (2.47). Note that it has been assumed that the electron chemical potential parameter ϕ_e is small, so that all terms depending on ϕ_e [2] can be expanded at first order in this parameter.

The other inputs are contained in the equations (6.20), and are the weak interaction and strong nuclear reaction rates. The corrected weak $n \leftrightarrow p$ rates are taken from our fits in Eqs. (6.2)-(6.5). The complete nuclear reaction network is composed of 88 reactions, which we report in appendix C; however, in many cases, one can also consider a limited number of reactions, introducing a negligible error in the computations. For brevity, we do not report the expressions for the nuclear reaction rates which can be found in [59].

6.3.1 Numerical tricks

The basics equations to be followed for evaluating the primordial abundances are (6.17) and (6.20). Eq. (6.16) can be directly substituted into (6.17), while the expression (6.18) for the electron chemical potential has to be used for calculating ρ_e, p_e but also ρ_γ, p_γ and ρ_ν (see the previous footnote). Instead, by means of Eq. (6.19) we can translate the time evolution into the temperature evolution of the interested quantities.

---

[2] Note that, in general, both ρ_e, p_e and ρ_γ, p_γ depend on the electron chemical potential, the last two quantitiex through the effective finite photon mass induced by the e^+e^- bath. Furthermore, observe that from the entropy conservation also ρ_ν, p_ν would depend on ϕ_e. However, this dependence is effective only in Eqs. (6.16), (6.17), while in Eq. (6.19) the presence of the theta-function makes it non operative (neutrino entropy is related to the electron one only when they are coupled to the plasma.

For numerical reasons, it is better to turn the variable n_B into the dimensionless quantity

$$\tilde{h} \; = \; \frac{n_B}{T^3} \quad , \tag{6.21}$$

which evolves more slowly with T than n_B. Furthermore, instead of T, we use the variable

$$z \; = \; \frac{m_e}{T} \quad . \tag{6.22}$$

In terms of these news variables Eq. (6.17) and Eqs. (6.20) take the form

$$\begin{aligned} \frac{d\tilde{h}}{dz} \; &= \; \left[\frac{\left(3\hat{\mathrm{p}}_\gamma - \hat{\rho}_\gamma + 3\hat{\mathrm{p}}_e - \hat{\rho}_e + z\frac{\partial \hat{\rho}_\gamma}{\partial z} + z\frac{\partial \hat{\rho}_e}{\partial z} + \frac{3}{2}\tilde{h}\sum_j Y_j\right)\widetilde{H} + \tilde{h}\sum_j \left(z\Delta\widetilde{M}_j + \frac{3}{2}\right)\widetilde{\Gamma}_j}{3\left(\hat{\rho}_\gamma + \hat{\mathrm{p}}_\gamma + \hat{\rho}_e + \hat{\mathrm{p}}_e + \frac{4}{3}\Theta(z_D - z)\hat{\rho}_\nu + \tilde{h}\sum_j Y_j\right)\widetilde{H} + \tilde{h}\sum_j \left(z\Delta\widetilde{M}_j + \frac{3}{2}\right)\widetilde{\Gamma}_j} \right] \cdot \\ &\cdot \quad \frac{3\tilde{h}}{z} , \end{aligned} \tag{6.23}$$

$$\begin{aligned} \frac{dY_i}{dz} \; &= \; \left[\frac{4\hat{\rho}_\gamma + 4\hat{\rho}_e + 4\Theta(z_D - z)\hat{\rho}_\nu - z\frac{\partial \hat{\rho}_\gamma}{\partial z} - z\frac{\partial \hat{\rho}_e}{\partial z} + \frac{3}{2}\tilde{h}\sum_j Y_j}{3\left(\hat{\rho}_\gamma + \hat{\mathrm{p}}_\gamma + \hat{\rho}_e + \hat{\mathrm{p}}_e + \frac{4}{3}\Theta(z_D - z)\hat{\rho}_\nu + \tilde{h}\sum_j Y_j\right)\widetilde{H} + \tilde{h}\sum_j \left(z\Delta\widetilde{M}_j + \frac{3}{2}\right)\widetilde{\Gamma}_j} \right] \cdot \\ &\cdot \quad \frac{\widetilde{\Gamma}_i}{z} \end{aligned} \tag{6.24}$$

with $\widetilde{H}$ denoting the dimensionless Hubble parameter $\widetilde{H} = H/m_e$

$$\widetilde{H} \; = \; \sqrt{\frac{8\pi}{3}\frac{m_e}{M_P}\frac{1}{z^2}\left[\hat{\rho}_\gamma + \hat{\rho}_e + \hat{\rho}_\nu + \tilde{h}\left(z\widetilde{M}_u + \sum_i \left(z\Delta\widetilde{M}_i + \frac{3}{2}\right)Y_i\right)\right]}^{\,1/2} \quad , \tag{6.25}$$

and $z_D = me/T_D$. In writing these equations we have used the following notations

$$\widetilde{M}_u \; = \; \frac{M_u}{m_e} \quad , \qquad \Delta\widetilde{M}_i \; = \; \frac{\Delta M_i}{m_e} \quad , \qquad \widetilde{\Gamma}_i \; = \; \frac{\Gamma_i}{m_e} \quad , \tag{6.26}$$

$$\hat{\rho}_\alpha \; = \; \frac{\rho_\alpha}{T^4} \quad , \qquad \hat{\mathrm{p}}_\alpha \; = \; \frac{\mathrm{p}_\alpha}{T^4} \quad , \tag{6.27}$$

with $\alpha = e, \gamma, \nu$.

As mentioned above, ρ_e, p_e and ρ_γ, p_γ, depend on the electron chemical potential. In the new numerical code we are writing, we use the following strategy. First of all, we have checked that the influence of ϕ_e on the various quantities of interest is very weak, justifying the expansion at first order in ϕ_e leading to Eq. (6.18). By virtue of this fact, we have then substituted Eq. (6.18) in the corrected expressions for ρ_e, p_e, ρ_γ, p_γ (given by Eqs. (2.53) - (2.54) plus Eqs. (5.18) - (5.21)) and subsequently we have performed a fit for these quantities as functions of z. To speed up the running of the BBN code we have finally used these fits in the evolution equations. The obtained values for the electron energy density and pressure are fitted (in the relevant temperature range) by the expressions

$$\begin{aligned}
\hat{\rho}_e &= 1.145 \;+\; 0.033981\; z \;-\; 0.14543\; z^2 \;+\; 0.025507\; z^3 - (0.54168\times10^{-3})\; z^4 \\
&- (0.11263\times10^{-3})\; z^5 - (0.29742\times10^{-5})\; z^6 \;+\; (0.38331\times10^{-6})\; z^7 \\
&+ (0.45263\times10^{-7})\; z^8 \;+\; (0.19241\times10^{-8})\; z^9 \;-\; (0.96597\times10^{-10})\; z^{10} \\
&- (0.19505\times10^{-10})\; z^{11} \;-\; (0.14079\times10^{-12})\; z^{12} \quad ,
\end{aligned} \tag{6.28}$$

$$\begin{aligned}
\hat{\mathrm{p}}_e &= \Big(0.3786 \;+\; 0.019126\; z \;-\; 0.063895\; z^2 \;+\; 0.032085\; z^3 \\
&- 0.0048501\; z^4 \;-\; 0.00016611\; z^5 \;+\; 0.000082922\; z^6 \;+\; (7.9884\times10^{-6})\; z^7 \\
&- (0.0619\times10^{-7})\; z^8 \;-\; (1.9568\times10^{-7})\; z^9 \;-\; (1.0921\times10^{-8})\; z^{10} \\
&+ (3.8564\times10^{-9})\; z^{11}\Big)\; e^{-0.13145\; z^2} \quad .
\end{aligned} \tag{6.29}$$

The expression for z derivative of $\hat{\rho}_e$, entering in (6.23) and (6.24), are obtained from (6.28).

Instead, in the considered temperature range, we have found that $\hat{\rho}_\gamma$ takes values between 0.6580 and 0.6573 while $\hat{\mathrm{p}}_\gamma$ varies from 0.2193 and 0.2187. For simplicity we have then taken the average values of 0.6577 and 0.2190 as the ones appropriate for $\hat{\rho}_\gamma$ and $\hat{\mathrm{p}}_\gamma$ respectively.

Finally, the most critical numerical part of the BBN code concerns the solution method of the set of differential equations (6.20) for Y_i. In fact, at high temperatures, nuclear reactions proceed in both forward and reverse directions almost equally rapidly, so that the right-hand-side of (6.20) is a small difference of large numbers, which causes severe numerical problems. To avoid this, we have used the Gear method of backward differentiation formulas for stiff problems, described for example in [93].

The implementation of the described code, using a Fortran Power Station, is currently under study, and represents the next step towards a precise determination of light element abundances in the Universe.

The preliminary results obtained by our code for ^4He mass fraction and D, ^7Li abundances as functions of η are shown in Figures 6.7, 6.8, 6.9.

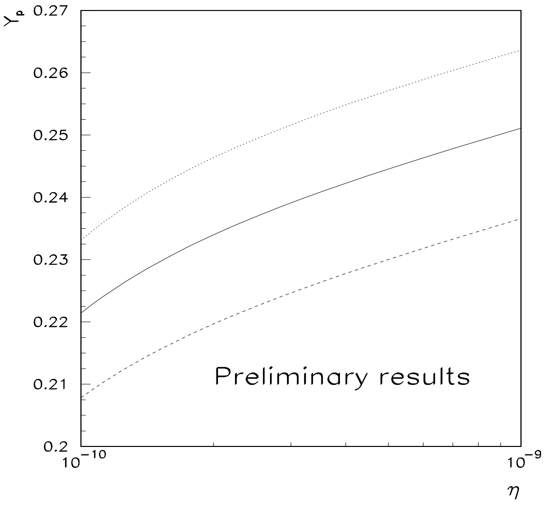

Figure 6.7: Our predictions for ^4He mass fraction Y_p versus η. The solid line refers to $N_\nu = 3$, while the dashed ones to $N_\nu = 2$ (below) and $N_\nu = 4$ (above).

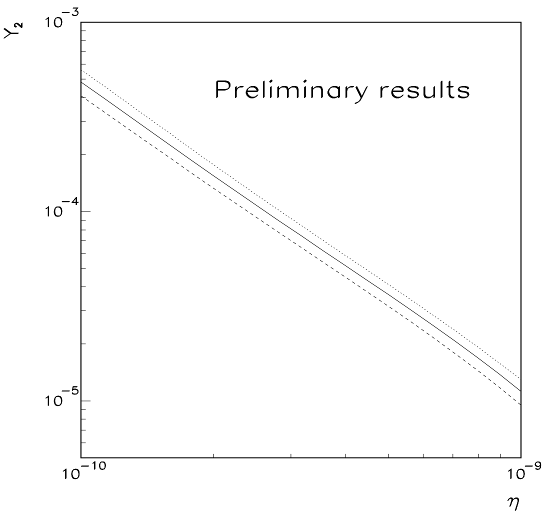

Figure 6.8: Our predictions for D abundance Y_2 versus η (notations as in Figure 6.7 .

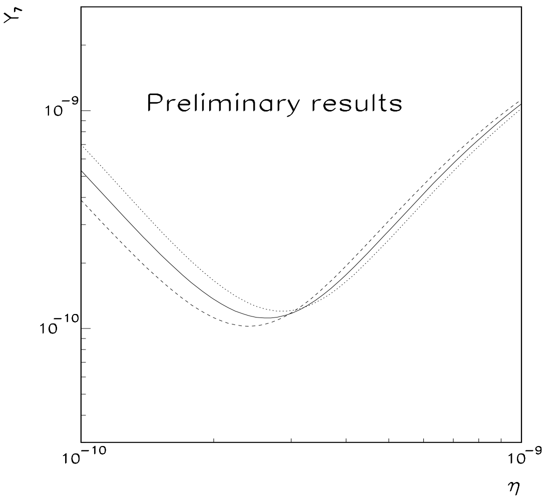

Figure 6.9: Our predictions for ^7Li abundance Y_7 versus η (notations as in Figure 6.7 .

Acknowledgments

I'm particularly indebted with Drs. Gianpiero Mangano, Gennaro Miele and O. Pisanti for their continuous unvaluable help, patience and encouragement during my Ph.D. thesis work. My sincere thanks for their friendship are here expressed. A special thank goes also to Prof. Franco Buccella and Prof. P. Strolin for their useful remarks and encouragement and to my friends F. Acerra, S. De Simone, E. Piedipalumbo, P. Santorelli and N. Tancredi.

Bibliography

[1] P.J.E. Peebles, *Physical Cosmology* (Princeton, 1971, Princeton University Press).

[2] D.N. Schramm and R.V. Wagoner, *Annu. Rev. Nucl. Sci.* **27** (1977) 37.

[3] A.M. Boesgaard and G. Steigman, *Annu. Rev. Astron. Astrophys.* **23** (1985) 919.

[4] E.W. Kolb and M.S. Turner, *The Early Universe*, (New York, 1990, Addison-Wesley Publishing Company).

[5] B.E.J. Pagel, *Observational and Physical Cosmology*, ed. F Sanchez *et al.*(Cambridge, 1992, Cambridge University Press).

[6] H. Reeves, *Rev. Mod. Phys.* **66** (1994) 193.

[7] S. Sarkar, *Rept. Prog. Phys.* **59** (1996) 1493.

[8] G. Gamow, *Phys. Rev.* **74** (1948) 505; G. Gamow, *Nature* **162** (1948) 680; R.A. Alpher and R.C. Herman, *Nature* **162** (1948) 774; R.A. Alpher and R.C. Herman, *Phys. Rev.* **75** (1949) 1089.

[9] N. Hata, R.J. Scherrer, G. Steigman, D. Thomas, and T.P. Walker, *Astrophys. J.***458** (1996) 637.

[10] K.A. Olive, University of Minnesota preprint UMN-TH-1735/99, astro-ph/9901231

[11] D.N. Schramm, M.S. Turner, *Rev. Mod. Phys.* **70** (1998) 303.

[12] R.E. Lopez and M.S. Turner, preprint FERMILAB-Pub-98/232-A (1998), astro-ph/9807279.

[13] S. Esposito, G. Mangano, G. Miele and O. Pisanti, *Nucl. Phys.* B in press, astro-ph/9808196.

[14] C. Hayashi, *Prog. Theo. Phys.* **5** (1950) 224; F. Hoyle and R.J. Tayler, *Nature* **203** (1964) 1108.

[15] R.A. Alpher, J.W. Follin and R.C. Herman, *Phys. Rev.* **92** (1953) 1347.

[16] S.L.Glashow, *Nucl. Phys.* **22** (1961) 579
S.Weinberg, *Phys. Rev. Lett.* **19** (1967) 1264
A.Salam, "Weak and Electromagnetic interactions", in Svartholm N., *Elementary Particle Theory*, Stockholm, Almquist and Wiksell, 1968.

[17] E. Lisi, S. Sarkar, F.L. Villante, preprint hep-ph/9901404.

[18] C. Caso *et al.*., *Eur. Phys. Jour.* **C3** (1998) 1.

[19] S. Esposito, G. Mangano, G. Miele and O. Pisanti, in progress.

[20] A. Songaila et al., *Nature* **371** (1994) 43.

[21] A. Reiss, R.P. Krishner, and W. Press, *Astrophys. J.* **438** (1995) L17; M. Hamuy et al, *Astron. J.* **109** (1995) 1; W. Freedman et al., *Nature* **371** (1994) 757; M. Bolte and C.J. Hogan, *Nature* **376** (1995) 399.

[22] C.J. Hogan, *Phys. Rev.* **D 54** (1996) 112.

[23] P.J.E. Peebles, *Principles of Physical Cosmology* (Princeton, 1993, Princeton University Press).

[24] G.F. Smoot and D. Scott, *Eur. Phys. J.* **C3** (1998) 127.

[25] S. Weinberg, *Gravitation and Cosmology* (New York, 1972, Wiley)

[26] W. Rindler, *Essential Relativity* (Berlin, 1977, Springer-Verlag).

[27] E.R. Harrison, *Astrophys. J.* **403** (1993) 28.

[28] E.R. Dekel, *Annu. Rev. Astron. Astrophys.* **32** (1994) 371.

[29] A. Guth, *Phys. Rev.* **D 23** (1981) 347; A.D. Linde, *Rep. Prog. Phys.* **47** (1984) 925; A.D. Linde *Particle Physics and Inflationary Cosmology* (New York, 1990, Harwood Academic); K.A. Olive, *Phys. Rep.* **190** (1990) 309.

[30] R.A. Lyttleton and H. Bondi, *Proc. Roy. Soc.* **A 252** (1959) 313; S. Sengupta and P.B. Pal, *Phys. Lett.* **B 365** 1996 175.

[31] G. Steigman, *Annu. Rev. Astron. Astrophys.* **14** (1976) 33.

[32] R.V. Wagoner, *Les Houches Session XXXII: Physical Cosmology* ed R Balian *et al.*(Amsterdam, 1980, North-Holland) p 395.

[33] D.A. Dicus, E.W. Kolb , A.M. Gleeson, E.C.G. Sudarshan, V.L. Teplitz and M.S. Turner, *Phys. Rev.* **D 26** (1982) 2694.

[34] K. Enqvist, K. Kainulainen and V. Semikoz, *Nucl. Phys.* **B 374** (1992) 392.

[35] G. Audi and A. H. Wapstra, *Nucl. Phys.* **A 595** (1995) 409.

[36] H.B. Niemann, et al. *Science* **272** (1996) 846.

[37] J.L. Linsky, et al., *Astrophys. J.***402** (1993) 694; J.L. Linsky, et al., *Astrophys. J.***451** (1995) 335.

[38] R. Epstein, J. Lattimer and D.N. Schramm, *Nature* **263** (1976) 198; J.M. Pasachoff and A. Vidal-Madjar, *Comm. Astroph.* **14** (1989) 61.

[39] R.F. Carswell, M. Rauch, R.J. Weymann, A.J. Cooke, and J.K. Webb, *MNRAS* **268** (1994) L1; A. Songaila, L.L. Cowie, C. Hogan, and M. Rugers, *Nature* **368** (1994) 599; M. Rugers and C.J. Hogan, *A.J.* **111** (1996) 2135; R.F. Carswell, et al. *MNRAS* **278** (1996) 518; E.J. Wampler, et al., *A.A. 316* (1996) 33; J.K. Webb, R.F. Carswell, K.M. Lanzetta, R. Ferlet, M. Lemoine, A. Vidal-Madjar, and D.V. Bowen, *Nature* **388** (1997) 250; D. Tytler et al., astro-ph/9810217 (1998).

[40] D. Tytler, X.-M. Fan, and S. Burles, *Nature* **381** (1996) 207; S. Burles and D. Tytler, *Astrophys. J.***460** (1996) 584.

[41] S. Burles and D. Tytler, *Astrophys. J.***499** (1998) 699; and astro-ph/9712109; A. Songaila, E.J. Wampler, and L.L. Cowie, *Nature* **385** (1997) 137.

[42] P.J. Kernan and S. Sarkar, *Phys. Rev.* **D 54** (1996) 3681.

[43] S.T. Scully, M. Cassé, K.A. Olive, D.N. Schramm, J.W. Truran, and E. Vangioni-Flam, *Astrophys. J.***462** (1996) 960; J. Geiss, in *Origin and Evolution of the Elements*, eds. N. Prantzos, E. Vangioni-Flam, and M. Cassé (Cambridge: Cambridge University Press, 1993), p. 89.

[44] D.S. Balser, T.M. Bania, C.J. Brockway, R.T. Rood, and T.L. Wilson, *Astrophys. J.***430** (1994) 667; T.M. Bania, D.S. Balser, R.T. Rood, T.L. Wilson, and T.J. Wilson, *Ap.J.S.* **113** (1997) 353; G. Gloeckler, and J. Geiss, *Nature* **381** (1996) 210.

[45] R.T. Rood, T.M. Bania, and T.L. Wilson, Nature **355** (1992) 618; R.T. Rood, T.M. Bania, T.L. Wilson, and D.S. Balser, 1995, in *the Light Element Abundances, Proceedings of the ESO/EIPC Workshop*, ed. P. Crane, (Berlin:Springer), p. 201; D.S. Balser, T.M. Bania, R.T. Rood, T.L. Wilson, *Astrophys. J.***483** (1997) 320.

[46] K.A. Olive, R.T. Rood, D.N. Schramm, J.W. Truran, and E. Vangioni-Flam, *Astrophys. J.***444** (1995) 680.

[47] J. Yang, M.S. Turner, G. Steigman, D.N. Schramm and K.A. Olive, *Astrophys. J.* **281** (1984) 493.

[48] B.E.J. Pagel, E.A. Simonson, R.J. Terlevich and M. Edmunds, *MNRAS* **255** (1992) 325; E. Skillman and R.C. Kennicutt, *Astrophys. J.***411** (1993) 655; E. Skillman, R.J. Terlevich, R.C. Kennicutt, D.R. Garnett, and E. Terlevich, *Astrophys. J.***431** (1994) 172.

[49] Y.I. Izotov, T.X. Thuan, and V.A. Lipovetsky, *Astrophys. J.***435** (1994) 647; *Ap.J.S.* **108** (1997) 1.

[50] K.A. Olive and G. Steigman, *Ap.J. Supp.* **97** (1995) 49.

[51] K.A. Olive, E. Skillman, and G. Steigman, *Astrophys. J.***483** (1997) 788.

[52] B.D. Fields and K.A. Olive, *Astrophys. J.***506** (1998) 177

[53] F. Spite, and M. Spite, *A.A.* **115** (1982) 357; M. Spite, J.P. Maillard, and F. Spite, *A.A.* **141** (1984) 56; F. Spite, and M. Spite, *A.A.* **163** (1986) 140; L.M. Hobbs,

and D.K. Duncan, *Astrophys. J.***317** (1987) 796; R. Rebolo, P. Molaro, J.E. and Beckman, *A.A.* **192** (1988) 192; M. Spite, F. Spite, R.C. Peterson, and F.H. Chaffee Jr., *A.A.* **172** (1987) L9; R. Rebolo, J.E. Beckman, and P. Molaro, *A.A.* **172** (1987) L17; L.M. Hobbs, and C. Pilachowski, *Astrophys. J.***326** (1988) L23; L.M. Hobbs, and J.A. Thorburn, *Astrophys. J.***375** (1991) 116; J.A. Thorburn, *Astrophys. J.***399** (1992) L83; C.A. Pilachowski, C. Sneden,and J. Booth, *Astrophys. J.***407** (1993) 699; L. Hobbs, and J. Thorburn, *Astrophys. J.***428** (1994) L25; J.A. Thorburn, and T.C. Beers, *Astrophys. J.***404** (1993) L13; F. Spite, and M. Spite, *A.A.* **279** (1993) L9. J.E. Norris, S.G. Ryan, and G.S. Stringfellow, *Astrophys. J.***423** (1994) 386.

[54] P. Molaro, F. Primas, and P. Bonifacio, *A.A.* **295** (1995) L47; P. Bonifacio and P. Molaro, *MNRAS* **285** (1997) 847.

[55] V.V. Smith, D.L. Lambert, and P.E. Nissen, *Astrophys. J.***408** (1992) 262; *Astrophys. J.*(1998) in press; L. Hobbs, and J. Thorburn, *Astrophys. J.***428** (1994) L25; M. Spite et al. *A.A.* (1998) submitted.

[56] G. Steigman, B. Fields, K.A. Olive, D.N. Schramm, and T.P. Walker, *Astrophys. J.***415** (1993) L35; M. Lemoine, D.N. Schramm, J.W. Truran, and C.J. Copi, *Astrophys. J.***478** (1997) 554; M.H. Pinsonneault, T.P. Walker, G. Steigman, and V.K. Naranyanan, *Astrophys. J.*(1998) submitted; B.D.Fields and K.A. Olive, *New Astronomy*, astro-ph/9811183, in press; E. Vangioni-Flam, et al. *New Astronomy*, in press.

[57] T.P. Walker, G. Steigman, D.N. Schramm, K.A. Olive and B. Fields, *Astrophys. J.***413** (1993) 562; K.A. Olive, and D.N. Schramm, *Nature* **360** (1993) 439.

[58] D. Thomas, D. Schramm, K.A. Olive, and B. Fields, *Astrophys. J.***406** (1993) 569.

[59] L. Kawano, preprint FERMILAB-Pub-88/34-A; preprint FERMILAB-Pub-92/04-A.

[60] R.V. Wagoner, W.A. Fowler and F. Hoyle, *Astrophys. J.* **148** (1967) 3.

[61] R.V. Wagoner, *Astrophys. J. Suppl.* **18** (1969) 247.

[62] R.V. Wagoner, *Astrophys. J.* **179** (1973) 343.

[63] M.S. Turner, Proceedings of the Nobel Symposium on Particle Physics and the Universe, Enkoping, Sweden, 20-25 Aug 1998, preprint astro-ph/9901109.

[64] A. Sirlin, *Phys. Rev.* **164** (1967) 1767.

[65] V.P. Gudkov and K. Kubodera, preprint nucl-th/9706074.

[66] W.J. Marciano and A. Sirlin, *Phys. Rev. Lett.* **56** (1986) 22 and references therein.

[67] W.J. Marciano and A. Sirlin, *Phys. Rev. Lett.* **46** (1981) 163.

[68] D.M. Wilkinson, *Nucl. Phys.* **A 377** (1982) 474.

[69] D. Seckel, preprint BA-93-16, hep-ph/9305311;
R. E. Lopez, M. S. Turner and G. Gyuk, *Phys. Rev.* **D 56** (1997) 3191.

[70] E.D. Commins and P.M. Bucksbaum, *Weak Interactions of Leptons and Quarks* (Cambridge University Press, Cambridge, England, 1983).

[71] F. Halzen and A.D. Martin, *Quarks and Leptons*, (Wiley, 1984, New York).

[72] J.L. Cambier, J.R. Primack and M. Sher, *Nucl. Phys.* **B 209** (1982) 372.

[73] J.F. Donoghue, B.R. Holstein and R.W. Robinett, *Ann. Phys.* (N.Y.) **164** (1985) 23.

[74] J.F. Donoghue and B.R. Holstein, *Phys. Rev.* **D28** (1983) 340; *Phys. Rev.* **D 29** (1984) 3004.

[75] A.E. Johansson, G. Peresutti and B.S. Skagerstam, *Nucl. Phys.* **B 278** (1986) 324.

[76] W. Keil, *Phys. Rev.* **D 40** (1989)1176.

[77] R. Baier, E. Pilon, B. Pire and D. Schiff, *Nucl. Phys.* **B 336** (1990) 157.

[78] W. Keil and R. Kobes, *Physica* **A 158** (1989) 47.

[79] M. LeBellac and D. Poizat, *Z. Phys.* **C 47** (1990) 125.

[80] T. Altherr and P.Aurenche, *Phys. Rev.* **D 40** (1989) 4171.

[81] R.L. Kobes and G.W. Semeneff, *Nucl. Phys.* **B 260** (1985) 714; ibidem **B 272** (1986) 329.

[82] R.F. Sawyer, *Phys. Rev.* **D 53** (1996) 4232.

[83] I.A. Chapman, *Phys. Rev.* **D 55** (1997) 6287.

[84] S. Esposito, G. Mangano, G. Miele and O. Pisanti, *Phys. Rev.* **D 58** (1998) 105023.

[85] A.J. Heckler, *Phys. Rev.* **D 49** (1994) 611.

[86] L. Dolan and R. Jackiw, *Phys. Rev.* **D 9** (1974) 3320; H.A. Weldon, *Phys. Rev.* **D 26** (1982) 1394.

[87] D. Bailin and A. Love, *Introduction to Gauge Field Theory* (Bristol, 1986, Adam Hilger).

[88] J. Kapusta, *Finite Temperature Field Theory* (Cambridge, 1988, Cambridge University Press).

[89] S. Dodelson and M.S. Turner, *Phys. Rev.* **D 46** (1992) 3372; A.D. Dolgov and M. Fukugita, *Phys. Rev.* **D 46** (1992) 5378; M.A.Herrera and S. Hacyan, *Astrophys. J.* **336** (1989) 539.

[90] G. Fiorentini, E. Lisi, S. Sarkar and F.L. Villante, *Phys. Rev.* **D 58** (1998) 063506.

[91] L.M. Krauss and P. Romanelli, *Astrophys. J.***358** (1990) 47;
P.J. Kernan and L.M. Krauss, *Phys. Rev. Lett.* **72** (1994) 3309.

[92] M. Srednicki, W. Watkins and K.A. Olive, *Nucl. Phys.* **B 310** (1988) 693; P. Gondolo and G. Gelmini, *Nucl. Phys.* **B 360** (1991) 145.

[93] C.W. Gear, *Numerical initial value problems in ordinary differential equations*, (Englewood, 1971, Cliffs, N.J.: Prentice Hall); J. Stoer and R. Bulirsch, *Introduction to numerical analysis*, (New York, 1980, Springer-Verlag).

Appendix A

Non equilibrium distribution of species

Decoupling of species from the background plasma is properly described by the evolution of the particles's phase space distribution function $f(p^\mu, x^\mu)$, given by the Boltzmann equation. In this appendix we follow the approach of [4] and restrict our analysis to an homogeneous and isotropic plasma, described by the Robertson-Walker metric. In this case $f = f(|\mathbf{p}|, t)$ or equivalently $f = f(E, t)$ and the Boltzmann equation is

$$E\,\frac{\partial f}{\partial t} \;-\; \frac{\dot{R}}{R}\,|\mathbf{p}|^2\,\frac{\partial f}{\partial E} \;=\; C[f] \quad , \tag{A.1}$$

where $C[f]$ is the collisional operator for the processes creating and destroying the given particle specie. It is more convenient to use the number density $n(t)$ rather than the distribution function, defined by

$$n(t) \;=\; g\int \frac{d^3p}{(2\pi)^3}\,f(E,t) \quad , \tag{A.2}$$

g being the internal degrees of freedom. For this quantity the Boltzmann equation becomes

$$\frac{dn}{dt} \;+\; 3H\,n \;=\; g\int \frac{d^3p}{(2\pi)^3}\,\frac{1}{E}\,C[f] \quad , \tag{A.3}$$

with $H = \dot{R}/R$. Let us focus on a given particle ψ, interacting with the other particles in the heat bath through the reaction $\psi + a + b + ... \longleftrightarrow i + j + ...$; for this process the collisional term can be written in the form

$$\begin{aligned} g\int \frac{d^3p}{(2\pi)^3}\,\frac{1}{E}\,C[f] \;&=\; -\int d\Pi_T\,(2\pi)^4\,\delta^4(\mathrm{p}_\psi + \mathrm{p}_a + \mathrm{p}_b ... - \mathrm{p}_i - \mathrm{p}_j ...)\times \\ &\times\;\; \Big(\overline{|M|^2}_{forward}\,\Phi_{forward} \;-\; \overline{|M|^2}_{backward}\,\Phi_{backward}\Big) \quad , \end{aligned} \tag{A.4}$$

with

$$\Phi_{forward} \;=\; f_\psi\, f_a\, f_b\, ...\,(1\pm f_i)\,(1\pm f_j)\,... \tag{A.5}$$

$$\Phi_{backward} \;=\; f_i\, f_j\, ...\,(1\pm f_\psi)\,(1\pm f_a)\,(1\pm f_b)\,... \tag{A.6}$$

where +/- refers to bosons/fermions. The phase space density is given by

$$d\Pi_T \;=\; d\Pi_\psi\, d\Pi_a\, d\Pi_b\, ...\, d\Pi_i\, d\Pi_j \quad , \tag{A.7}$$

$$d\Pi_\alpha \;=\; \frac{g_{|}\alpha}{(2\pi)^3}\,\frac{d^3p_\alpha}{2E_\alpha} \quad , \tag{A.8}$$

while the squared matrix elements $|M|^2$ are averaged over initial and final spins and, assuming CP invariance, $\overline{|M|^2}_{forward} = \overline{|M|^2}_{backward} = |M|^2$.

For illustrative purposes, we consider only situations in which Bose condensation or Fermi degeneracy can be neglected, so that we may safely disregard the stimulated emission or blocking factors in (A.4): $(1 \pm f_\alpha) \simeq 1$. In these approximations, the evolution equation (A.3) simplifies to

$$\begin{aligned} \frac{dn_\psi}{dt} \;+\; 3H\,n_\psi \;&=\; -\;\int d\Pi_T\,(2\pi)^4\,\delta^4(\mathrm{p}_\psi + \mathrm{p}_a + \mathrm{p}_b ... - \mathrm{p}_i - \mathrm{p}_j ...)\,\overline{|M|^2}\times \\ &\times\;\; (f_\psi\, f_a\, f_b\, ... \;-\; f_i\, f_j\, ...) \quad . \end{aligned} \tag{A.9}$$

Note that the $3H\,n_\psi$ term accounts for the dilution effect of the expansion of the Universe, while the right hand side term accounts for the number changing ψ interactions. The dilution factor can be absorbed by considering the particle number in the comoving volume R^3, proportional to the quantity

$$Y \;=\; \frac{n_\psi}{s} \quad , \tag{A.10}$$

where $s \propto R^{-3}$ is the entropy density. In fact, in this case the left hand side of (A.9) becomes simply

$$\frac{dn_\psi}{dt} \;+\; 3H\,n_\psi \;=\; \frac{1}{s}\,\frac{dY}{dt} \quad . \tag{A.11}$$

We are now in a position to describe the decoupling (i.e. the exit from chemical equilibrium) of the given specie from the background plasma. Restricting ourselves to the case in which this specie is stable, the only number changing processes are of the type

$$\psi\,\overline{\psi} \;\longleftrightarrow\; X\,\overline{X} \quad . \tag{A.12}$$

With X we generically denote all the species into which ψ can annihilate. These particles are, of course, in thermal equilibrium and hereafter we neglect, for simplicity, any chemical potential. Then we have

$$f_{X,\overline{X}} \;\simeq\; \exp\left\{-\,\frac{E_{X,\overline{X}}}{T}\right\} \tag{A.13}$$

but, by means of energy conservation, the following condition

$$f_X\, f_{\overline{X}} \;\simeq\; \exp\left\{-\,\frac{E_\psi}{T}\right\}\, \exp\left\{-\,\frac{E_{\overline{\psi}}}{T}\right\} \;\simeq\; f_\psi^{EQ}\, f_{\overline{\psi}}^{EQ} \tag{A.14}$$

holds, where with the index EQ we have indicated the equilibrium distributions. Hence the statistical factor in (A.9) takes the form

$$f_\psi\, f_{\overline{\psi}} \;-\; f_X\, f_{\overline{X}} \;=\; f_\psi\, f_{\overline{\psi}} \;-\; f_\psi^{EQ}\, f_{\overline{\psi}}^{EQ} \tag{A.15}$$

and the Boltzmann equation for the present case becomes

$$\frac{dn_\psi}{dt} \;+\; 3H\, n_\psi \;=\; -\, <\sigma_{\psi\overline{\psi}\to X\overline{X}}\, v>\, \left(n_\psi^2 \;-\; (n_\psi^{EQ})^2\right) \tag{A.16}$$

where $<\sigma v>$ is the thermally averaged annihilation cross section times velocity:

$$\begin{aligned} <\sigma_{\psi\overline{\psi}\to X\overline{X}} v> \;&=\; \frac{1}{(n_\psi^{EQ})^2} \int d\Pi_T\, (2\pi)^4\, \delta^4(\mathrm{p}_\psi + \mathrm{p}_{\overline{\psi}} - \mathrm{p}_X - p_{\overline{X}}) \times \\ &\times\;\; \overline{|M|^2}\, \exp\left\{-\,\frac{E_\psi}{T}\right\}\, \exp\left\{-\,\frac{E_{\overline{\psi}}}{T}\right\} \quad . \end{aligned} \tag{A.17}$$

We stress that the rate of change of $\psi, \overline{\psi}$ is proportional to the annihilation rate, while it tends to zero when the equilibrium is approaching since creation processes balance destruction ones.

Another impressive form of (A.16) is obtained by considering the Boltzmann equation for the quantity Y and rewriting the t dependence in terms of the temperature or, better, in terms of the adimensional parameter $z = m_\psi/T$:

$$\frac{z}{Y_{EQ}}\, \frac{dY}{dz} \;=\; -\,\frac{\Gamma}{H}\, \left\{\left(\frac{Y}{Y_{EQ}}\right)^2 \;-\; 1\right\} \tag{A.18}$$

$$\Gamma \, = \, n_{EQ} < \sigma \, v > \quad . \tag{A.19}$$

From these we immediately see that the rate of change of ψ per comoving volume is set by the factor Γ/H: when this is less than order unity, the relative change in the number of ψ in the comoving volume becomes small, annihilations freeze out and the abundance of ψ “freezes in”.

Appendix B

Neutrino-photon temperature relation

When neutrinos decouple (at T_ν^D around $1\,MeV$) from the background primordial plasma, their thermal distribution retains the equilibrium Fermi-Dirac form with a temperature T_ν scaling (approximately) as the inverse of the cosmic scale factor R. As discussed in 1.4.1, their entropy S_ν in the comoving volume is conserved also after decoupling

$$S_\nu(T_\nu^D) \; = \; S_\nu(T_\nu) \quad . \tag{B.1}$$

On the other side, photons still remain in equilibrium with the $e^\pm$ pairs until these disappear when become non relativistic (around $T \sim m_e$). However, since the total entropy in the comoving volume is conserved as well as neutrino entropy, it follows that the entropy S_I of the species still in equilibrium ($I = e^\pm, \gamma$) is conserved too

$$S_I(T_D) \; = \; S_I(T) \quad . \tag{B.2}$$

Note that, until neutrinos decouple, $T_\nu = T$; consequently $T_\nu^D = T_D$. According to Eqs. (1.77) and (1.49), (1.50), the entropy of a specie is explicitly given by

$$S_i \; = \; \frac{g_i}{6\pi^2}\, I(x_i)\, R^3\, T_i^3 \quad , \tag{B.3}$$

$$I(x_i) \; = \; \int_0^\infty dy\, \frac{(y^2 + 2x_i y)^{1/2}\,(4y^2 + 8x_i y + 3x_i^2)}{e^{x_i+y} \pm 1} \quad , \tag{B.4}$$

where $x_i = m_i/T_i$, $y = (E_i - m_i)/T_i$. Here, the effective (T dependent) degrees of freedom are parametrized by $g_i(T) = (g_i/6\pi^2)\, I(x_i)$. Substituting (B.3) in (B.1), (B.2) and dividing side by side these two equations, the following relation between T_ν and T is obtained [92]

$$\left(\frac{T_\nu}{T}\right)^3 \; = \; \frac{g_\nu(T_D)}{g_I(T_D)}\, \frac{g_I(T)}{g_\nu(T)} \tag{B.5}$$

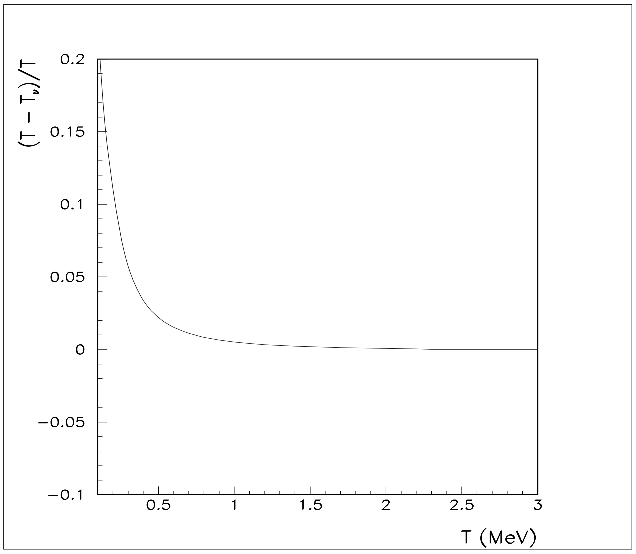

Figure B.1: Neutrino - photon temperature difference.

or, more explicitly,

$$\frac{T_\nu}{T} = \left(\frac{2\pi^4 + 15\, I(x_e)}{2\pi^4 + 15\, I(x_e^D)}\right)^{\frac{1}{3}} \quad . \tag{B.6}$$

In the limit (considered in 1.4.1) in which $g_I(T) \simeq 2$, $g_I(T_D) \simeq 11/2$ $(g_\nu(T_D) = g_\nu(T))$, from (B.5) the relation (1.119) follows. Instead (B.6) gives the generalization for T_ν as function of T we looked for. In Figure B.1 we plot the relative difference in temperature between neutrinos and photons; of course, before decoupling the two temperature coincide (the plotted curve is evaluated from (B.6) adopting the value $2.3\, MeV$ for the decoupling temperature; results practically unchange by shifting this temperature in the range $2 \div 3\, MeV$).

Appendix C

Nuclear reaction network

In the following Tables C.1 - C.9 we show the complete nuclear reaction network relevant for the calculations of the primordial abundances of light elements [60, 61, 62, 59].

Table C.1: Nuclear β-decay reactions.

^{3}H	$\rightarrow$	$e^{-}+\overline{\nu}_{e}+{}^{3}He$
^{8}Li	$\rightarrow$	$e^{-}+\overline{\nu}_{e}+2{}^{4}He$
^{12}B	$\rightarrow$	$e^{-}+\overline{\nu}_{e}+{}^{12}C$
^{14}C	$\rightarrow$	$e^{-}+\overline{\nu}_{e}+{}^{14}N$
^{8}B	$\rightarrow$	$e^{+}+\nu_{e}+2{}^{4}He$
^{11}C	$\rightarrow$	$e^{+}+\nu_{e}+{}^{11}B$
^{12}N	$\rightarrow$	$e^{+}+\nu_{e}+{}^{12}C$
^{13}N	$\rightarrow$	$e^{+}+\nu_{e}+{}^{13}C$
^{14}O	$\rightarrow$	$e^{+}+\nu_{e}+{}^{14}N$
^{15}O	$\rightarrow$	$e^{+}+\nu_{e}+{}^{15}N$

Table C.2: Nuclear neutron-photon reactions.

H	(n,γ)	D
D	(n,γ)	^{3}H
^{3}He	(n,γ)	^{4}He
^{6}Li	(n,γ)	^{7}Li
^{7}Li	(n,γ)	^{8}Li
^{10}B	(n,γ)	^{11}B
^{11}B	(n,γ)	^{12}B
^{12}C	(n,γ)	^{13}C
^{13}C	(n,γ)	^{14}C
^{14}N	(n,γ)	^{15}N

Table C.3: Nuclear neutron-proton and proton-neutron reactions.

^{3}He	(n,p)	^{3}H
^{7}Be	(n,p)	^{7}Li
^{11}C	(n,p)	^{11}B
^{13}N	(n,p)	^{13}C
^{14}N	(n,p)	^{14}C
^{15}O	(n,p)	^{15}N
^{12}B	(p,n)	^{12}C

Table C.4: Nuclear neutron-α and α-neutron reactions.

^{6}Li	(n,α)	^{3}H
^{7}Be	(n,α)	^{4}He
^{10}B	(n,α)	^{7}Li
^{15}O	(n,α)	^{12}C
^{8}Li	(α,n)	^{11}B
^{9}Be	(α,n)	^{12}C
^{10}B	(α,n)	^{13}N
^{11}B	(α,n)	^{14}N
^{12}B	(α,n)	^{15}N
^{13}C	(α,n)	^{16}O

Table C.5: Nuclear proton-photon reactions.

D	(p,γ)	^{3}He
^{3}H	(p,γ)	^{4}He
^{6}Li	(p,γ)	^{7}Be
^{7}Be	(p,γ)	^{8}B
^{9}Be	(p,γ)	^{10}B
^{10}B	(p,γ)	^{11}C
^{11}B	(p,γ)	^{12}C
^{11}C	(p,γ)	^{12}N
^{12}C	(p,γ)	^{13}N
^{13}C	(p,γ)	^{14}N
^{14}C	(p,γ)	^{15}N
^{13}N	(p,γ)	^{14}O
^{14}N	(p,γ)	^{15}O
^{15}N	(p,γ)	^{16}O

Table C.6: Nuclear proton-α and α-proton reactions.

^{6}Li	(p,α)	^{3}He
^{7}Li	(p,α)	^{4}He
^{9}Be	(p,α)	^{6}Li
^{10}B	(p,α)	^{7}Be
^{12}B	(p,α)	^{9}Be
^{15}N	(p,α)	^{12}C
^{8}B	(α,p)	^{11}C
^{10}B	(α,p)	^{13}C
^{11}B	(α,p)	^{14}C
^{11}C	(α,p)	^{14}N
^{12}N	(α,p)	^{15}O
^{13}N	(α,p)	^{16}O

Table C.7: Nuclear α-photon reactions.

D	(α,γ)	^{6}Li
^{3}H	(α,γ)	^{7}Li
^{3}He	(α,γ)	^{7}Be
^{6}Li	(α,γ)	^{10}B
^{7}Li	(α,γ)	^{11}B
^{7}Be	(α,γ)	$^{11}C)$
^{12}C	(α,γ)	^{16}O

Table C.8: Nuclear deuterium-nucleon reactions.

D	(d,n)	^{3}He
D	(d,p)	^{3}H
^{3}H	(d,n)	^{4}He
^{3}He	(d,p)	^{4}He
^{9}Be	(d,n)	^{10}B
^{10}B	(d,p)	^{11}B
^{11}B	(d,n)	^{12}C

Table C.9: Nuclear three-body reactions.

^3He	$(^3He, 2p)$	^4He
^7Li	$(d, n\,\alpha)$	^4He
^7Be	$(d, p\,\alpha)$	^4He
^4He	$(\alpha\, n, \gamma)$	^9Be
^4He	$(2\alpha, \gamma)$	^{12}C
^8Li	$(p, n\,\alpha)$	^4He
^8B	$(n, p\,\alpha)$	^4He
^9Be	$(p, d\,\alpha)$	^4He
^{11}B	$(p, 2\alpha)$	^4He
^{11}C	$(n, 2\alpha)$	^4He

Appendix D

Nuclide mass excess

In this appendix we report the measured mass excess Δm_i for the 26 nuclides used in BBN calculations [35].

Table D.1: Nuclear mass excess Δm_i in KeV (referred to ^{12}C).

n	8071.323 ± 0.002	^{11}B	8667.984 ± 0.420
p	7288.969 ± 0.001	^{11}C	10650.531 ± 0.952
D	13135.720 ± 0.001	^{12}B	13368.901 ± 1.400
^{3}H	14949.794 ± 0.001	^{12}C	0.0
^{3}He	14931.204 ± 0.001	^{12}N	17338.083 ± 1.000
^{4}He	2424.911 ± 0.001	^{13}C	3125.011 ± 0.001
^{6}Li	14086.312 ± 0.475	^{13}N	5345.456 ± 0.270
^{7}Li	14907.673 ± 0.473	^{14}C	3019.892 ± 0.004
^{7}Be	15769.489 ± 0.472	^{14}N	2863.417 ± 0.001
^{8}Li	20946.195 ± 0.488	^{14}O	8006.456 ± 0.075
^{8}B	22921.002 ± 1.107	^{15}N	101.438 ± 0.001
^{9}Be	40818.362 ± 62.471	^{15}O	2855.388 ± 0.503
^{10}B	12050.761 ± 0.370	^{16}O	-4736.998 ± 0.001

Appendix E

Finite nucleon mass corrected matrix element

In this appendix we report the result for the spin summed squared modulus of Eq. (4.1)

$$
\begin{aligned}
\sum_{\text{spins}} |M|^2 \;=\; 16\,(\;& {C_A}^2\,(M_1^2\,M_2^2 + 2\,M_1^2\,M_3^2 + M_2^2\,M_3^2 + 2\,M_1^2\,M_2\,M_4 + 2\,M_2\,M_3^2\,M_4 + \\
+ \;& M_1^2\,M_4^2 + 2\,M_2^2\,M_4^2 + M_3^2\,M_4^2 - 2\,M_1^2\,s - 2\,M_2^2\,s + \\
- \;& 2\,M_3^2\,s - 2\,M_4^2\,s + 2\,s^2 - M_1^2\,t - M_2^2\,t + \\
- \;& M_3^2\,t - 2\,M_2\,M_4\,t - M_4^2\,t + 2\,s\,t + t^2) + \\
+ \;& {C_V}^2\,(M_1^2\,M_2^2 + 2\,M_1^2\,M_3^2 + M_2^2\,M_3^2 - 2\,M_1^2\,M_2\,M_4 - 2\,M_2\,M_3^2\,M_4 + \\
+ \;& M_1^2\,M_4^2 + 2\,M_2^2\,M_4^2 + M_3^2\,M_4^2 - 2\,M_1^2\,s - 2\,M_2^2\,s + \\
- \;& 2\,M_3^2\,s - 2\,M_4^2\,s + 2\,s^2 - M_1^2\,t - M_2^2\,t + \\
- \;& M_3^2\,t + 2\,M_2\,M_4\,t - M_4^2\,t + 2\,s\,t + t^2) + \\
+ \;& 2\,C_A\,f_{ps}\,(-M_1^2\,M_2\,M_3^2 + M_2^3\,M_3^2 + M_2\,M_3^4 + M_1^4\,M_4 - M_1^2\,M_3^2\,M_4 + \\
- \;& M_2^2\,M_3^2\,M_4 - M_1^2\,M_2\,M_4^2 + M_1^2\,M_4^3 + M_1^2\,M_2\,s - M_2\,M_3^2\,s + \\
- \;& M_1^2\,M_4\,s + M_3^2\,M_4\,s - M_2\,M_3^2\,t - M_1^2\,M_4\,t) + \\
- \;& 2\,C_A\,\frac{f_2}{M_N}\,(M_1^2\,M_2^3 - M_2^3\,M_3^2 + M_1^2\,M_2^2\,M_4 - M_2^2\,M_3^2\,M_4 - M_1^2\,M_2\,M_4^2 + \\
+ \;& M_2\,M_3^2\,M_4^2 - M_1^2\,M_4^3 + M_3^2\,M_4^3 - M_1^2\,M_2\,t - M_2^3\,t + \\
- \;& M_2\,M_3^2\,t - M_1^2\,M_4\,t - M_2^2\,M_4\,t - M_3^2\,M_4\,t - M_2\,M_4^2\,t + \\
- \;& M_4^3\,t + 2\,M_2\,s\,t + 2\,M_4\,s\,t + M_2\,t^2 + M_4\,t^2) + \\
+ \;& 2\,C_V\,f_3\,(-M_1^2\,M_2\,M_3^2 + M_2^3\,M_3^2 + M_2\,M_3^4 - M_1^4\,M_4 + M_1^2\,M_3^2\,M_4 +
\end{aligned}
$$

$$\begin{aligned}
+ \quad & M_2^2\, M_3^2\, M_4 \,-\, M_1^2\, M_2\, M_4^2 \,-\, M_1^2\, M_4^3 \,+\, M_1^2\, M_2\, s \,-\, M_2\, M_3^2\, s \,+ \\
+ \quad & M_1^2\, M_4\, s \,-\, M_3^2\, M_4\, s \,-\, M_2\, M_3^2\, t \,+\, M_1^2\, M_4\, t) \,+ \\
+ \quad & 2\, C_V\, C_A\, (\,-\, M_1^2\, M_2^2 \,+\, M_2^2\, M_3^2 \,+\, M_1^2\, M_4^2 \,-\, M_3^2\, M_4^2 \,+\, M_1^2\, t \,+ \\
+ \quad & M_2^2\, t \,+\, M_3^2\, t \,+\, M_4^2\, t \,-\, 2\, s\, t \,-\, t^2) \,+ \\
+ \quad & 2\, C_V\, \frac{f_2}{M_N}\, (M_1^2\, M_2^3 \,+\, M_1^2\, M_2\, M_3^2 \,-\, M_2\, M_3^4 \,-\, M_1^4\, M_4 \,-\, M_1^2\, M_2^2\, M_4 \,+ \\
+ \quad & M_1^2\, M_3^2\, M_4 \,-\, M_2\, M_3^2\, M_4^2 \,+\, M_3^2\, M_4^3 \,-\, M_1^2\, M_2\, s \,+\, M_2\, M_3^2\, s \,+ \\
+ \quad & M_1^2\, M_4\, s \,-\, M_3^2\, M_4\, s \,-\, M_1^2\, M_2\, t \,-\, M_2^3\, t \,+\, M_2^2\, M_4\, t \,+ \\
- \quad & M_3^2\, M_4\, t \,+\, M_2\, M_4^2\, t \,-\, M_4^3\, t \,+\, M_2\, t^2 \,+\, M_4\, t^2))
\end{aligned} \tag{E.1}$$

In the above formula, neutrino mass has not been set to zero to give a general expression holding for all reactions. For the two-body scattering processes in (3.1), (3.2), (3.3) it is

$$\begin{aligned}
s &= (p_1 + p_2)^2 = (p_3 + p_4)^2 \quad , \\
t &= (p_1 - p_3)^2 = (p_2 - p_4)^2 \quad .
\end{aligned}$$

As in section (3.1), p_1 and p_3 are the initial and final lepton momentum while p_2 and p_4 are the initial and final nucleon momentum, respectively. Instead for $n \rightarrow p\, e^-\, \overline{\nu}_e$ it is

$$\begin{aligned}
s &= (-\,p_1 + p_2)^2 = (p_3 + p_4)^2 \quad , \\
t &= (-\,p_1 - p_3)^2 = (-\,p_2 + p_4)^2 \quad .
\end{aligned}$$

while for $p\, e^-\, \overline{\nu}_e \rightarrow n$ it is

$$\begin{aligned}
s &= (p_1 + p_2)^2 = (-\,p_3 + p_4)^2 \\
t &= (p_1 + p_3)^2 = (-\,p_2 + p_4)^2
\end{aligned}$$

Appendix F

Finite temperature and density QED

F.1 The Real Time Formalism

At finite temperatures, physical processes take place in a heat bath consisting of a background of a plasma of particles and antiparticles. All interaction processes must be therefore considered as occurring in a thermal "vacuum" state, which does not coincide with the usual Poincaré invariant vacuum of zero temperature quantum field theory. Manifest Lorentz invariance therefore breaks down due to the choice of the preferred frame of the bath, and the zero temperature renormalization prescription cannot be applied straightforwardly. The covariant formalism that enables to consider the interactions of a given particle with the surrounding medium is the Finite Temperature and Density Quantum Field Theory [86, 87, 88]. Here we adopt the Real Time formulation of this theory, in which the Feynman rules for the vertices are identical to the corresponding ones in the vacuum. The effect of the temperature and of the density is taken into account in the expressions of the free particle propagators. For fermions and bosons we have respectively

$$\begin{aligned} S_F(p) &= (\not p + m)\left(\frac{1}{p^2 - m^2} + i\,\Gamma_F(p)\right) \quad , &\text{(F.1)}\\ D_{\mu\nu}(p) &= -\,g_{\mu\nu}\left(\frac{1}{p^2 - m^2} - i\,\Gamma_B(p)\right) \quad , &\text{(F.2)}\end{aligned}$$

where

$$\Gamma(p) = 2\pi\,\delta(p^2 - m^2)\,\left(\theta(p{\cdot}u)\,n(p) + \theta(-p{\cdot}u)\,\overline{n}(p)\right) \quad , \qquad \text{(F.3)}$$

and

$$
\begin{aligned}
n_F(p) &= \frac{1}{e^{\beta(|p\cdot u|-\mu)} + 1} \quad , && \text{(F.4)} \\
n_B(p) &= \frac{1}{e^{\beta(|p\cdot u|-\mu)} - 1} \quad , && \text{(F.5)}
\end{aligned}
$$

($\beta = 1/T$) are the Fermi-Dirac and Bose-Einstein distribution functions ($\overline{n}_F$ and $\overline{n}_B$ are the distribution for the antiparticles, obtained replacing μ with $-\mu$). Note that in a plasma, another 4-vector must be considered, the 4-velocity u^μ of the medium, which in its rest frame is given by $u^\mu = (1, \mathbf{0})$.

The additional contributions in the above formulas (denoted with $\Gamma_{F,B}$) pick up *real* particles through the mass shell δ-functions and are proportional to the particle densities in the thermal bath. They take into account the role played by the medium in the single particle propagation.

The heat bath we are interested in is the primordial plasma at the epoch of BBN, i.e. at temperature around 1 MeV. At these temperatures the $W^\pm$ and Z^0 gauge bosons degrees of freedom are not excited, so we can safely neglect the temperature dependent term $\Gamma_B(p)$ in $D_{\mu\nu}$ for these bosons.

Our primordial plasma consists of nucleon, $e^\pm$ pairs, photons and neutrinos. The temperature dependent term in the propagator of nucleons would be suppressed by a Boltzmann factor smaller than $\exp(-100)$, compared with the ones for the other particles, in the temperature range relevant for BBN, so it will be neglected in the following as well.

The most important finite temperature effects induced by the remaining particles in the heat bath come from the QED interactions of $e^\pm$ and photons, which are of order α. Neutrinos only interact weakly, thus their contribution is at least of order G_F.

In this appendix we calculate the $e^\pm$ self-energy and wavefunction renormalization at finite temperature and photon self-energy, which are relevant for the thermal radiative corrections considered in chapter 5.

F.2 Electron self-energy

The Feynman diagram for electron self-energy Σ is reported in Figure F.1; it gives

$$
-\,i\,\Sigma \;=\; \int \frac{d^4k}{(2\pi)^4}\,(i\,e\,\gamma^\mu)\;i\,S_F(p-k)\;(i\,e\,\gamma^\nu)\;i\,D_{\mu\nu}(k) \qquad \text{(F.6)}
$$

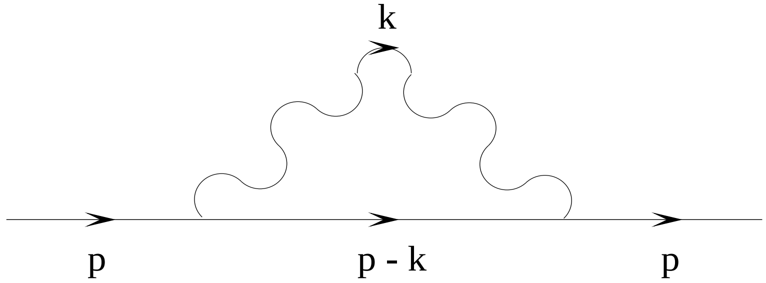

Figure F.1: Self-energy diagram for an electron in a plasma.

where $S_F(p-k)$ and $D_{\mu\nu}(k)$ are the (RTF) Fermi and Bose propagators in a plasma, which are reported in (F.1), (F.2). Here we are only interested in the temperature dependent part Σ_T of the self-energy; moreover, we neglect possible damping effects (which are suppressed with respect to coherent ones) and then consider only its real part:

$$\begin{aligned} \Re(\Sigma_T) \;=\; \Re(\Sigma_T^B) \;+\; \Re(\Sigma_T^F) \;&=\; 2\,e^2 \int \frac{d^4k}{(2\pi)^4} \left((\not{p} - \not{k} \,-\, 2m_e)\, \frac{\Gamma_B(k)}{(p-k)^2 \,-\, m_e^2} \;+ \right. \\ &\left. -\;\; (\not{k} \,-\, 2m_e)\, \frac{\Gamma_F(k)}{(p-k)^2} \right) \end{aligned} \tag{F.7}$$

From Lorentz invariance, it follows that the self-energy has the general form

$$\Re\Sigma_T \;=\; a\;\not{p} \;+\; b\;\not{u} \;+\; c \tag{F.8}$$

where a, b, c are functions of the only two invariants p^2,$p{\cdot}u$ (obviously $u^2 = 1$). In the following, when necessary, we shall adopt the plasma rest frame, where $u^\mu = (1, \mathbf{0})$. We then have

$$a \;=\; -\frac{1}{\mathbf{p}^2}\,(T_p \,-\, p_0\,T_u) \tag{F.9}$$

$$b \;=\; -\frac{1}{\mathbf{p}^2}\,\Big((p_0^2 \,-\, \mathbf{p}^2\,T_u \,-\, p_0\,T_p\Big) \tag{F.10}$$

$$c \;=\; \frac{1}{4}\,Tr\,\Re\Sigma_T \tag{F.11}$$

where

$$T_p \;=\; \frac{1}{4}\,Tr\,(\not{p}\,\Re\Sigma_T) \tag{F.12}$$

$$T_u \;=\; \frac{1}{4}\,Tr\,(\not{u}\,\Re\Sigma_T) \tag{F.13}$$

For the Bose parts, after some calculations we obtain ($p = |\mathbf{p}|,\ k = |\mathbf{k}|$)

$$T_p^B \;=\; -\frac{\alpha}{2\pi}\int dk\,k\,B(k)\left(-4 + \frac{\eta^2 + 2m_e^2}{2k}\,\left(I_1(p_0,p,k) + I_1(-p_0,p,k)\right)\right) \tag{F.14}$$

$$T_u^B \;=\; -\frac{\alpha}{2\pi}\int dk\,B(k)\,\left((p_0\,-\,k)\,I_1(p_0,p,k)\;+p_0\,+\,k)\,I_1(-p_0,p,k)\right) \tag{F.15}$$

$$c_B \;=\; \frac{\alpha\,m_e}{\pi}\int dk\,B(k)\,\left(I_1(p_0,p,k)\;+\;I_1(-p_0,p,k)\right) \tag{F.16}$$

where $\eta \,=\, p_0^2\,-\,\mathbf{p}^2\,-m_e^2$. Instead for the Fermi parts we get:

$$T_p^F \;=\; -\frac{\alpha}{2\pi}\int dk\,\frac{k^2}{E}\,F(E)\,\left(I_2(p_0,p,k)\;+\;I_2(-p_0,p,k)\right) \tag{F.17}$$

$$T_u^F \;=\; -\frac{\alpha}{2\pi}\int dk\,k^2\,F(E)\,\left(I_3(p_0,p,k)\;-\;I_3(-p_0,p,k)\right) \tag{F.18}$$

$$c_F \;=\; \frac{\alpha\,m_e}{\pi}\int dk\,\frac{k^2}{E}\,F(E)\,\left(I_3(p_0,p,k)\;+\;I_3(-p_0,p,k)\right) \tag{F.19}$$

with $E \,=\, \sqrt{\mathbf{p}^2\,+\,m_e^2}$. The quantities I_i are defined by [1]

$$I_1(p_0,p,k) \;=\; \int_{-1}^{1}\frac{dx}{p_0\,-\,\frac{\eta}{2k}\,-\,px} \;=\; \frac{1}{p}\,\ln\frac{|p_0\,-\,\frac{\eta}{2k}\,+\,p|}{|p_0\,-\,\frac{\eta}{2k}\,-\,p|} \tag{F.20}$$

$$\begin{aligned} I_2(p_0,p,k) \;&=\; \int_{-1}^{1}dx\,\frac{2(p_0E\,-\,pkx)}{\eta\,+\,2m_e^2\,-\,2p_0E\,+\,2pkx} \;= \\ &=\; \frac{\eta\,+\,2m_e^2}{2pk}\,\ln\frac{|\eta\,+\,2m_e^2\,-\,2p_0E\,+\,2pk|}{|\eta\,+\,2m_e^2\,-\,2p_0E\,-\,2pk|} \end{aligned} \tag{F.21}$$

$$\begin{aligned} I_3(p_0,p,k) \;&=\; \int_{-1}^{1}\frac{2\,dx}{\eta\,+\,2m_e^2\,-\,2p_0E\,+\,2pkx} \;= \\ &=\; \frac{1}{pk}\,\ln\frac{|\eta\,+\,2m_e^2\,-\,2p_0E\,+\,2pk|}{|\eta\,+\,2m_e^2\,-\,2p_0E\,-\,2pk|} \end{aligned} \tag{F.22}$$

In the above formulas we have treated p_0 and $\mathbf{p}$ as two independent variables. Since the expressions in (F.14)-(F.19) are already of order α, in these we can substitute the vacuum dispersion relation $p_0^2 \,=\, \mathbf{p}^2\,+\,m_e^2$, thus obtaining the following results for the coefficients a, b, c

$$a \;=\; \frac{\alpha\,\pi\,T^2}{3\,p^2}\left(-1\,+\,\frac{\omega}{2p}\,\ln\frac{\omega\,+\,p}{\omega\,-\,p}\right)\;+$$

---

[1] We have chosen a reference frame in which the electron momentum lies along the z axis ($x \,=\, \cos\theta$).

$$+ \quad \frac{\alpha}{2\pi p^2} \int dk \, \frac{k^2}{E} \, F(E) \left(-4 + \frac{\omega E + m_e^2}{pk} \ln A + \frac{\omega E - m_e^2}{pk} \ln B \right) \quad , \tag{F.23}$$

$$\begin{aligned} b &= \frac{\alpha \, \pi \, T^2}{3 \, p^2} \, \omega \left(1 - \frac{m_e^2}{2\omega p} \ln \frac{\omega + p}{\omega - p} \right) + \\ &- \frac{\alpha \, \omega}{2\pi p^2} \int dk \, \frac{k^2}{E} \, F(E) \left(-4 + \frac{m_e^2}{pk} \left(\frac{E + \omega}{\omega} \ln A + \frac{E - \omega}{\omega} \ln B \right) \right) \quad , \end{aligned} \tag{F.24}$$

$$c = \frac{\alpha \, m_e}{\pi \, p} \int dk \, \frac{k}{E} \, F(E) \, (\ln A - \ln B) \quad , \tag{F.25}$$

$$A = \frac{\omega E + m_e^2 + pk}{\omega E + m_e^2 - pk} \quad , \qquad B = \frac{\omega E - m_e^2 + pk}{\omega E - m_e^2 - pk} \quad , \tag{F.26}$$

with $\omega = \sqrt{\mathbf{p}^2 + m_e^2}$.

From the calculated electron self-energy, we can now proceed to evaluate the mass shift correction.

If we denote with ψ the wavefunction of the electron in the plasma, it satisfies the correct Dirac equation

$$(\not{p} - m_e - \Sigma) \, \psi = 0 \quad , \tag{F.27}$$

with Σ in (F.8). We can rewrite this in the form

$$(\tilde{\not{p}} - \tilde{m}) \, \psi = 0 \quad , \tag{F.28}$$

with

$$\tilde{p}_\mu = (1 - a) \, p_\mu - b \, u_\mu \tag{F.29}$$

$$\tilde{m} = m_e + c \tag{F.30}$$

By left-multiplying Eq. (F.28) by $\tilde{\not{p}} + \tilde{m}$ we then deduce the correct dispersion relation for an electron in a medium

$$\tilde{p}^2 - \tilde{m}^2 = 0 \quad , \tag{F.31}$$

or

$$p_0^2 - \mathbf{p}^2 - \frac{2b}{1-a} \, p_0 + \frac{b^2 - (m_e + c)^2}{(1-a)^2} = 0 \quad . \tag{F.32}$$

At first order in α we finally obtain the energy shift

$$p_0 \simeq \sqrt{p^2 + m_e^2} + \left(\hat{a} \, \frac{m_e^2}{\omega} + \hat{b} + \hat{c} \, \frac{m_e}{\omega} \right) = \omega + \mu \quad , \tag{F.33}$$

where $\hat{a}$, $\hat{b}$, $\hat{c}$ are a, b, c evaluated in $p_0 = \omega$.

F.3 Wavefunction renormalization

In general, the Dirac spinors corresponding to a particle propagating in a plasma are different from the ones travelling in vacuum. This results in effective temperature dependent energy projection operators $\Lambda_R^{\pm}$ which replace the usual vacuum ones $\Lambda_0^{\pm}$ in the computation of spin summed squared amplitudes

$$\Lambda_0^{+} \;=\; \frac{\not{p} + m_e}{2\omega} \;\longrightarrow\; \Lambda_R^{+} \quad , \tag{F.34}$$

and similarly for the negative energy projector. Thus, we first have to calculate the effective energy projection operators and then evaluate the corresponding corrections for the decay rates for the reaction in (3.1), (3.2), (3.3) .

An electron propagating through a plasma is described by the equation of motion in (F.27), so that the field propagator is given by

$$G \;=\; \frac{1}{\not{p} \,-\, m_e \,-\, \Sigma} \;=\; \frac{1}{\tilde{\not{p}} - \tilde{m}} \;=\; \frac{\tilde{\not{p}} + \tilde{m}}{\tilde{p}^2 \,-\, \tilde{m}^2} \quad . \tag{F.35}$$

We identify the particle states as corresponding to the energy poles in the propagator; the wavefunction renormalization can then be read off by evaluating the residue of G at the pole. For definiteness, let us focus on the positive energy projection operator; a similar procedure will hold for the negative energy one. If we expand G in (F.35) around the positive energy pole, say ω_R, we obtain

$$\begin{aligned}
\left(\tilde{p}^2 \,-\, \tilde{m}^2\right)^{-1} \;&=\; \left(p^2 \,-\, m_e^2 \,-\, 2\,a\,p^2 \,-\, 2\,b\,p{\cdot}u \,-\, 2\,c\,m\right)^{-1} \;\simeq \\
&\simeq\; \Big\{p_0^2 \,-\, \omega^2 \,-\, 2\,\left(\hat{a} \,+\, \hat{a}'\,(p_0 - \omega_R)\right)(p_0^2 - \mathbf{p}^2) + \\
&+\; 2\,\left(\hat{b} \,+\, \hat{b}'\,(p_0 - \omega_R)\right)\,p{\cdot}u \,-\, 2\,m\,\left(\hat{c} \,+\, \hat{c}'\,(p_0 - \omega_R)\right)\Big\}^{-1} \;\simeq \\
&\simeq\; \Big\{p_0^2 \,-\, \omega^2 \,-\, 2\,\hat{a}\,p_0^2 \,-\, 2\,\hat{a}'\,\omega^2\,(p_0 - \omega_R) + \\
&+\; 2\,\mathbf{p}^2\,\left(\hat{a} \,+\, \hat{a}'\,(p_0 - \omega_R)\right) \,-\, 2\,\hat{b}\,p{\cdot}u \,-\, 2\,\hat{b}'\,\hat{p}{\cdot}u\,(p_0 - \omega_R) \,+ \\
&-\; 2\,m\,\left(\hat{c} \,+\, \hat{c}'\,(p_0 - \omega_R)\right)\Big\}^{-1} \quad .
\end{aligned}$$

Here we have used the "hat" to denote that a given quantity is evaluated at $p_0 = \omega_R$, while a "prime" is used to indicate differentiation with respect to p_0. Note that throughout the entire calculation we retain only terms which are of the first order in α. Substituting the relation $\hat{b}\, p{\cdot}u \,\simeq\, \hat{b}\,\hat{p}{\cdot}u \,+\, \hat{b}\, u_0\, (p_0 - \omega_R)$ in the above formula, we get

$$\begin{aligned} \left(\tilde{p}^2 \,-\, \tilde{m}^2\right)^{-1} \;&=\; \Big\{(1 - 2\hat{a})\, \Big[p_0^2 - \Big(\omega^2 \,+\, 2a\, m_e^2 \,+\, 2\hat{b}\,\hat{p}{\cdot}u \,+\, 2\hat{c}\, m\Big)\Big] \,+ \\ &-\;\; (p_0 - \omega_R)\, \Big[2\hat{b}\, u_0 \,+\, 2\hat{a}'\, m_e^2 \,+\, 2\hat{b}'\,\hat{p}{\cdot}u \,+\, 2\hat{c}'\, m\Big]\Big\}^{-1} \quad . \end{aligned}$$

By requiring that G (and then $(\tilde{p}^2 \,-\, \tilde{m}^2)^{-1}$) has a pole for $p_0 = \omega_R$ we deduce that

$$\omega_R^2 \;=\; \omega^2 \,+\, 2a\, m_e^2 \,+\, 2\hat{b}\,\hat{p}{\cdot}u \,+\, 2\hat{c}\, m \quad , \tag{F.36}$$

which exactly corresponds to the energy shift in (F.33). Around $p_0 = \omega_R$ we then obtain

$$\left(\tilde{p}^2 \,-\, \tilde{m}^2\right)^{-1} \;\simeq\; \frac{1}{p_0 - \omega_R}\,\frac{1}{2\omega_R} \left(1 \,+\, 2\hat{a} \,+\, \frac{\hat{b}}{\omega}\, u_0 \,+\, \hat{a}'\, \frac{m_e^2}{\omega} \,+\, \hat{b}'\, \frac{\hat{p}{\cdot}u}{\omega} \,+\, \hat{c}'\, \frac{m_e}{\omega}\right) \quad , \tag{F.37}$$

thus the expansion around the positive energy pole $p_0 = \omega_R$ of the propagator G in (F.35) finally gives

$$\begin{aligned} G \;\;&\simeq\;\; \frac{1}{p_0 - \omega_R} \left\{\left(1 \,+\, \hat{a} \,+\, \frac{\hat{b}}{\omega}\, u_0 \,+\, \hat{a}'\, \frac{m_e^2}{\omega} \,+\, \hat{b}'\, \frac{\hat{p}{\cdot}u}{\omega} \,+\, \hat{c}'\, \frac{m_e}{\omega}\right) \frac{\not{\hat{p}} + m_R}{2\omega_R} \,+ \right. \\ &\left. -\;\; \frac{\hat{b}}{2\omega} \left(\not{u} \,+\, \frac{\omega}{m_e}\right)\right\} \quad . \end{aligned} \tag{F.38}$$

Here, we also report an alternative writing of the same expression

$$\begin{aligned} G \;\;&\simeq\;\; \frac{1}{p_0 - \omega_R} \left\{\left(1 \,+\, \hat{a} \,+\, \frac{\hat{b}}{\omega}\, (u_0 - 1) \,+\, \hat{a}'\, \frac{m_e^2}{\omega} \,+\, \hat{b}'\, \frac{\hat{p}{\cdot}u}{\omega} \,+\, \hat{c}'\, \frac{m_e}{\omega}\right) \frac{\not{\hat{p}} + m_R}{2\omega_R} \,+ \right. \\ &\left. -\;\; \frac{\hat{b}}{2\omega^2} \left((\omega\;\; \not{u} -\;\; \not{p}) \,+\, \frac{\mathbf{p}^2}{m_e}\right)\right\} \end{aligned} \tag{F.39}$$

The quantity m_R is the effective mass corresponding to the effective energy ω_R in (F.33)

$$m_R \,\simeq\, m_e \,+\, \delta m \,\simeq\, m_e \,+\, \hat{a}\, m_e \,+\, \hat{b}\, \frac{\omega}{m_e} \,+\, \hat{c} \quad . \tag{F.40}$$

In the particularly relevant case in which $u_\mu = (1, \mathbf{0})$ (plasma rest frame) we obtain

$$G \,\simeq\, \frac{1}{p_0 - \omega_R} \left\{\left(1 \,+\, \hat{a} \,+\, \hat{a}'\, \frac{m_e^2}{\omega} \,+\, \hat{b}' \,+\, \hat{c}'\, \frac{m_e}{\omega}\right) \frac{\not{\hat{p}} + m_R}{2\omega_R} \,-\, \frac{\hat{b}}{2\omega^2} \left(\mathbf{p}{\cdot}\gamma \,+\, \frac{\mathbf{p}^2}{m_e}\right)\right\} \tag{F.41}$$

The positive energy projection operator is then simply the residue of G at the corresponding pole; for example, in the plasma rest frame we have

$$\Lambda_R^+ \;=\; (1 \,+\, \lambda)\, \frac{\not{\hat{p}} \,+\, m_R}{2\omega_R} \,-\, \frac{\hat{b}}{2\omega^2} \left(\mathbf{p}{\cdot}\gamma \,+\, \frac{\mathbf{p}^2}{m_e}\right) \quad , \tag{F.42}$$

with

$$\lambda \,=\, \hat{a} \,+\, \hat{a}' \, \frac{m_e^2}{\omega} \,+\, \hat{b}' \,+\, \hat{c}' \, \frac{m_e}{\omega} \quad . \tag{F.43}$$

For the negative energy projector, one has simply to make the substitutions $\omega \to -\omega$, $\omega_R \to -\omega_R$, $\mathbf{p} \to -\mathbf{p}$ in all the quantities appearing in (F.42), (F.43) (in particular these substitutions have to be made also in the expressions for $\hat{a}$, $\hat{a}'$, ...).

Some considerations are now in order. We mainly note that differently from the usual vacuum case, wavefunction renormalization at finite temperature is not simply given by a multiplicative renormalization factor (in the vacuum case $\Lambda_R \,=\, (1 + Z_2)\,\Lambda_0$), but also introduces an additional term proportional to $\hat{b}$ and with a different spinorial structure. This is a pure matter effect, which is given by the presence of the medium 4-velocity u_μ. This dependence is, however, also present in the multiplicative renormalization factor (the first term between {...} in (F.38) or (F.39) or in λ in (F.42)); we point out that, in the plasma rest frame, the peculiar medium dependence of λ only occurs through the energy derivative of b, differently to what happens in the general case in which also a term proportional to b is present (see the first term in (F.39)). One can easily check that in the limiting case of no medium, we recover the usual expression for the renormalized projection operator. We note, however, that this is not true [84] for the result quoted in [82], although an approach similar to ours is used. Other different approaches to the problem of wavefunction renormalization have been proposed in literature [74]-[81], but the final results striking differ. For example, in [74] the authors start introducing finite temperature spinors chosen as the solution of the (nonlinear) Dirac equation (F.27) whose corresponding creation and annihilation operators are assumed to satisfy ordinary, zero temperature, anticommutation relations. Expanding the propagator in terms of these spinors they obtain a wavefunction renormalization factor which is only multiplicative. In particular, this multiplicative factor is exactly the same as our factor $(1 + \lambda)$ in (F.42), but the additional term proportional to $\hat{b}$ is absent. The essential difference with our approach is the assumption made in [74] on the canonical spinor basis to be used; here, however, we do not make any hypothesis on the renormalized field to be used, but simply recover the particle content and the corresponding projector operators from the poles of G and their residues, respectively. Comparative analysis of different approaches have been carried out in Refs. [83, 84].

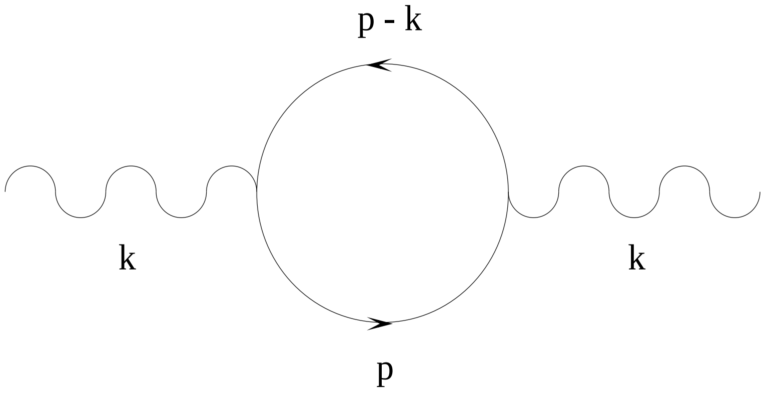

Figure F.2: Self-energy diagram for a photon in a plasma.

F.4 Photon self-energy

The Feynman diagrams for photon self-energy $\Pi_{\mu\nu}$ is shown in Figure F.2; it gives

$$i\,\Pi_{\mu\nu} \;=\; -\int \frac{d^4p}{(2\pi)^4}\, Tr\left\{(i\,e\,\gamma^{\mu})\; i\,S_F(p)\;(i\,e\,\gamma^{\nu})\; i\,S_F(p-k)\right\} \quad , \tag{F.44}$$

where again $S_F(p)$ is the electron propagator in the plasma given by (F.1). As for the electron self-energy, we are interested only in the real part of $\Pi_{\mu\nu}$ which, after some algebra, is given by

$$\begin{aligned} \Re(\Pi_{\mu\nu}) \;&=\; -2e^2 \int \frac{d^3p}{(2\pi)^3}\,\frac{1}{2E}\left(\frac{2p_\mu p_\nu \,-\, \mathrm{p}_\mu k_\nu \,-\, p_\nu k_\mu \,+\, p{\cdot}k g_{\mu\nu}}{k^2 \,-\, 2p{\cdot}k} + \right. \\ &+ \left. \frac{2p_\mu p_\nu \,+\, \mathrm{p}_\mu k_\nu \,+\, p_\nu k_\mu \,-\, p{\cdot}k g_{\mu\nu}}{k^2 \,+\, 2p{\cdot}k}\right)(n_e \,+\, \overline{n}_e) \end{aligned} \tag{F.45}$$

where $E = \sqrt{\mathbf{p}^2 + m_e^2}$. It is now convenient to express $\Pi_{\mu\nu}$ in terms of form factors by using Lorentz and gauge invariance, which give the following constraints

$$k^{\mu}\,\Pi_{\mu\nu} \;=\; k^{\nu}\,\Pi_{\mu\nu} \;=\; 0 \quad . \tag{F.46}$$

In presence of a medium, $\Pi_{\mu\nu}$ may be expressed in terms of the tensor $g_{\mu\nu}$ and the 4-vectors k_μ and u_μ. Then, noting that

$$\tilde{g}_{\mu\nu} \;\equiv\; g_{\mu\nu} \;-\; \frac{k_\mu k_\nu}{k^2} \quad , \tag{F.47}$$

and

$$\frac{\tilde{u}_\mu \tilde{u}_\nu}{\tilde{u}^2} \quad , \tag{F.48}$$

with $\tilde{u}_\mu = \tilde{g}_{\mu\nu} u^\nu$, are the only two tensors orthogonal to k_μ that can be built with $g_{\mu\nu}$, k_μ and u_μ, the most general form of $\Pi_{\mu\nu}$ (assuming parity conservation) results

$$\Pi_{\mu\nu} \; = \; \Pi_T \, R_{\mu\nu} \; + \; \Pi_L \, Q_{\mu\nu} \quad , \tag{F.49}$$

with

$$R_{\mu\nu} \; = \; \tilde{g}_{\mu\nu} \; - \; \frac{\tilde{u}_\mu \tilde{u}_\nu}{\tilde{u}^2} \qquad , \qquad Q_{\mu\nu} \; = \; \frac{\tilde{u}_\mu \tilde{u}_\nu}{\tilde{u}^2} \quad . \tag{F.50}$$

The quantities Π_T, Π_L are scalar functions of the only two invariants k^2, $k{\cdot}u$ and in terms of $\Pi_{\mu\nu}$ are given by

$$\Pi_L \; = \; Q^{\mu\nu} \, \Pi_{\mu\nu} \quad , \tag{F.51}$$

$$2\Pi_t \; = \; R^{\mu\nu} \, \Pi_{\mu\nu} \quad . \tag{F.52}$$

It is now simple to explicitly evaluate these form factors from (F.45); at first order in α, substituting the vacuum dispersion relation $\omega^2 - \mathbf{k}^2 = 0$ in the expression (F.45), after some algebra we obtain

$$\Re(\Pi_L) \; \simeq \; O(\alpha^2) \quad , \tag{F.53}$$

$$\Re(\Pi_T) \; \simeq \; \frac{2\alpha}{\pi} \int_0^\infty dp \, \frac{p^2}{\sqrt{p^2 \, + \, m_e^2}} \, (n_e \, + \, \overline{n}_e) \; + \; O(\alpha^2) \quad . \tag{F.54}$$

From the equation of motion for the 4-vector potential field A^μ

$$\Big(-k^2 \, g_{\mu\nu} \; + \; \Pi_{\mu\nu} \Big) \; A^\nu \quad , \tag{F.55}$$

which more usefully can be written more usefully in the form

$$\Big(k^2 \; - \; \Pi_T \Big) \; R_{\mu\nu} \; + \; \Big(k^2 \; - \; \Pi_L \Big) \; Q_{\mu\nu} \; = \; 0 \quad , \tag{F.56}$$

we can deduce the perturbed dispersion relation of the transverse modes, which is

$$\omega^2 \; - \; \mathbf{k}^2 \; = \; \Pi_T \quad , \tag{F.57}$$

with Π_T given, at first order in α, in (F.54).